Impact of the degradation products of an ion exchange resin (UP2W) on the uptake of radionuclides by cement

Zur Erlangung des akademischen Grades eines

DOKTORS DER NATURWISSENSCHAFTEN

(Dr. rer. nat.)

von. der KIT-Fakultät für Chemie und Biowissenschaften

des Karlsruher Instituts für Technologie (KIT)

genehmigte

DISSERTATION

von

Dipl. Chem. Peter Gyula Szabó

KIT-Dekan :	Dr. Hans-Achim Wagenknecht
Referent:	Prof. Dr. Horst Geckeis
Korreferentin:	Prof. Dr. Petra Panak

Tag der mündlichen Prüfung: 20.04.2023

Erklärung

Ich bestätige hiermit, dass ich die oben genannte Arbeit allein verfasst und nur die aufgeführten Quellen und Hilfsmittel verwendet habe. Des Weiteren versichere ich, dass alle wörtlich oder teilweise aus anderen Quellen kopierten Teile der Arbeit als solche gekennzeichnet sind, dass die elektronische Version der Arbeit mit der schriftlichen entspricht und dass die Arbeit keiner Prüfung Vollmacht in gleicher oder ähnlicher Form unterzogen wurde. Die Satzung des Karlsruher Instituts für Technologie (KIT) zum Schutz guter wissenschaftlicher Praxis wurde in der aktuellen Fassung beachtet. Die hier beschriebenen Studien waren zum Zeitpunkt der Einreichung dieser Arbeit bereits in ähnlicher Form von mir als federführender Erstautorin in internationalen, peer-reviewed Zeitschriften publiziert und werden im Folgenden nicht als solche gekennzeichnet [1-3].

Datum, Ort Unterschrift

Acknowledgement

First, I would like to thank to my scientific advisor Prof. Horst Geckeis and Dr. Marcus Altmaier, who gave me guidance and endless support to achieve my PhD thesis.
I am deeply grateful to my supervisors, Dr. Xavier Gaona and Dr. Tasi Agost for their assistance through my study. For their invaluable aid, I am very pleased.
Next to my advisor within the KIT-INE, I am highly thankful to Dr. Svante Hedström and Dr. Annika Maier for the fruitful discussions and to the Swedish Nuclear Fuel and Waste Management Co. for funding my PhD work in which I was involved.
I am profoundly obliged to Dr. Barbara Lonthenbach from Swiss EMPA institute for her advices during our discourses.
Frank Geyer, Annika Kaufmann and Cornelia Walschburger are appreciated for the measurement of (SF-)ICP-MS. Contribution of Dr. Robert Polly in theoretical calculations, advice of Dr. David Fellhauer on Pu chemistry, assist of Jonas Rentmeister in NPOC examination, Dr. Muriel Bouby in LC-OCD-OND measurement, the exceptional support of Stephanie Kraft, Tanja Kisely and Melanie Böttle in ICP-OES/MS, TG-DSC and LSC, outstanding help of Thomas Sittel in NMR characterization, helping hand of Dr. Johannes Lützenkirchen in Zeta potential measurement, in addition of Dr. Nicolas Finck in XRD and FT-IR data collection and evaluation are greatly acknowledged.
My sincere gratitude towards to my lab mates Dr. Sarah Duckworth, Dr. Androniuk Iuliia, Dr. Sanduni Ratnayake, Dr. Daniel Glückmann, and among other fellow colleagues within KIT-INE, providing me excessive knowledge, endless support and joyful atmosphere, which made the daily work more bearable.
Last but not least, I would like to express my appreciation to my father, Gyula Szabó, my mother, Csilla Lukács and my brother, Viktor Szabó next to my friends in Hungary for constant supporting me in my life and my PhD term as well.

This project was partially funded by Swedish Nuclear Fuel and Waste Management Company (SKB). The EURAD project leading to this application has received funding from the European Union's Horizon 2020 research and innovation programme under grant agreement No 847593. The work was performed as part of the WP CORI and coordinated by KIT-INE.

Abstract

The internationally favored concept for the management of nuclear waste considers the final disposal in near surface and deep underground repositories. Disposal in three main host-rock formations are considered: clay, crystalline and salt. Multibarrier systems are considered to minimize the migration of radionuclides from the repository into the biosphere. Water intrusion into the repositories could not be excluded, that may ruin the barriers and mobilize the radionuclides. This process most likely improbable in rock salt, whilst in clay or granite (also in granitic host rock with a copper coated container), this can be expected in more standard scenarios.

Cementitious materials are widely used for the stabilization of the waste and for construction purposes in repositories for the disposal of low and intermediate level waste, L/ILW. The contact of groundwater with cement results in strongly alkaline conditions ($10 \leq pH \leq 13$), that influence the chemical behaviour of the radionuclides. In this context, an accurate knowledge of the sorption properties of key radionuclides in cementitious systems provides important inputs for the assessment of the long-term performance of repositories for L/ILW.

Organic materials are disposed of together with the radionuclides in L/ILW. Among others, this includes high molecular weight materials *e.g.* paper, cloths, filters etc. Under hyperalkaline and Ca(II) abundant conditions, the abovementioned materials may degrade into low molecular weight organic molecules, which may contribute to the mobilization of the radionuclides. In the recent years, the impact of the organic materials on the retention of radionuclides on cementitious materials have been broadly investigated with some well-known polyhydroxycarboxylic acids *e.g.* isosaccharinic acid (ISA), gluconic acid (GLU).

The UP2W filter aid, built-up mostly by polyacrylonitrile (PAN), is utilized in the nuclear facilities as ion exchange filter aid. In hyperalkaline milieu, nitrile functional groups are transformed to carboxylic and/or carboxamide functional groups during the hydrolysis process. In previous studies, various types of organic fragments *e.g.* malonic acid, decanoic acid, aromatic acids etc. were assigned from the hydrolyzed UP2W, albeit these molecules cannot be traced back to the original PAN material, and the degradation products remain ill-defined. In a first stage of this project conducted outside this PhD thesis, three proxy ligands were defined as representative of the degradation products of UP2W: glutaric acid (GTA, representing the bulk of PAN), as well as α-hydroxyisobutyric acid (HIBA) and 3-hydroxybutyric acid (HBA) (representing the end-groups of the polymer chain).

In order to assess the influence of the ascertained organic ligands derived from the degraded UP2W material on the sorption processes of radionuclides onto hardened cement paste (HCP), stepwise experiments were performed as follows:

1. Investigation of the impact of the defined proxy ligands on the solubility of Ca(II), Ni(II), Nd(III) and Pu(III/IV) in cement porewater and under alkaline conditions.
2. Determining the interaction of the organic ligands with the HCP.
3. Characterization of RN sorption onto HCP in the absence and in the presence of the proxy ligands.

All experiments were performed under Ar atmosphere. The solubility of $Ca(OH)_2$(cr), β-$Ni(OH)_2$(cr), $Nd(OH)_3$(s) and PuO_2(ncr,hyd) in the presence of proxy ligands was examined in alkaline conditions. Due to the possible formation of various oxidation states of Pu in reducing conditions, the experiments with this radionuclide were buffered with the redox agents hydroquinone (HQ) and $SnCl_2$. The mild reducing environment imposed by HQ ensures the predominance of Pu(IV), whilst both Pu(IV) and Pu(III) may occur in the strongly reducing conditions imposed by Sn(II). The effect of the proxy ligands on the uptake of radionuclides (^{63}Ni, ^{152}Eu, ^{242}Pu) by HCP (CEM I 42.5N BV/SR/LA, supplied by the Swedish Nuclear Fuel and Waste Management Company, SKB) was monitored thoroughly. These measurements were conducted at various solid-to-liquid ratios (S:L), RN and organic ligand concentrations. Besides investigating the alteration of RN and organic ligand concentration in respect of the solubility and sorption measurement, the solid phase in solubility experiments was further analyzed by XRD. For the Pu system, Density Functional Theory (DFT) calculations were also conducted by Robert Polly (KIT-INE).

Topic 1: Solubility of $Ca(OH)_2$(cr), β-$Ni(OH)_2$(cr), $Nd(OH)_3$(s) and PuO_2(ncr,hyd) in the presence of defined proxy ligands

Solubility of these four solid phases was monitored in cement porewater containing the proxy ligands at various concentration of $-6 \leq \log ([Lig]_{aq} /M) \leq -1$. Experimental results showed that in most of the cases there were no solubility increase in the presence of the organic ligands. From this observation, their inefficiency to form stable complexes with the investigated elements could be deduced. However, slight increase of Ni concentration in aqueous phase was detected, which suggests the possible formation of Ni(II)-OH-Ligand complexes.

XRD diffractograms confirmed that the four solid phases initially considered remain as main phase after terminating the solubility experiments, yet additional signals on the XRD patterns indicate the formation of secondary phases. Comparing to the solubility data of the same solid phases in the presence of isosaccharinic acid (ISA), the stronger complexation of the latter ligand under alkaline condition can be clearly observed. Although the HIBA and HBA containing similar functional groups (–COOH and –OH) as ISA, stable chelates require the presence of more than one hydroxyl group besides the carboxylate groups. Thus, ISA with its four hydroxyl groups is able to form more stable complexes than the two butyric acids. This theory was further supported via DFT calculations on the system Pu(IV)-OH-Ligand, which indicate that the hydroxyl functional groups of HIBA and HBA do not contribute to the complexation of plutonium, neither as protonated nor in the deprotonated form.

Topic 2: Investigation on the sorption of assigned proxy ligands by hardened cement paste representative to CEM I, degradation stage II

Sorption experiments with the binary system HCP – proxy ligands revealed only minor uptake for of HIBA (R_d = (2.2 ± 1.3)·10^{-3} $m^3 \cdot kg^{-1}$) and HBA (R_d = (1.6 ± 0.9)·10^{-3} $m^3 \cdot kg^{-1}$) by HCP. GTA has moderately higher sorption than the other two proxy ligands using either inactive (R_d = (1.0 ± 0.5)·10^{-2} $m^3 \cdot kg^{-1}$) or active (^{14}C-labelled GTA, R_d = (1.3 ± 0.5)·10^{-2} $m^3 \cdot kg^{-1}$) batch solutions. From these results, it appears evident that the secondary carboxylic functional group present in GTA plays an important role in the sorption process.

Taking into consideration the relevant GTA retention, the sorption data were modelled using a one-site Langmuir isotherm. This evaluation confirms the high adsorption capacity of GTA onto HCP (q = 0.45 ± 0.12·mol·kg^{-1}), which is in line with previous studies with ISA. However, the adsorption affinity constant of GTA is considerably lower (K = 22.5 ± 6.1 $dm^3 \cdot mol^{-1}$) than the one reported for the stronger binding sites of ISA.

Electrophoretic mobility of suspended HCP colloidal particles in proxy ligands solutions was monitored and their results were evaluated as zeta potentials (ζ, mV) to obtain a picture on the effect of the proxy ligands on the surface properties of HCP. A small decrease in the surface charge of HIBA- and HBA-HCP suspensions was only observed at $[Lig]_{tot} \geq 10^{-1.5}$ M. On the other hand, a clear drop in the zeta

potential and the inversion of the surface charge from positive to negative were observed in the case of GTA at $[GTA]_{tot} = 6 \cdot 10^{-2}$ M. These results validated the results obtained in the sorption experiments.

The comparison of the sorption data obtained in this PhD thesis with other results reported in the literature with organic ligands containing carboxylic and hydroxyl groups demonstrated the relevance of the number of these functional groups participating in the uptake process. This comparison underpins also the key role of alcoholic groups in the sorption, most likely in the deprotonated form. Other key parameters affecting sorption are pH, the stability of the complexes Ca(II)-Ligand, as well as steric constrains.

Topic 3: RN sorption processes in Cement-RN-Ligand systems under alkaline and reducing conditions

The uptake of the ^{63}Ni, ^{152}Eu and ^{242}Pu by HCP was investigated in the absence and presence the proxy ligands in the cement degradation stage II. Experimental results of the Cement-Pu(IV), Cement-Eu(III) and Cement-Ni(II) after solid phase separation coincide with the results found in the literature under analogue conditions. In case of Cement-Eu(III) measurements, experiments without appropriate solid phase separation (*e.g.* filtration, centrifuge etc.) resulted in significantly lower R_d values, which are attributed to the possible presence of Eu(III) colloids. The influence of the proxy ligands, which were assigned from UP2W degradation solutions, indicated a slight decrease in the sorption of Ni(II) at $[Lig]_{tot} \geq 10^{-2}$ M. This observation correlates well to solubility data, where Ni(II) concentration was enhanced by the presumed formation of Ni(II)-OH-Ligand ternary complexes. On the contrary, no effect of the proxy ligands was observed for the uptake of Pu(III/IV) and Eu(III). For the three investigated radionuclide systems, the retention remained strong even at the highest ligand concentration. Subsequently, it was verified the proxy ligands were not able to mobilize these cations remarkably comparing to the well investigated polyhydroxycarboxylic acids *i.e.* ISA and GLU.

This study underpins the limited effect of the proxy ligands identified for the degradation of UP2W on the solubility and sorption of Ni(II), Eu(III) and Pu(III/IV) in cementitious systems under reducing conditions. These results provide important inputs to assess the role of the

degradation products of UP2W under boundary conditions relevant for cement-based repositories for the disposal of L/ILW.

Abstract

Das international favorisierte Konzept zur Entsorgung nuklearer Abfälle sieht die Endlagerung in oberflächennahen und tiefen unterirdischen Endlagern vor. Die Lagerung in drei Hauptgesteinsformationen wird in Betracht gezogen: Ton, Kristallin und Salz. Multibarrieren Systeme gelten als Minimierung der Migration von Radionukliden aus dem Endlager in die Biosphäre. Ein Eindringen von Wasser in die Endlager konnte nicht ausgeschlossen werden, das die Barrieren zerstören und die Radionuklide mobilisieren könnte. In Steinsalz ist dieser Vorgang höchstwahrscheinlich unwahrscheinlich, während in Ton oder Granit (auch in granitischem Wirtsgestein mit kupferbeschichtetem Behälter) dies in Standardszenarien zu erwarten ist.

Zementhaltige Materialien werden in großem Umfang zur Stabilisierung des Abfalls und für Bauzwecke in Endlagern für die Endlagerung von schwach- und mittelaktiven Abfällen, S/MA, verwendet. Der Kontakt von Grundwasser mit Zement führt zu stark alkalischen Bedingungen ($10 \leq pH \leq 13$), die das chemische Verhalten der Radionuklide beeinflussen. In diesem Zusammenhang liefert eine genaue Kenntnis der Sorptionseigenschaften wichtiger Radionuklide in zementgebundenen Systemen wichtige Inputs für die Bewertung der langfristigen Leistungsfähigkeit von Endlagern für S/MA.

Organische Materialien werden zusammen mit den Radionukliden in Klein- und SMA entsorgt. Dazu gehören unter anderem Materialien mit hohem Molekulargewicht, *z.B.* Papier, Tücher, Filter usw. Unter hyperalkalischen und Ca(II)-reichen Bedingungen können die oben genannten Materialien zu niedermolekularen organischen Molekülen abgebaut werden, die zur Mobilisierung der Radionuklide beitragen können. In den letzten Jahren wurde der Einfluss organischer Materialien auf die Retention von Radionukliden auf zementartigen Materialien umfassend mit einigen wohlbekannten Polyhydroxycarbonsäuren untersucht, *z.B.* Isosaccharinsäure (ISA), Gluconsäure (GLU).

Das meist aus Polyacrylnitril (PAN) aufgebaute Filterhilfsmittel UP2W wird in kerntechnischen Anlagen als Ionenaustausch-Filterhilfsmittel eingesetzt. Im hyperalkalischen Milieu werden funktionelle Nitrilgruppen während des Hydrolyseverfahrens in funktionelle Carboxyl- und/oder Carboxamidgruppen umgewandelt. In früheren Studien wurden verschiedene Arten von organischen Fragmenten, *z.B.* Malonsäure, Decansäure, aromatische Säuren usw. wurden aus dem hydrolysierten UP2W zugeordnet, obwohl diese Moleküle nicht auf das ursprüngliche PAN-Material zurückgeführt werden können und die Abbauprodukte schlecht definiert bleiben. In einer ersten Phase dieses Projekts, das außerhalb dieser

Dissertation durchgeführt wurde, wurden drei Proxy-Liganden als repräsentativ für die Abbauprodukte von UP2W definiert: Glutarsäure (GTA, stellt den Großteil von PAN dar), sowie α-Hydroxyisobuttersäure (HIBA) und 3-Hydroxybuttersäure (HBA) (repräsentiert die Endgruppen der Polymerkette).
Um den Einfluss der ermittelten organischen Liganden aus dem abgebauten UP2W-Material auf die Sorptionsprozesse von Radionukliden auf Zementstein (HCP) zu beurteilen, wurden schrittweise Experimente wie folgt durchgeführt:

1. Untersuchung des Einflusses der definierten Proxy-Liganden auf die Löslichkeit von Ca(II), Ni(II), Nd(III) und Pu(III/IV) in Zementporenwasser und unter alkalischen Bedingungen.
2. Bestimmung der Wechselwirkung der organischen Liganden mit dem HCP.
3. Charakterisierung der RN-Sorption auf HCP in Abwesenheit und in Gegenwart der Proxy-Liganden.

Alle Experimente wurden unter Ar-Atmosphäre durchgeführt. Unter alkalischen Bedingungen wurde die Löslichkeit von $Ca(OH)_2$(cr), β-$Ni(OH)_2$(cr), $Nd(OH)_3$(s) und PuO_2(ncr,hyd) in Gegenwart von Proxy-Liganden untersucht. Wegen der möglichen Bildung verschiedener Oxidationsstufen von Pu unter reduzierenden Bedingungen wurden die Versuche mit diesem Radionuklid mit den Redoxmitteln Hydrochinon (HQ) und $SnCl_2$ gepuffert. Die durch HQ auferlegte milde reduzierende Umgebung gewährleistet das Vorherrschen von Pu(IV), während sowohl Pu(IV) als auch Pu(III) unter den durch Sn(II) auferlegten stark reduzierenden Bedingungen auftreten können. Die Wirkung der Proxy-Liganden auf die Aufnahme von Radionukliden (^{63}Ni, ^{152}Eu, ^{242}Pu) durch HCP (CEM I 42,5N BV/SR/LA, geliefert von der Swedish Nuclear Fuel and Waste Management Company, SKB) wurde sorgfältig überwacht. Diese Messungen wurden bei verschiedenen Feststoff-zu-Flüssigkeit-Verhältnissen (S:L), RN und Konzentrationen organischer Liganden durchgeführt. Neben der Untersuchung der Veränderung der RN- und organischen Ligandenkonzentration im Hinblick auf die Löslichkeits- und Sorptionsmessung wurde die Festphase in Löslichkeitsexperimenten weiter durch XRD analysiert. Für das Pu-System wurden von Robert Polly (KIT-INE) auch Berechnungen der Dichtefunktionaltheorie (DFT) durchgeführt.

Thema 1: Löslichkeit von $Ca(OH)_2(cr)$, β-$Ni(OH)_2(cr)$, $Nd(OH)_3(s)$ und $PuO_2(ncr,hyd)$ in Gegenwart definierter Proxy-Liganden

Die Löslichkeit dieser vier festen Phasen wurde in Zementporenwasser überwacht, das die Proxy-Liganden bei verschiedenen Konzentrationen von $-6 \leq \log([Lig]_{aq}/M) \leq -1$ enthielt. Experimentelle Ergebnisse zeigten, dass es in den meisten Fällen zu keiner Erhöhung der Löslichkeit in Gegenwart der organischen Liganden kam. Aus dieser Beobachtung konnte ihre Ineffizienz zur Bildung stabiler Komplexe mit den untersuchten Elementen abgeleitet werden. Es wurde jedoch ein leichter Anstieg der Ni-Konzentration in der wässrigen Phase festgestellt, was auf die mögliche Bildung von Ni(II)-OH-Ligand-Komplexen hindeutet. XRD-Diffraktogramme bestätigten, dass die zunächst betrachteten vier festen Phasen nach Beendigung der Löslichkeitsexperimente als Hauptphase verbleiben, jedoch deuten zusätzliche Signale auf den XRD-Mustern auf die Bildung von Nebenphasen hin. Im Vergleich zu den Löslichkeitsdaten der gleichen Festphasen in Gegenwart von Isosaccharinsäure (ISA) ist die stärkere Komplexierung des letztgenannten Liganden unter alkalischen Bedingungen deutlich zu beobachten. Obwohl HIBA und HBA ähnliche funktionelle Gruppen (–COOH und –OH) wie ISA enthalten, erfordern stabile Chelate das Vorhandensein von mehr als einer Hydroxylgruppe neben den Carboxylatgruppen. So kann ISA mit seinen vier Hydroxylgruppen stabilere Komplexe bilden als die beiden Buttersäuren. Diese Theorie wurde weiter gestützt durch DFT-Rechnungen am System Pu(IV)-OH-Ligand, die zeigen, dass die funktionellen Hydroxylgruppen von HIBA und HBA weder in protonierter noch in deprotonierter Form zur Komplexierung von Plutonium beitragen.

Thema 2: Untersuchung zur Sorption zugeordneter Proxy-Liganden durch ausgehärteten Zementleim repräsentativ für CEM I, Abbaustufe II

Sorptionsexperimente mit dem binären System HCP – Proxy-Liganden zeigten nur eine geringe Aufnahme von HIBA (R_d = (2,2 ± 1,3)·10^{-3} $m^3 \cdot kg^{-1}$) und HBA (R_d = (1,6 ± 0,9)·10^{-3} $m^3 \cdot kg^{-1}$) von HCP. GTA hat eine mäßig höhere Sorption als die beiden anderen Proxy-Liganden, wenn entweder inaktives (R_d = (1,0 ± 0,5)·10^{-2} $m^3 \cdot kg^{-1}$) oder aktives (^{14}C-markiertes GTA, R_d = (1,3 ± 0,5)·10^{-2} $m^3 \cdot kg^{-1}$) Ansatzlösungen verwendet wird. Aus diesen Ergebnissen scheint ersichtlich, dass die in GTA vorhandene sekundäre funktionelle Carboxylgruppe eine wichtige Rolle im Sorptionsprozess spielt.

Unter Berücksichtigung der relevanten GTA-Retention wurden die Sorptionsdaten mit einer einseitigen Langmuir-Isotherme modelliert. Diese Bewertung bestätigt die hohe Adsorptionskapazität von GTA an HCP (q = 0,45 ± 0,12 $mol \cdot kg^{-1}$), was mit früheren Studien mit ISA übereinstimmt. Allerdings ist die Adsorptionsaffinitätskonstante von GTA erheblich niedriger (K = 22,5 ± 6,1 $dm^3 \cdot mol^{-1}$) als die für die stärkeren Bindungsstellen von ISA berichtete.

Die elektrophoretische Mobilität von suspendierten kolloidalen HCP-Partikeln in Lösungen von Proxy-Liganden wurde überwacht und ihre Ergebnisse wurden als Zeta-Potentiale (ζ, mV) ausgewertet, um ein Bild über die Wirkung der Proxy-Liganden auf die Oberflächeneigenschaften von HCP zu erhalten. Eine geringe Abnahme der Oberflächenladung von HIBA- und HBA-HCP-Suspensionen wurde nur bei $[Lig]_{tot} \geq 10^{-1,5}$ M beobachtet. Andererseits wurde ein deutlicher Abfall des Zeta-Potentials und die Umkehrung der Oberflächenladung von positiv beobachtet zu negativ wurden im Fall von GTA bei [GTA]tot = 6·10^{-2} M beobachtet. Diese Ergebnisse bestätigten die in den Sorptionsexperimenten erhaltenen Ergebnisse.

Der Vergleich der in dieser Dissertation erhaltenen Sorptionsdaten mit anderen in der Literatur berichteten Ergebnissen mit organischen Liganden, die Carboxyl- und Hydroxylgruppen enthalten, zeigte die Relevanz der Anzahl dieser am Aufnahmeprozess beteiligten funktionellen Gruppen. Dieser Vergleich untermauert auch die Schlüsselrolle alkoholischer Gruppen bei der Sorption, höchstwahrscheinlich in der deprotonierten Form. Andere Schlüsselparameter, die

die Sorption beeinflussen, sind der pH-Wert, die Stabilität der Komplexe Ca(II)-Ligand sowie sterische Beschränkungen.

Thema 3: RN-Sorptionsprozesse in Zement-RN-Ligand-Systemen unter alkalischen und reduzierenden Bedingungen

Die Aufnahme von ^{63}Ni, ^{152}Eu und ^{242}Pu durch HCP wurde in Abwesenheit und Anwesenheit der Proxy-Liganden in der Zementabbaustufe II untersucht. Experimentelle Ergebnisse von Cement-Pu(IV), Cement-Eu(III) und Cement-Ni(II) nach Festphasentrennung stimmen mit den in der Literatur unter analogen Bedingungen gefundenen Ergebnissen überein. Bei Zement-Eu(III)-Messungen ergaben Versuche ohne geeignete Festphasentrennung (*z.B.* Filtration, Zentrifuge uzw.) deutlich niedrigere R_d-Werte, die auf die mögliche Anwesenheit von Eu(III)-Kolloiden zurückgeführt werden. Der Einfluss der Proxy-Liganden, die aus UP2W-Abbaulösungen zugeordnet wurden, deutete auf eine leichte Abnahme der Sorption von Ni(II) bei $[Lig]_{tot} \geq 10^{-2}$ M hin. Diese Beobachtung korreliert gut mit Löslichkeitsdaten, wobei Ni(II)-Konzentration wurde durch die vermutete Bildung von ternären Ni(II)-OH-Ligand-Komplexen erhöht. Im Gegensatz dazu wurde kein Einfluss der Proxy-Liganden auf die Aufnahme von Pu(III/IV) und Eu(III) beobachtet. Für die drei untersuchten Radionuklidsysteme blieb die Retention sogar bei der höchsten Ligandenkonzentration stark. Anschließend wurde verifiziert, dass die Proxy-Liganden nicht in der Lage waren, diese Kationen bemerkenswerterweise im Vergleich zu den gut untersuchten Polyhydroxycarbonsäuren, *d. h.* ISA und GLU, zu mobilisieren.

Diese Studie unterstreicht die begrenzte Wirkung der für den Abbau von UP2W identifizierten Proxy-Liganden auf die Löslichkeit und Sorption von Ni(II), Eu(III) und Pu(III/IV) in zementartigen Systemen unter reduzierenden Bedingungen. Diese Ergebnisse liefern wichtige Inputs, um die Rolle der Abbauprodukte von UP2W unter Randbedingungen zu bewerten, die für zementbasierte Endlager für die Endlagerung von S/MA relevant sind.

Table of Contents

List of figures

List of tables

List of abbreviation and acronyms

$[i]_{tot}$	Total concentration of species "*i*" in solution [mol·dm^{-3} or M]
β	Cumulative or overall stability constant
ACW	Artificial cement pore water
AFm	Aluminate ferrite monosulfate
AFm-CO_3	Calcium monocarboaluminate
AFt	Aluminoferrite trisulfate
AFt-SO_4	Ettringite
An	Actinides / actinoids
COSMO	Conductor-like screening model
C-S-H	Calcium-silicate-hydrate
DFT	Density functional theory
DP	Degradation product
DRS	Diffuse reflectance spectroscopy
E_h	Standard electrode potential
eV	Electronvolt (unit of energy, 1.602176634·10^{-19} J)
EXAFS	Extended X-ray absorption fine structure
FCW	Fresh Cement Pore Water
FT-IR	Fourier-transform infrared spectroscopy
g	Gravitational force-equivalent [9.80665 m·s^{-2}]
GLU	Gluconic acid / gluconate ion
GTA	Glutaric acid
HBA	3-hydroxybutyric acid
HCP	Hardened cement paste
HIBA	α-hydroxyisobutyric acid
HLW	High-level radioactive waste
HQ	Hydroquinone (Benzene-1,4-diol)
HSAB	Hard and soft (Lewis) acids and bases
hyd	Hydrated
I	Ionic strength [mol·dm^{-3}]
ICP-MS	Inductively coupled plasma-mass spectrometry
ICP-OES	Inductively coupled plasma-optical emission spectrometry
IEP	Isoelectric point
ILW-LL	Intermediate-level long-lived waste
INE	Institut für Nukleare Entsorgung (Institute for Nuclear Waste Disposal)
ISA	Isosaccharinic acid / α-D-isosaccharinate ion
JCPDS	Joint Committee on Powder Diffraction Standards
K	Adsorption affinity constant [dm^3·mol^{-1}]
K°	Equilibrium constant (T = 25 °C)
K_d	Distribution coefficient [dm^3·kg^{-1}or m^3·kg^{-1}]
kD	Kilodalton
KIT	Karlsruher Institut für Technologie (Karlsruhe Institute of Technology)

LC-OCD-OND	Liquid Chromatography – Organic Carbon Detection – Organic Nitrogen Detector
LCPW	Leached Cement Pore Water
LDH	Layered Doubled Hydroxide
LILW-SL	Low- and intermediate-level short-lived waste
L/ILW	Low- and intermediate-level radioactive waste
LLW-LL	Low-level long-lived waste
Ln	Lanthanides / lanthanoids
Log $K°$	Base 10 logarithm of equilibrium constant
LSC	Liquid scintillation counting
M	Metallic constituent / molarity [$mol \cdot dm^{-3}$]
MWCO	Molecular weight cut-off
N	Coordination number
ncr	Nano-crystalline
NEA-TDB	Nuclear Energy Agency – Thermochemical Database
NMR	Nuclear magnetic resonance
NPOC	Non-Purgeable Organic Carbon
OPC	Ordinary Portland cement
p.a.	Per analysis
PAN	Polyacrylonitrile
PDF	Powder Diffraction File
pe	Negative decimal logarithm of free electron concentration / activity in solution
pH	Potential of proton [$-\log_{10}[H^+]$]
PP	Polypropylene
ppb	Parts per billion, [$\mu g \cdot dm^{-3}$]
ppm	Parts per million, [$mg \cdot dm^{-3}$]
PTFE	Polytetrafluorethylene
p.w.	Present work
q	Adsorption capacity [$mol \cdot kg^{-1}$]
Q_d	Other abbreviation for distribution coefficient [$m^3 \cdot kg^{-1}$]
R_d	Distribution ratio [$dm^3 \cdot kg^{-1}$ or $m^3 \cdot kg^{-1}$]
RMS	Root-mean-square
RN	Radionuclide
RT	Room temperature (T = (22 ± 2) °C)
SF-ICP-MS	Sector field-inductively coupled plasma-mass spectrometry
SHE	Standard hydrogen electrode
SKB	Svensk Kärnbränslehantering AB (Swedish Nuclear Fuel and Waste Management Company)
S:L	Solid-to-liquid phase ratio [$g \cdot dm^{-3}$]
SNF	Spent nuclear fuel
$t_{1/2}$	Half-life [second or day]
TG-DSC	Thermogravimetric-differential scanning calorimetry
TOC	Total organic carbon

TRLFS	Time-resolved fluorescence spectroscopy
TRU	Transuranic nuclear waste
u	Unified atomic mass unit
UP2W	Polyacrylonitrile (PAN) based ion exchange resin
V	Volume [dm^3]
VLLW	Very low-level radioactive waste
w/o	Without
XAS	X-ray absorption spectroscopy
XRD	X-ray diffraction

1. Introduction

The nuclear industry mostly considers the use of enriched uranium as fuel to generate electricity via nuclear fission (^{235}U), although other fuels such as MOX are also used in some countries. Besides the generation of energy, the nuclear reactions taking place in the reactor produce different types of short- and long-lived radionuclides, for instance ^{90}Sr, ^{137}Cs, ^{131}I, ^{239}Pu, ^{99}Tc, ^{241}Am, ^{237}Np and several activation products *e.g.* ^{14}C, ^{55}Fe, ^{59}Ni, ^{63}Ni, ^{93}Mo, ^{94}Nb etc. The long-term management of radioactive waste considers the disposal of those wastes in surface, near surface, underground or deep underground disposal facilities. Such installations should ensure the safety of the waste disposal. The safety concept of such facilities relies on a multi-barrier system aiming at minimizing the release of the radionuclides from the repository into the biosphere [4, 5].

Type of radioactive wastes

The categorization of radioactive waste changes from country to country. Germany classifies them according to heat generating and negligibly heat generating waste, but generally, they are frequently separated into five main groups [6-11]:

- **Very low-level radioactive waste (VLLW)**: comprising materials which activity is less than 100 Bq/g. This type of waste can be originated from concretes, soils, and scrap metals. Due to the low activity, it can be stored in near-surface disposal
- **Low-level long-lived waste (LLW-LL)**: radioactivity of this nuclear waste can come from different sources, *e.g.* radium-bearing wastes (^{226}Ra, ^{232}Th), graphite, among other. The activity concentration of these types of wastes is in the range of 10 and 1000 kBq/g. Although they are planned to be disposed in near-surface facilities, yet they require robust isolation from the environment.
- **Low- and intermediate-level short-lived waste (LILW-SL)**: this group contains mostly β-emitting radionuclides with half-life of less than 30 years and limited amounts of long-lived radionuclides which can come from maintenance operations (*e.g.* tools, cleaning rags), operation facilities (*e.g.* ion exchange resins and metals wastes), and dismantling operations. Their activity is usually below 0.37 GBq/kg. They are usually encapsulated in cementitious medium and placed them into near surface or underground disposal.

- **Intermediate-level long-lived waste (ILW-LL)** encompasses metallic wastes, which come from the fuel reprocessing *i.e.* hulls and end-pieces from zircaloy cladding, among others. The activity concentration of this waste is in the range of 0.37-370 GBq/kg. Due to high activity and long half-lives ($t_{1/2} \geq 31$ a) of radionuclides within the waste, they are usually considered to be disposed in deep geological repositories.
- **High-level radioactive waste (HLW)**, which contains spent fuel and residues from its reprocessing, vitrified and transuranic nuclear waste (TRU). It comprises actinides (^{239}Pu, ^{244}Cm), fission products (^{144}Ce, ^{137}Cs) and activation products (^{59}Ni). Total activity coming mostly from spent nuclear fuel is between 90 and 170 TBq/kg.

Fundamentals of repositories for nuclear waste disposal

The repositories' main purposes are based on two major safety functions: isolation of the nuclear waste from biosphere and containment as long as the waste represents a potential hazard [12]. According to a widely considered concept for radioactive waste disposal of L/ILW, the wastes are deposited into steel canisters, then the canisters filled with cement (generally with ordinary Portland cement, OPC) and finally the packages are housed to a well-design concrete vault or tunnels (also referred to as galleries) [5, 13, 14]. The formerly mentioned waste disposal process follows the principle of a multibarrier system, which consists of geoengineered/technical (metallic canister, waste form and backfill material) and natural (host rock) barriers. Some countries choose for natural barriers the host rock formations of granitic (crystalline) rocks, clay rocks (boom clay, Opalinus clay), and salt domes and flat bedded rock salt, while other countries prefer to emplace L/ILW in surface disposal sites. Cementitious materials are used extensively in radioactive waste disposal facilities. They are applied as packaging of the L/ILW and as construction materials [5].
In regards of close collaboration with the Swedish Nuclear Fuel and Waste Management Company (SKB), the present work in this thesis focused on the disposal of radioactive wastes under given conditions within the SKB waste repositories. A final repository for radioactive waste (SFR 1) was built by SKB for storing L/ILW waste, which can come from for instance from operation of Swedish nuclear power plants (filters, protective clothes etc.). Unlike the SNF, which is disposed of as HLW, it contains short-lived radionuclides of low activities with no heat generation, but also low activities of long-lived radionuclides [15]. The SFR repository is built-up by various vaults for the disposal of different types of waste according

to their activity levels *i.e.* one SILO and four vaults (BMA, 1 BTF, 2 BTF and BLA) [15-17]. A brief description of these vaults is provided below:

- The BMA vault wastes contain of intermediate level materials, mostly ion exchange resins, scraps and trash covered with cement or bitumen.
- BTF has been constructed to keep intermediate level wastes, such as de-watered ion-exchange resins, ashes and scraps. The former wastes are placed to concrete, whilst the latter two are placed to steel drummer or concrete containers.
- In BLA, only low-level waste is stored, primarily metals, cellulose and other organic materials and placed to standard steel containers.
- SILO is designed to keep ion exchange resins and small amounts of scraps and trashes. These wastes are conditioned around 80 % in cement and 20% in bitumen.

In underground repositories, the anoxic corrosion of steel and iron components is expected to result in the development of reducing condition with redox potentials close to the lower border line of the water stability field. This can affect the chemical behaviour of redox-sensitive radionuclides, which is strongly dependent on the redox boundary conditions. In the event of water intrusion, the possible formation of aqueous systems involving radionuclides needs to be considered.

Organic materials in L/ILW and their behaviour

Some organic materials are disposed of together with the radionuclides in some waste streams, especially in L/ILW. High molecular weight organic components may undergo degradation in the alkaline conditions defined by the cement systems in many repository concepts for L/ILW, resulting the potential formation of low molecular weight compounds with the capacity to complex radionuclides. For instance, under cement porewater conditions (Section 1.2), the cellulose is not stable and decomposes into isosaccharinic acid (ISA) [14], which is capable of forming stable complexes with different radionuclides. The α-D-isosaccharinic acid (α-D-ISA) is one of the major degradation products of several cellulosic materials [18, 19]. Regarding the cellulose final degradation product is ISA, which is accepted by scientific community, we used ISA for comparison purpose through our work. The organic material investigated in this PhD thesis, UP2W, is used as filter aid in nuclear and conventional power plants. This macromolecule technically consists of polyacrylonitrile (PAN), with additional other ingredients, such as water, N,N-dimethylacetamide and an

unknown component called "finish" [16]. Nowadays approximately 53 t are disposed within the repository after its exhaustion [20]. The UP2W filter aid was reported to undergo hydrolytic degradation within previously mentioned condition. The degradation products of UP2W may complex radionuclides thus decreasing their retention properties.

In high alkaline conditions, organic polymers could degrade to short-carbon chained organic molecules containing carboxylic and alcoholic functional groups, which are capable of establishing complexes with metal ions. Furthermore, appearance of Ca(II) in solution may enhance the stabilization of organic ligands and metal ions through the formation of ternary or quaternary complexes (Ca(II)-RN-Ligand and /or Ca(II)-RN-OH-Ligand) [19]. Therefore, the understanding on the nature and strength of the interactions between radionuclides and polymers degradation products are of utmost importance.

1.1 Historical aspects, abundance and aqueous chemistry of the radionuclides investigated in this PhD thesis

1.1.1 Nickel and its complex formation with organic molecules

This transition metal is situated in the group of the periodic table VIII/B, Period 4. Its electron configuration is [Ar] $3d^8\ 4s^2$ and in ambient conditions and aqueous media, the oxidation state is +2, but in extreme conditions, it could be stabilized in +1, +3, +4 oxidation states [21].

Of its isotopes, five are stable in nature: ^{58}Ni, ^{60}Ni, ^{61}Ni, ^{62}Ni and ^{64}Ni. There are 26 radioactive isotopes, but among them, the ^{59}Ni and ^{63}Ni are the most important. ^{59}Ni, ($t_{1/2}$ = $7.6{\cdot}10^4$ a) is applied in isotope geology as a standard, whereas ^{63}Ni ($t_{1/2}$ = 100.1 a) is used in gas chromatography in electron capture detectors. These two isotopes are activation products of Ni, (^{58}Ni and ^{62}Ni), Zn and Co. Both isotopes ^{59}Ni and ^{63}Ni appear in the structural steels and internal components of nuclear reactor vessels [22-24]. The activation products enter cooling water through corrosion of structural components.

Multiple experiments prove that the hydrolysis of Ni(II) produces several hydroxide forms, such as $NiOH^+$, $Ni(OH)_2(aq)$, $Ni(OH)_3^-$ and so-called polynuclear species (Ni_2OH^{3+} and $Ni_4(OH)_4^{4+}$), which turn up as Ni aqueous species in solutions. However, the recent literature stated $NiOH^+$, Ni_2OH^{3+} and $Ni_4(OH)_4^{4+}$ are developed in acidic or neutral condition and in the case of $Ni_4(OH)_4^{4+}$ at $[Ni(II)]_{tot} > 5{\cdot}10^{-3}$ M [23, 25]. Recent studies have shown that $Ni(OH)_2(aq)$ is the main hydrolysis species prevailing in alkaline conditions, although the

formation of $Ni(OH)_3^-$ may occur at pH > 13 [23]. Hydrolysis reactions of Ni(II) and corresponding equilibrium constants at the reference state are summarized in Appendix Table A-1 [23, 25].

The solubility of β-$Ni(OH)_2$(cr) and the speciation of Ni(II) in cement porewater have been surveyed over the last years [26-30]. Ochs *et* al. [31] analyzed the solubility of $Ni(OH)_2$(s) in fresh cement (FCW, pH ≈ 13.3) and aged Portland cement (ACW, pH ≈ 12.5) porewater at 22 °C and 50 °C. This study indicated that in fresh cement porewater the $Ni(OH)_2$(s) solubility was slightly higher than in the ACW. The authors suggested that this could be attributed to the formation of higher-order Ni-hydroxo complexes at high pH. At room temperature (22 °C) in FCW, the mean Ni concentration was around $3.1 \cdot 10^{-7}$ M, whereas in ACW, despite the large uncertainty in the course of time, it was around $1.3 \cdot 10^{-7}$ M. Furthermore, the degradation products of long-chain organic compounds can also inflict significant changes in the solubility of $Ni(OH)_2$(s) within analogous conditions. Warwick and co-workers [32] investigated the interaction of ISA and GLU at pH = 7 – 13 varying organic ligand concentration (approximately $10^{-6} \leq ([Lig]_{in}\ /M) \leq 10^{-1}$) with 0.1 M $NiCl_2$. Aside of assessing the structure and stability constant (β) of Ni(II)-L (L = ISA, GLU) with a stoichiometry of NiL, Ni_2L and $Ni_2(OH)_4L$ at pH = 13.3, the impact of GLU and ISA on the solubility of Ni(II) was observed at $[GLU]_{in} \geq 10^{-6}$ M and $[ISA]_{in} \geq 10^{-2}$ M. Complexation of Ni(II)-ISA was further analyzed by González-Siso *et* al. [23]. The authors used β–$Ni(OH)_2$(cr) with or without ISA at 7.5 ≤ pH ≤ 13, using 0.5 – 3.0 M NaCl-NaOH solutions. In the absence of ISA, they have come to the conclusion that $Ni(OH)_3^-$ was not formed at $[Ni]_{in} = 10^{-7}$ M within the pH range of 10 to 13 and the solubility of Ni(II) was pH independent. Although, their experiments are corresponding to $Ni(OH)_2$ solubility data of [28, 33], yet their result was in disagreement with the increase of the solubility of Ni in the pH range of 12.5 – 13.5 according to the calculation of NEA-TDB [25, 34], where the development of $Ni(OH)_3^-$ species was considered. In the presence of ISA as organic ligand, due to formation of $Ni(OH)_2ISA^-$ and $Ni(OH)_3ISA^{2-}$ species in analogous pH conditions, the solubility was increased by two orders of magnitude in solutions with $[ISA]_{in} \geq 10^{-2}$ M comparing with the ISA free systems. This signified that the organic ligand is capable of outcompeting the hydrolysis under hyperalkaline conditions. Moreover, this phenomenon proves that the ISA could have the capacity to form complexes in alkaline environment due to the deprotonation of the carboxylic and hydroxyl groups.

Solubility experiments with Ni in the context of the UP2W degradation products (DP) were executed in the literature of [16]. Under ambient conditions, the effect of the organic

fragments derived from the degradation of UP2W at pH = 12.5 in artificial cement pore water and at pH =13.5 in artificial fresh cement pore water was investigated. The authors studied the solubility considering (i) added degradation solution volume, (ii) required time for reaching the equilibrium, (iii) order of addition of compounds to the system and (iv) comparison of the effect of organic leachates obtained during hydrolytic degradation at pH = 12.5 and 13.5. As a consequence of the precipitation of $Ca(OH)_2$, the porewater solution was filtered through either Munktell filter papers or 0.2 µm syringe filters prior analysis. During the monitoring of (i) experiments at pH = 12.5, it was observed that the increase of DP concentration contributed to the enhancement of Ni(II) concentration in aqueous phase from $3.75 \cdot 10^{-7}$ M to $3.41 \cdot 10^{-6}$ M. In the second study (ii), the equilibrium was reached at [Ni] = $6.82 \cdot 10^{-6}$ M after $t_{eq} \approx 48$ d. It was concluded within (iii) experimental study that the order of addition (whether it was prepared in pore water + RN + DP or pore water + DP + RN) had no impact on the solubility of Ni after the same equilibration time as in (ii) measurement. The influence of the organic fragments of UP2W at pH = 12.5 (DP1) was compared with the effect of the degradation products obtained at pH = 13.5 and containing [TOC] = 5116 ppm (DP2). Utilizing same order of addition of (i) or (ii) in the presence of DP2, the Ni concentration increased up ≈ 6 ppm, which is not surprising, since the organic carbon concentration was ≈ 6 times higher in DP2 than in DP1.

1.1.2 Introduction to lanthanides

Those metallic elements, which are situated in the periodic table from the atomic number of 57 to 71, namely from lanthanum to lutetium, are called lanthanides or lanthanoids. These elements, together with scandium and yttrium, are also referred to as rare-earth elements. The standard electron configuration of the lanthanides is represented as [Xe] $4f^n\ 5d^{0-1}\ 6s^2$ (n = 0 – 14). The most common oxidation state of these elements is +3, but some lanthanides also appear with +2 and +4 state. Moving from La to Lu in the periodic table, a significant decrease of the atomic and ionic radii can be perceived, which is known as “lanthanide contraction”. This theory emphasizes that as the nuclear charge increases, the nuclear attraction of electrons in outer-shell is amplified due to weak shielding effect of 4*f* electrons in inner-shell orbital. This results decrease in the size of electron cloud [35, 36]. However, the Eu and Yb do not follow this trend, because due to their tendency to adopt the 2+, they have the structure of $[Ln^{2+}(e^-)_2)]$ with greater radii, which is more comparable to barium [35, 36]. The alteration caused by the contraction has a great impact on (i) the atomic size of the

elements, (ii) strength of the ionic interaction, (iii) complex formation and (iv) electronegativity of the lanthanides [37]. The lanthanides are characterized by high coordination numbers (N). Normally, the coordination number is in the range of 7 and 9 for the interaction with simple ligands (*i.e.* H_2O), but can increase up to 12 for the interaction with organic molecules (*i.e.* EDTA) [38]. Another property of the lanthanides is their basicity, which affects the type of bonding developed in their oxide or hydroxide compounds. It is acknowledged by the Fajan's rule that by decreasing the size of Ln(III), the strength of its covalent character increases, whilst the ionic character between the metal ion and OH^- decreases. Hence, the size and the basicity of the Ln(III) decrease according to [39]:

$La^{3+} > Ce^{3+} > Pr^{3+} > Nd^{3+} > Pm^{3+} > Sm^{3+} > Eu^{3+} > Gd^{3+} > Tb^{3+} > Dy^{3+} > Ho^{3+} > Er^{3+} > Tm^{3+} > Yb^{3+} > Lu^{3+}$

The discovery of neodymium (Nd) belongs to Carl Auer von Welsbach, who used the method of fractional crystallization in 1885 to separate the didymium, a mixture of neodymium and praseodymium from each other. The main oxidation state of Nd is +3, but appears as +2 and +4 [40]. Electron configuration of this element is [Xe] $4f^4$ $6s^2$. Natural Nd can be found with the atomic number of ^{142}Nd, ^{143}Nd, ^{145}Nd, ^{146}Nd, ^{148}Nd and two radioisotopes of ^{144}Nd and ^{150}Nd. The latter two isotopes are the most stable from the other 24 synthetic radioisotopes [41].

Europium, with an atomic number of 63, is one of rarest among lanthanide elements. The oxidization states of this lanthanide element are usually +2 and +3. Its electron configuration is [Xe] $4f^7$ $6s^2$ and it has six main isotopes, the ^{150}Eu, ^{151}Eu, ^{152}Eu, ^{153}Eu, ^{154}Eu and ^{155}Eu. Naturally occurring europium is composed of two isotopes, *i.e.* ^{151}Eu and ^{153}Eu. Plenty of minerals contain europium along with other lanthanides. The most widely used sources are bastnäsite, monazites, xenotime, loparite and ore with small concentrations of rare-elements [42-44].

1.1.2.1 Solubility of lanthanides (Nd(III) and Eu(III)) and their complexation with organic ligands

Lanthanides and actinides with same oxidization states are often considered as chemical analogues. This is due to the same charge and similar ionic radii, *e.g.* for Nd^{3+}, Am^{3+}, Cm^{3+} and Pu^{3+} with 111, 110, 112 and 109 pm, respectively [45]. Trivalent lanthanides and

actinides are characterized by a high solubility in acidic to weakly alkaline solutions, but the formation of sparingly soluble oxy-hydroxides in alkaline to hyperalkaline systems.

Tobias and Garett [46] indicated that between Nd^{3+} and hydroxyl group ion bond was weak and formed by electrostatic attraction. The dissolution of $Nd(OH)_3(s)$ in distilled water resulted in pH = 9.1 due to low solubility of the solid phase. In another article, Icenhower and his co-workers [47] studied the $Nd(OH)_3(s)$ solubility equilibrium for 670 days under de-aerated NaCl media and inert atmosphere. They observed that from pH 10 to 13 the $[Nd]_{tot}$ remained constant and low ($[Nd]_{tot} \leq 10^{-8}$ M). With own results and data reported in the literature, Neck *et* al. [45] discussed the solubility of Nd(III), Cm(III) and Am(III) at pH = 7 – 13 in various ionic strengths I = 0.1, 0.5, 2.5 and 5.0 M NaCl and 0.25, 1.0, 2.5 and 3.5 M $MgCl_2$ / $CaCl_2$ at room temperature (T = (22 ± 2) °C) and in Ar atmosphere. The authors observed an increase of the solubility with ionic strength, and derived accordingly chemical, thermodynamic and (SIT, Pitzer) activity models. A large scattering of the data was observed at pH > 10, which is attributed to the predominance of the neutral species $Nd(OH)_3(aq)$, its tendency to the formation of colloids $Nd_m(OH)_{3m}$, and their sorption on the vessel's walls and filters. In systems containing moderate to high $CaCl_2$ concentrations, the authors reported the formation of ternary complexes Ca(II)-Nd(III)-OH. However, these complexes are not expected to form within the boundary conditions defined by cement environment in dilute systems (*i.e.* $[Ca] \leq 0.02$ M).

Observations in the context of interactions of organic ligands with Ln(III) solubility at various pH are systematically discussed in the next paragraphs.

Giroux *et* al. [48] simulated the complex formation of lanthanides (La(III), Eu(III), Dy(III), Er(III) and Lu(III)) in the presence of gluconic acid (GLU) and Pr(III) in the presence of some polyhydroxycarboxylic acids (glyceric acid, threonic acid, 2-hydroxybutanoic acid and 3-hydroxybutanoic acid) by using pH potentiometric titrations and NMR under acidic to weakly alkaline conditions. For the Pr(III)-Ligand systems, the authors proposed the predominance of the complexes $ML_{-2}H_{-3}$ and $ML_{-2}H_{-2}$ (glyceric acid), MLH_{-2}(theornic acid) and ML(butanoic acids) at 8 < pH. Moreover, it was highlighted that the hydroxyl groups in the α-, γ-position could play main role in the complex formation, but organic molecules with longer carbon-chain established stronger bound with the Ln(III) than with those which have shorter carbon-chain.

Vercammen and co-workers [49] conducted sorption experiments with Th(IV) ($[Th]_{tot}$ = 1.2 – $1.6 \cdot 10^{-13}$ M) and Eu(III) ($[Eu]_{tot}$ =$5 \cdot 10^{-10}$ M) using of ISA as complexing agent in the pH range of 10.7 to 13.3, N_2 atmosphere and at I = 0.3 M. The addition of $Ca(NO_3)_2$ was utilized

to simulate the cementitious environment at the investigated pH. In case of Th(IV) the results showed strong Ca(II) interaction with Th(IV)-ISA to develop $CaTh(OH)_4(ISA)_2$. However, no effect of Ca(II) on Eu(III)-ISA complexation was found, and the formation of a complex with a ratio 1:1 was proposed. The impact of ISA on $Nd(OH)_3(am)$ solubility was studied at 0.1 M, 1.0 M and 5.0 M NaCl (pH = 8 – 14), 0.1 M NaCl-$CaCl_2$ (pH = 8 – 13) and 10^{-5} M ≤ $[ISA]_{tot}$ ≤ $4 \cdot 10^{-2}$ M solutions under Ar atmosphere and room temperature (22 ± 2) °C by Gugau. [50]. From this study, it could be deduced that the increase of the Nd(III) concentration in aqueous phase starts from 10^{-3} M ≤ $[ISA]_{tot}$, in various NaCl solutions, whereas in $CaCl_2$ system no significant change was detected in the investigated conditions, which implies that ternary complexes of Ca(II)-Ln(III)-ISA do not form in alkaline conditions. Based on her experimental observations, the author reported the formation of the complexes $Nd(OH)(ISA_{-H})(aq)$ (log K^0 = 5.83 ± 0.2) and $Nd(OH)_2(ISA_{-H})^-$ (log K^0 = -(5.92 ± 0.2)).
Tasdigh [16] studied the influence of the UP2W DP on the solubility of Ni(II) and Eu(III) in alkaline, ambient conditions using different approaches. Increasing concentrations of DP resulted in the enhancement of the Eu(III) concentration from 0.027 to 1.12 ppm. Furthermore, the order of addition of the individual components has no striking influence on the mobilization of the radionuclide.

1.1.3 Introduction to actinides

All isotopes of actinides are radioactive and their half-lives are in the range between $1.41 \cdot 10^{10}$ years and 0.38 millisecond (for ^{232}Th and ^{258}Fm, respectively). Some early actinides are characterized by a rich redox chemistry, as shown in Figure 1. The chemical behaviour of the actinides is accordingly strongly dependent on the redox boundary conditions.

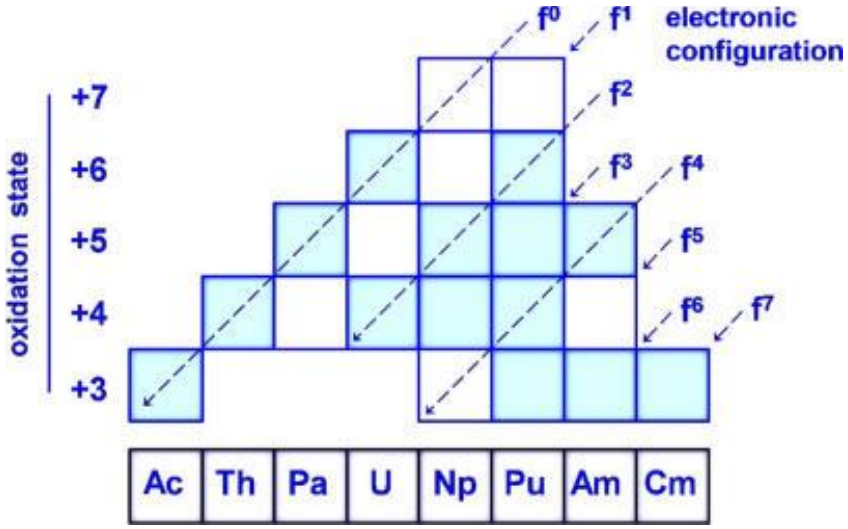

Figure 1. *Possible oxidation states of actinide from actinium to curium. The blue-blocks symbolize the most stable redox state of actinides in aqueous media [51].*

The actinide group contains 15 elements, starting from actinium (atomic number 89) and ending with lawrencium (atomic number 103). With the discovery of the transuranic elements, it became clear that electrons can populate the 5*f* shell. Except for actinium and thorium, all other actinides comprise electron(s) in 5*f* orbitals. Comparing with lanthanides, they have some similar chemical properties, however the binding energies of lanthanides 4*f* electrons are much higher than the binding energies of actinides 5*f* electrons. Since binding energies of actinides 5*f* electrons are lower than lanthanides, they can be easily get rid of electrons from their shells and therefore actinides are characterized by several oxidization states. As underlined for the lanthanides, the size of the actinides decreases gradually with increasing atomic numbers. The main difference between the "actinides contraction" and "lanthanides contraction" is that the former is greater due to the higher radial extension of the valence orbital. Analogously with the lanthanides, the actinide ions are coloured in the specific oxidization state in which one or more single *f* electrons exist. The heaviest natural elements, thorium, protactinium and uranium, lie in corresponding positions just below the 6th period transition metals hafnium, tantalum and tungsten. These three elements, which are in the process of filling up the 5*d* electron shelf are similar in their chemical properties to the corresponding transition elements, zirconium, niobium and molybdenum, which are in the process of filling up the 4*d* shell. To same extend, thorium and protactinium display some resemblance with 4*d* and 5*d* elements. However, the resemblance of uranium to tungsten and molybdenum is much weaker. [35, 36, 52]. Actinides are categorized as hard Lewis acids

based on the Pearson's HSAB (hard and soft (Lewis) acids and bases) theory due to their high effective nuclear charge (Z_{eff}) (and minor polarizability), and thus they are prone to establish stable ionic bonding with hard Lewis bases involving oxygen and nitrogen atom(s) (and fluoride and chloride ions) [53]. The actinides demonstrate perfect ion-dipole interaction with water molecules. The strength of the ionic bonding between the "hard" bases and actinides ions depends on the effective charge of the metal cation. Therefore, the decrease of the effective charge (displayed the numbers in the brackets) shows the decrease the ability to form stable complexes:

$$An^{4+}(4) > AnO_2^{2+}(3.3) > An^{3+}(3) > AnO_2^{+}\ (2.2)\ [5, 54]$$

The actinide cations are unstable in the oxidation states +V and +VI and transform to the linear dioxocation moieties called actinyl ions. The central actinide ion creates covalent bonds with the two oxygen forming the linear structure $(O=An=O)^{n+}$, with n = 1 or 2.

Plenty of articles underline that not only the factors of pH and E_h in the water contribute to the solubility and migration of the actinides, but also the complex reactions with inorganic and organic ligands, sorption to colloidal or mineral surfaces, etc. The hydrolysis of the actinides depends on their oxidation states, namely the aforementioned effective charges, which is the key driving force for interaction with hard bases. Subsequently, the lower the effective charge of the actinide, the higher the pH value at which the hydrolysis starts [5, 54, 55]. At the same time, properties of actinides highly rely on the oxidation state. Consequently, actinides with the same oxidization state possess similar chemical reactivity and they are often considered as analogous. For example, trivalent lanthanides as well as Am(III) and Cm(III) are often used as analogues of the redox-sensitive Pu(III). This method is applicable for actinides in the +4 oxidation state as well *i.e.* Th(IV) as analogue of Pu(IV) [5, 56]. A convenient way to visualize the actinide species in aqueous solution is the Pourbaix-diagram, which shows the predominant species of a given element as a function of the redox potential (E_h) and pH. The Figure 2 shows the stable complexes and solid phases within an aqueous system [5].

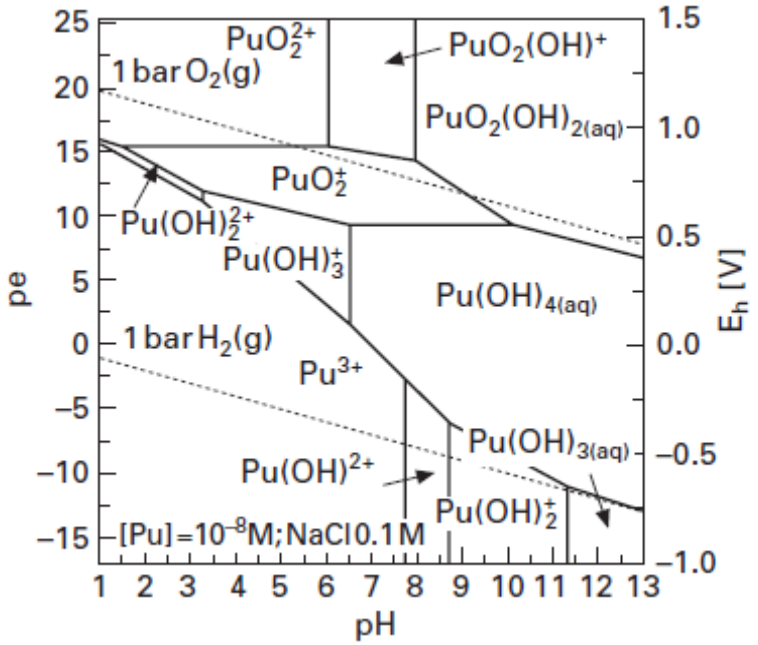

Figure 2*. Pourbaix-diagram of plutonium cited from Poinssot and co-workers [5]. Calculation was carried out for 0.1 M NaCl, $[Pu]_{tot} = 10^{-8}$ M and room temperature (T = 25 °C) without the involvement of carbonate complex formation. Solid dash lines illustrate the borderlines between the aqueous species, whilst dot lines correspond to the upper and lower stability field of water.*

Another relevant aspect of the actinides is the formation of An-colloid particles. During the hydrolysis, the transuranic elements have the susceptibility to develop so-called intrinsic or eigencolloids [5, 14]. Tetravalent actinides are able to develop the strong colloid formation, also in line with their very strong hydrolysis [14, 57, 58]. To less extent, the formation of colloids of An(III) and Ln(III) is also described in the literature, however this effect is still not comprehended or defined [14, 59].

1.1.3.1 Solubility of plutonium and its complexation with organic ligands

The discovery of this transuranic element was a huge milestone for mankind. In 1940, Arthur C. Wahl and Glenn T. Seaborg in collaboration with Dr. Joseph W. Kennedy in Department of Chemistry at the University of California, Berkley, were capable of producing ^{239}Pu with a cyclotron, using uranium-oxide bombarded with 16 MeV deuterons. Years later, they recognized that plutonium is not only a good nuclear energy source, but also a fissile source for making the first atomic bomb (Manhattan Project) [60]. Next to ^{239}Pu, the other isotopes of Pu must be highlighted, because in the nuclear reactor, they are also formed through

neutron capture of ^{238}U. These isotopes are the ^{240}Pu, ^{241}Pu and ^{242}Pu. Its electron configuration is [Rn] $5f^6 7s^2$ [61].

Plutonium may well be unique in that four oxidation states can coexist in aqueous solution. Due to its electropositive nature, the Pu has the tendency to lose electrons from its outer electrons in order to create oxidation states of +3, +4, +5, +6 and +7. Since their redox potentials are close to each other, for certain boundary conditions, there is the possibility that the first 4 (stable) redox states appear simultaneously in aqueous system, making it difficult to understand the Pu chemistry in the aqueous phase. In presence of non-complexing acidic solutions (*i.e.* perchloric acid), the Pu(III) and Pu(IV) exist hydrated or in aquo ions, with high number of valence shell orbitals and coordination number (N). These numbers typically vary between n = 8–10 and depend on ionic strength and ligands [62].

As stated in the scientific literature [14, 63-65], the solubility equilibriums of PuO_2 (Pu(IV)) and its hydrolysis constants can be described in accordance of Appendix Table A-3.

In some environment systems or in underground repositories, reducing condition are expected to be developed thus affecting the oxidation state of plutonium. In these conditions, the formation of both Pu(IV) and Pu(III) can be envisaged. Altmaier and co-workers, reported the thermodynamic data of the log *K*/log β values for solubility and hydrolysis of Pu(III) and Pu(IV) (Appendix Table A-4). The studies of the Pu(III/IV) solubility and hydrolysis, especially in alkaline and reducing conditions, are limited [66]. Due to this fact, large uncertainties are related to the thermodynamic data on Pu(III) aqueous species and solid compounds. A thorough summary and selection of the available data is provided within the NEA-TDB project [64]. Recently, Tasi *et* al. studied the solubility of PuO_2(ncr,hyd) under inert atmosphere, controlled reducing and alkaline milieu [65]. The experiments confirmed that the solubility was pH-independent above pH > 8, which reflects the same observation as Neck and Kim. [58]. Tasi and co-workers [65] reported that the solubility in mild reducing media ($pe + pH_m = 9.5 \pm 1$; HQ) is controlled by PuO_2(ncr,hyd), whilst in strong reducing solution ($pe + pH_m = 2 \pm 1$; Sn(II)), the co-existence of PuO_2(ncr,hyd) and $Pu(OH)_3$(am) was proposed.

Experimental results of Pu solubility measurement in the presence of low molecular weight carboxylic acids, for instance formic acid, acetic acid, citric acid etc. under hyperalkaline (pH > 11) conditions are scarce in the scientific reports, but the impact of main degradation product of cellulose (ISA) on the Pu solubility has been investigated in numerous articles.

Moreton [67] conducted Pu solubility experiments in the present of various soluble organic molecules comprising carboxylic and/or hydroxyl functional groups *i.e.* GLU, sorbitol, citric

acid, ISA etc. under alkaline conditions (pH = 12) and $-6 \leq \log ([Lig]_{in} /M) \leq -2$. It was determined that the Pu(IV) form complexes in the terms of 1:1 or 1:2 with the organic ligands under the following criteria: (i) the organic compounds, which contain at least four hydroxyl groups, $Pu(LH_{-4})$ formation was proposed; (ii) organic ligands, which comprise less than four hydroxyl groups, were able to form $Pu(LH_{-m})(OH)_{(4-m)}^{-}$ (where the m is the number of hydroxyl groups on the carbon chain) and (iii) in pH regions where [Pu] *vs.* [L] experimental datapoints illustrated a slope of 2, the complex formation of $Pu(LH_{-2})_2^{2-}$ was presumed. Besides these statements, the findings confirmed, that the strength of Pu-ligand stability relies on various functional groups, in which, next to carboxylic groups, the amount of hydroxyl groups contribute in large scale. Log *K* values in this report were reevaluated in later studies available in the literature [63, 68]. Considering these processes, for instance using the recalculated solubility data at pH = 12 in regards of ISA, the appearance of $Pu(OH)_4(ISA)^{-}$ and $Pu(OH)_4(ISA)_2^{2-}$ as complex species were suggested [14]. Effect of ISA on Pu solubility under typical conditions of underground waste repositories in post closure period has been thoroughly studied in the recent years [18, 19]. Regarding the existence of Pu in various oxidation states, the redox environment for gaining Pu(III) and Pu(IV) was ensured by applying Sn(II) and HQ redox buffers, respectively. The experiments were performed varying the concentrations of ISA, Ca and/or NaCl. Density Functional Theory (DFT) calculations were used for determining the preferential Pu(IV)-ISA complex configuration. This study indicated that from pH > 11 the dominant species in the presence of Ca were $Ca(II)Pu(IV)(OH)_3ISA_{-H}^{+}$ and $Ca(II)Pu(IV)(OH)_3ISA_{-2H}(aq)$ quaternary complexes. This hints that Ca(II) further enhances the stability of the Pu(IV)-ISA complexes.

1.2 Cementitious materials: composition, application and degradation stages.

Cement is one of the main components in the multi-barrier system in several concepts for the disposal of L/ILW. Cement is used for the stabilization of the waste and for construction purposes.

The cement is fundamentally build-up by a complex mixture of different elements and compounds, mostly by calcium-silicates. It is basically manufactured with the help of heating limestone with clay around 1450 °C in a kiln. The gained hard cement clinker is added and gridded with a small portion of gypsum to the powder in order to prepare Ordinary Portland Cement (OPC), the most widely used cement type all over the world. This Portland cement

encompasses regularly five particular components (numbers in brackets exemplify the percentage distribution of the components) [34]:

- **Alite** (50 – 70 %): Tricalcium silicate, C_3S or Ca_3SiO_5, whose reaction with water results in calcium silicate hydrate gel and portlandite ($Ca(OH)_2$).
- **Belite** (20 – 30 %): Also known as dicalcium silicate, C_2S or β-Ca_2SiO_4, generates C-S-H and portlandite via the reaction with water as well, but at a slower pace.
- **Aluminate** (5 – 12 %): Ferrite and tricalcium aluminate (C_3A or $Ca_3Al_2O_6$). In the presence of appropriate amount of gypsum, C_3A leads to the formation of AFt (calcium aluminosulphate, $F = Fe_2O_3$) or with the lack of gypsum AFm (calcium monosulphoaluminate).
- **Ferrite** (5 – 12 %): Calcium aluminoferrite $C_2(F,A)_5$. Reacts with water the same way as the C_3A does.
- **Gypsum** (~2 %): Addition of this component to cement during the mixture with water promotes slow hydration. This "retarding agent" of cement prevents from fast setting caused by an immediate hydration of aluminates. Hence, it provides longer working time for mixing, transporting and placing the cement material.

The hydration of the mineral phases present in the clinker results in the following components:

- Major solid phases: Amorphous C-S-H phases and crystalline portlandite ($Ca(OH)_2$).
- Minor solid phases: ettringite (aluminoferrite trisulfate, AFt); monosulphate (aluminoferrite monosulphate, AFm), hydrogarnet and hydrotalcite.

C-S-H phases are of special relevance as a sink of radionuclides, especially of (cationic) metal ions, and to less extent anionic species. Characterization of different cement materials indicated the surface area of hardened cement paste (HCP) is above 50 m^2/g, portlandite is around 6 m^2/g, whilst C-S-H phases is 148 m^2/g [34, 69]. Accordingly, sorption processes can be also evaluated considering the surface area, thus resulting in mol/m^2 or $sites/nm^2$. Consequently, a high amount of cement creates significant sorption capacity for radionuclides and other pollutants [34, 70-73].

1.2.1 Degradation stages of hydrated cement

Upon contact with aqueous solutions (*e.g.* groundwater), cement materials undergo degradation, which induces significant changes in the structure and composition of cement. The degradation can be classified in four stages (see Figure 3):

Stage I

The porewater composition is dominated by dissolved Na- and K-oxo/hydroxides, which results in very high pH values between 13 – 13.5. Furthermore, the solubility of portlandite here is low (10^{-3} M) and only a small portion of Ca(II) is released to the aqueous phase from solid phases.

Stage II

After the washing out of alkali ions by the effluent water from pore fluid, the pH level decreases to 12.5. In this instance, the pore fluid is basically a 20 mM $Ca(OH)_2$ solution. By the removal of the alkali ions, the pH and pore fluid are controlled by solubility equilibria of portlandite.

Stage III

This Stage happens after the total dissolution of portlandite at end of Stage II. From this perspective, C-S-H phases undergo incongruent dissolution, evolving from high Ca/Si (> 1.5) to low Ca/Si (< 0.6) ratios. This results in a evolution of the pH from 12.5 to ca. 10 [74].

Stage IV

In this stage C-S-H phases have been fully dissolved, and only calcite remains as main degradation product of cement. The $[Ca]_{tot}$ in the solution are between $10^{-3} – 10^{-4}$ M [34, 75, 76].

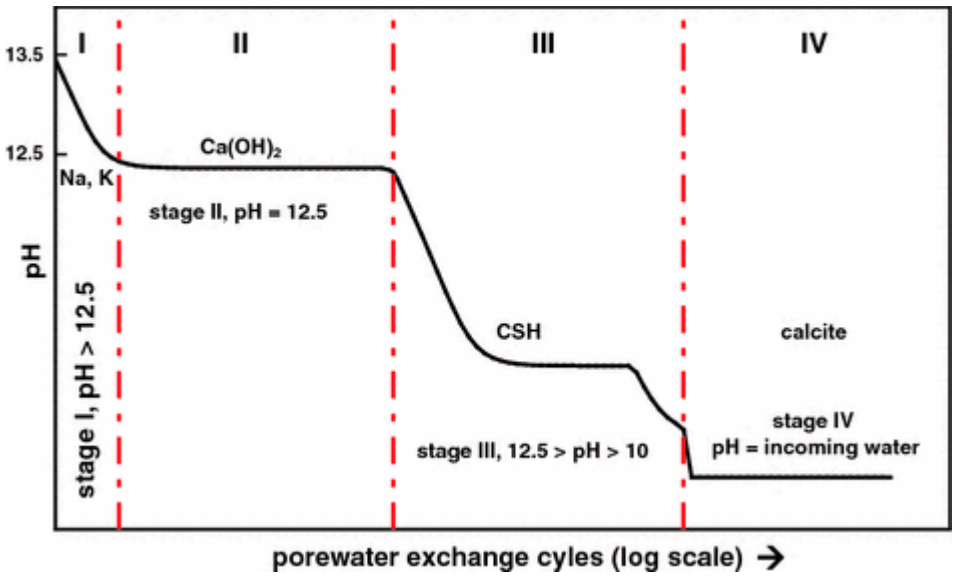

Figure 3. *Evolution of pH in cement porewater during cement degradation at 25 °C in accordance with Ochs and co-workers publication [34].*

1.3. UP2W filter aid: structure, application and hydrolytic degradation

Ion exchange resins are used widely in nuclear power plants for the purpose of extracting chemical impurities and radionuclides from coolant and waste streams. After the exhaustion of these different type of polymers, they are disposed of generally as L/ILW in cementitious environments [77]. In the highly alkaline media expected in cementitious environments, the polymeric materials may degrade over time to short-carbon chain organic molecules, which might be able to form complexes with radionuclides in aqueous media, eventually decreasing sorption and promoting their mobilization into the biosphere.

This chapter focuses on the description of the UP2W material, particularly on the main ingredient, the polyacrylonitrile (PAN).

1.3.1 Polyacrylonitrile, PAN

The UP2W is technically a filter aid, which is used in nuclear and conventional power plants. This material consists of polyacrylonitrile (PAN), water, additional unknown component called “finish” and negligibly minor portion of N,N-dimethylacetamide. The polymer is prepared by the polymerization of its monomer (Figure 4) [16].

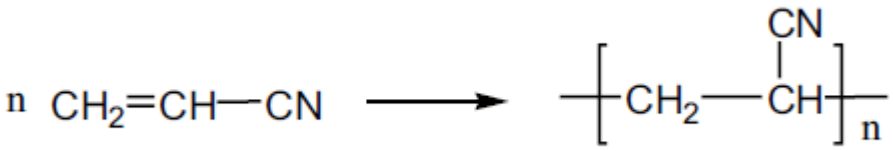

Figure 4. *Acrylonitrile (left) and Polyacrylonitrile (PAN) (right).*

The polymer is manufactured from its monomer in two ways: ionic reaction and radical reaction [17]. In general, three different spatial structures might appear during the synthesis process. These formed polymers are usually called isotactic, syndiotactic and atactic. Along the main carbon chain, the neighboring nitrile groups can either be on only the same side (isotactic) or different side (syndiotactic) or in some special cases, when the configuration varies between both forms (atactic). Usually, the latter form occurs after the polymerization. Molecular mass of PAN in UP2W is in the range of 100,000 and 150,000 u. The polymer is commercially declared stable between pH 2 and 12 [17]. In general, the polymer decomposes above 150 °C and melts at 300 °C. At these temperatures, the polymer releases nitrogen in the form of N_2, NH_3 and other small organic molecules containing nitrogen. On top of that, the polymer itself is susceptible to oxidization, which results the formations of alcoholic and carboxylic groups [17, 78, 79].

Due to functional groups along the polymer fibers, the PAN has so-called reactive points. In these specific sites, the degradation reactions start taking place, forming eventually degradation products. Thus, nitrile groups are sensitive against any nucleophilic attack on the carbon atom, which are connected directly to the polymer chain. Since the resin is in a highly alkaline media in the repository, this degradation path is expected to occur. This degradation expectedly results in the production of smaller organic molecules, which could lead to the mobilization of radionuclides inside the cementitious system [17].

1.3.2 Hydrolytic degradation of PAN: state-of-art

Tracking the degradation of PAN is not new among scientists. Research on this phenomenon started decades ago with Glazkovskii *et* al. [80], who analyzed the hydrolysis of the nitrile groups, with the degradation proceeding via amide until formation of carboxylic groups. In 1985, Bajaj and co-workers [81] continued the experiments with saponification of the polymer and they came to the conclusion that the PAN went through cyclization by the formation of C=N conjugated systems during hydrolysis.

Few years later, Bashir *et* al. [82] indicated that the treatment of PAN with bases (*e.g.* Et_2NH, NaOH, NaOEt etc.) produced coloured materials, which underwent cyclization reactions. However, later they investigated the degradation using ^{13}C-NMR to see what type of configuration change occurred within process and they observed that no cyclization was induced even when reddish-black colour emerged. It was presumed that there is no relationship between the cyclization and colour forming. Instead, they found out that the syndiotactic formation increased at expense of the isotactic sequences. The following arguments were provided to explain these observations [17, 82]:

a. Besides the colouration of the solution, its viscosity was decreased, which could be related to breakage of the carbon backbone
b. After a certain period, the viscosity increased again, which was attributed to an enhanced crosslinking effect between the chains of carbon atoms
c. The nitrile groups were hydrolysed to amides and then later to carboxylic acids or their salts
d. NMR revealed that the PAN structure underwent configuration changes. It was proposed, that the hydroxyl anion attacked the proton of the carbon atom in the α-position, which was stabilized to carbanion by resonance. The free hydroxyl ion could be responsible for breaking the polymer chain, crosslinking reactions or the abstraction of the proton from the solvent. The PAN also goes through inversion in its configuration from isotactic to syndiotactic caused by the methine proton abstraction and/or the chain scission on the isotactic formation.

A thorough investigation of the hydrolytic degradation of the PAN polymer was conducted by Litmanovich and Platé [79]. The experiments indicated that the final composition of the degradation product contains carboxylate and amide groups. These measurements also indicated that amidine groups function were intermediate species between the nitrile and

carboxylate groups. The release of NH_3 during the degradation process (Figure 5) and its impact on the cement porewater are another factors, which must be taken into consideration. The generation of NH_3 confirmed that the hydrolysis was still in progress, and ammonia has also the ability to act as ligand for some radionuclides (*e.g.* Ni(II), Ag(I), etc.) [17, 83]. Hence, the produced NH_3 has to be explicitly involved during characterization of the hydrolysed filter aid.

However, despite the detailed articles of developed intermediate and small organic compounds from the UP2W, controversial statements were found in these studies. For example, Duro *et* al. [17] reported the presence of some aromatic compounds among the degradation products, which cannot be traced back to the structure of PAN. Due to lack of information about the dissolution of UP2W and its main/final degradation products, more experiments need to be accomplished. In current work, we have determined 3 possible "final" degradation products of UP2W ion exchange filter, which results can be seen in Section 1.3.3.

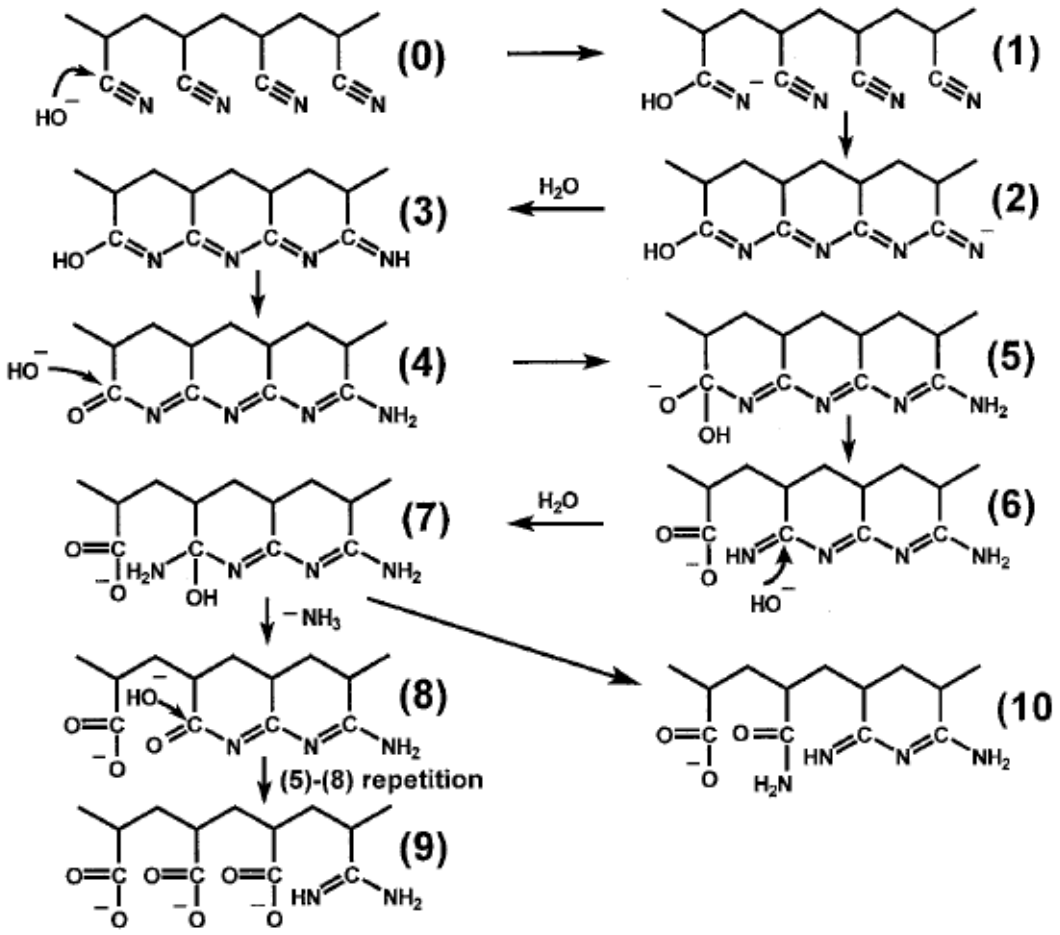

Figure 5. *Conjugated sequences of PAN during the hydrolysis (Litmanovich and Platé, 2000) [79].*

1.3.3 Review: Degradation studies of UP2W

This chapter of the PhD thesis provides a brief insight on the degradation / dissolution process of PAN-based UP2W filter aid in NaOH and portlandite-buffered media investigated at KIT-INE, which was reported by Tasi *et* al. [84]. The work was performed within the EU funded CORI project mainly by A. Tasi with significant contributions by myself.

Degradation of the UP2W material was systematically monitored by following the increase of NPOC concentration in liquid phase as function of time in different solutions reproducing cementitious environments:

- $Ca(OH)_2$-buffered system at T = 22 °C
- $Ca(OH)_2$-buffered system at T = 22 °C in the presence of Fe(0)
- $Ca(OH)_2$-buffered system at T = 80 °C

- NaOH system at pH ≈ 12.5
- 0.1 M NaOH system
- 1.0 M NaOH system

With increasing contact time, the concentration of NPOC increased in NaOH solutions, up to ~ 1000 ppm in the 1.0 M NaOH. A much slower degradation / dissolution of the UP2W fiber was observed in $Ca(OH)_2$-buffered systems. NPOC concentrations of ~ 50 ppm were measured after a contact time of ~ 1250 days. Moreover, in 1.0 M NaOH, the polymer was completely disintegrated after t ≈ 2 a, resulting a coloured (orange) and viscous solution. This is in good agreement with the study of Bashir and co-workers [82]. These observations support that degradation occurs at an enhanced rate in NaOH systems as compared to $Ca(OH)_2$-buffered solutions.

The degradation leachate obtained in 1.0 M NaOH was further analyzed with ^{1}H and ^{13}C liquid phase NMR in order to identify the main fragments of the degraded polymer. It is well documented that nitrile groups (–C≡N) of PAN hydrolyze under hyperalkaline conditions resulting in carboxylate and / or carboxamide groups [79, 81]. Based on the previous studies and the obtained results, Tasi *et* al. [84] proposed three plausible proxy ligands consistent with NMR observations and representing possible fragments of the PAN degradation products. These were (i) the glutaric acid (GTA), which represents the bulk chain of the generated polymer fragments, whereas (ii) α-hydroxyisobutyric acid (HIBA) and (iii) 3-hydroxybutyric acid (HBA) both simulate the end groups of the main polymer chain. The assigned organic molecules shown in Figure 6 were applied in all solubility (Section 3.2) and sorption experiments (Section 3.3).

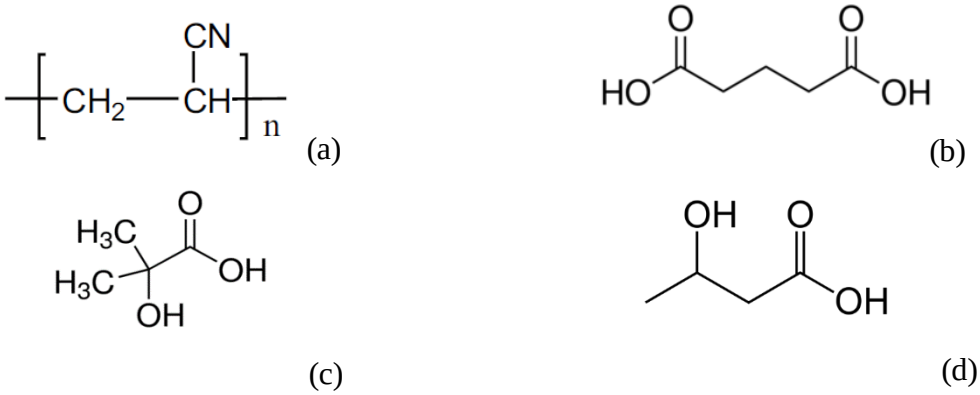

Figure 6. *Chemical composition of polyacrylonitrile (PAN, a), glutaric acid (GTA, b), α-hydroxyisobutyric acid (HIBA, c) and 3-hydroxybutyric acid (HBA, d).*

The degradation leachates were analyzed with Liquid Chromatography – Organic Carbon Detection – Organic Nitrogen Detector (LC-OCD-OND) to characterize the length and molecular weight of the generated organic fragments. Measurements conducted with $NaHCO_3$ and Na_2HPO_4/KH_2PO_4 eluents. Chromatograms indicated that larger molecular weight fragments are developed in NaOH- (> 150 kDa) than in $Ca(OH)_2$-buffered solutions (~ 3.5 kDa).

In addition to the liquid phase characterization, the degraded solid phase was also characterized with various techniques, *i.e.* FT-IR or TG-DSC. Prior any measurement could take place, the solid material was washed with 0.05 – 1.0 M HCl and Milli-Q water in order to extract the traces of background electrolytes. Fourier-transform infrared spectroscopy (FT-IR) was conducted with the fresh UP2W fibers and compared to the hydrolyzed UP2W material to gain insight on the hydrolyzed functional groups forming in hyperalkaline conditions. The spectra of UP2W equilibrated in $Ca(OH)_2$-buffered media at T = 22 °C showed that the nitrile signal at 2239 cm^{-1} decreased significantly compared to the original PAN material, supporting the significant progress of the hydrolysis process. Moreover, signals corresponding to carboxamide and carboxylate functional groups appeared along with $Ca(OH)_2$ and CO_3^{2-}, from which the manifestation of the $Ca(OH)_2$ signal was attributed to the insufficient washing of the degrading material. The observation of the CO_3^{2-} signal was attributed to the characterization conducted under air atmosphere. Tasi and co-workers [84] proposed that the observation of carboxamide and carboxylate functional groups is most likely related to the formation of Ca-carboxamide/carboxylate complexes. In NaOH systems, the main peak of the PAN nitrile groups decreased gradually with increasing NaOH concentration, according to 0.03 M (pH = 12.5) < 0.1 M < 1.0 M. However, the peak of the PAN nitrile groups remained after a long degradation process (t ≈ 2 a), although with clearly lower intensities. From these observations, the authors deduced that hydrolysis is more pronounced in $Ca(OH)_2$ than in NaOH environment. This hypothesis was further supported by TG-DSC analysis. The thermograms showed the exothermic signal of nitrile groups at T = 200 – 300 °C. This exothermic signal is associated to the cyclization of vicinial nitrile groups resulting in a conjugated polyimine-structure [78, 85, 86]. It was concluded that this specific peak cannot be detected in portlandite buffered system, whilst in NaOH solution, these functional groups are still on the polymer chain.

The study by Tasi and co-workers at KIT-INE underpins that the dissolution of the UP2W filter-aid is more pronounced in NaOH solutions than $Ca(OH)_2$-buffered solutions. The weak influence in portlandite-buffered media can be attributed to the hindering effect of the Ca(II)

during the chain scission on the polymer. Regarding the formation of Ca(II) complexes with the carboxamide / carboxylic functional groups, the electron density would be with high plausibility decreased, with eventually results in less intensive dissolution in $Ca(OH)_2$–buffered systems than in NaOH.

The proxy ligands proposed to represent the degradation products of the PAN-based UP2W material, *i.e.* GTA, HIBA and HBA have been considered in this PhD thesis to evaluate the impact of the degradation products (see Section 1.3.3) on the solubility and sorption of key radionuclides such as Ni(II), Nd(III)/Eu(III) and Pu(III/IV).

1.4 Overview of chosen radionuclides and some organic ligands behaviour under cementitious environment

This section is dedicated to the systems M(II/III/IV)-cement (Ni(II), Eu(III) and Pu(III/IV)) and some selected small molecular weight organic ligand / cement interactions in the binary system. The available data with di-, tri- and tetravalent metals with the interaction of cement are discussed in detail. Despite the lack of investigations dealing with the ternary system cement-RN-UP2W degradation products, several studies have targeted other families of organic compounds, which are reviewed in the Section 1.4.3.

1.4.1 Main aspects of organic ligands sorption onto cementitious materials

Key processes controlling the (free) concentration of the organic compounds in the porewater under cementitious environment can be classified as:

(i) Reaction with other components of the aqueous phase (complexation with metal ions, precipitation etc.)
(ii) Degradation reactions (chemical or microbial)
(iii) Reactions with hydrated cement phases, *e.g.* sorption via chemi- or physisorption, or surface precipitation etc.

Sorption phenomena are often quantitatively described by means of the distribution ratio (R_d, expressed in $m^3 \cdot kg^{-1}$ or $dm^3 \cdot kg^{-1}$). It refers to the partitioning of the species between the solid phase (cement, mineral phases, etc.) and liquid phase (cement porewater, groundwater, etc.) [14]:

$$R_d = (C_{ads}/C_{aq}) \quad (1)$$

where the C_{ads} is the sorbed material on the solid phase ($mol \cdot kg^{-1}$ or $mol \cdot g^{-1}$), C_{aq} is the concentration of the material in aqueous phase ($mol \cdot dm^{-3}$ or $mol \cdot dm^{-3}$).

Over the years various reports on the uptake of organic compounds by cement, boom-clay, bitumen etc. have been published. Wieland *et* al. [87] investigated the sorption of methanol, ethanol, formaldehyde, acetaldehyde, formic and acetic acid on sulphate-resisting Portland cement (CEM I) at pH = 12.5 – 13.3 under inert atmosphere within the timeframe 1 h to 390 d. The experiments indicated that after 390 days, the concentration of Ca(II) increased from 4 mM to 59 mM, altering the pH from 13.3 to 12.5. This phenomenon was related to the dissolution of portlandite caused by high concentration of formate and acetate. Nevertheless, the report emphasized that the organic molecules have only minor impact on the mineral composition of the cement paste.

Miyashita and co-workers [88] conducted adsorption experiments using calcite and aragonite as sorbent at pH ≤ 10. The organic molecules of oxalic, malonic and glutaric acids were utilized in order to understand how dicarboxylic acids sorb on the solid minerals surface when the carbon number in their homologous series is increased. Generally, the organic molecules with two carboxylic functional groups have a certain tendency to form chelate complexes. The authors found that the adsorption affinity of the 3 acids decreased in the order: oxalic acid

> malonic acid > glutaric acid, thus pointing to a higher stability of surface complexes for organic ligands with shorter carbon chains.

The sorption of ISA on cementitious materials has been studied extensively in the literature [26, 89]. PSI research group dedicated huge efforts to depict ISA sorption behaviour on CEM I hardened cement paste (CPA 55 HTS cement). Van Loon and co-workers [89] applied artificial cement pore water (ACW) containing the concentration of 0.114 M Na, 0.18 M K and $2 \cdot 10^{-3}$ M Ca, with a pH = 13.4. The uptake experiments were performed in N_2 atmosphere with ISA concentration ranging between 10^{-5} and 0.3 M at S:L = 25 and 500 $g \cdot dm^{-3}$ and centrifugation and filtration with 0.45 μm membrane filter to separate the solid and liquid phase properly. It was concluded that the equilibrium was reached after 1 day of contact time. The concentration of sorbed organic molecules on the cement matrix ($[Lig]_{ads}$ ($mol \cdot kg^{-1}$)) was determined according to Equation (2).

$$[Lig]_{ads} = ([Lig]_{in} - [Lig]_{aq}) \cdot V(porewater,\ dm^3) \cdot m(cement,\ kg)^{-1} \quad (2)$$

Following the sorption of the ISA on the solid phase, initially, the authors suggested the implementation of a one-site Langmuir isotherm (Equation (3)) because this was the simplest way for describing the uptake of the ISA. However, this attempt failed, and the authors finally fit their data using a two-site Langmuir isotherm (Equation (4)) [89].

$$[Lig]_{ads} = K \cdot q \cdot [Lig]_{aq} \cdot (1 + K \cdot [Lig]_{aq})^{-1} \quad (3)$$

$$[Lig]_{ads} = K_1 \cdot q_1 \cdot [Lig]_{aq} \cdot (1 + K_1 \cdot [Lig]_{aq})^{-1} + K_2 \cdot q_2 \cdot [Lig]_{aq} \cdot (1 + K_2 \cdot [Lig]_{aq})^{-1} \quad (4)$$

where q, q_1 and q_2 are the theoretical maximum binding capacity of binding sites of cement for the uptake of the ligand ($mol \cdot kg^{-1}$) and K, K_1 and K_2 are the adsorption affinity constant ($dm^3 \cdot mol^{-1}$) in one (Equation (3)) and two sorption sites (Equation (4)).

A fundamental factor, which influences the sorption of the organic ligands on cement, is the electrostatic charge on the surface of the cement. Under alkaline conditions, these organic molecules become negatively charged due to deprotonation of the organic functional groups (*e.g.* carboxylic, hydroxyl), which can interact with the cement surface [6].

The parameter often used to assess the surface charge is the zeta potential (ζ). This value represents the electrical potential that is generated at the interface between solid surface and liquid phase. It is usually affected by the chemical composition of solvent, ionic strength, temperature, ionic species and the charge of these species. It is well-known that negatively

charged solid phases do not adsorb high amounts of organic ligands containing negatively charged functional groups, in contrast with positively charged surfaces [71, 90, 91]. In the report of Viallis-Terrisse and co-workers [92], the alteration of zeta-potential in C-S-H as a function of $Ca(OH)_2$ concentration was monitored. This experiment confirmed that the Ca(II) level in the systems governs the electrical potential of the double layer of the interface. At pH = 10 – 11, the silica layer owing to deprotonation of silanols (>SO^-) remains overall negatively charged, but as the Ca(II) concentration reached 2 mM, the zeta potential becomes neutral, indicating the point of zero charge, also known as isoelectric point (IEP) of the system. Moreover, the cement at pH = 12 – 12.5 and $[Ca]_{tot} \approx 22$ mM shows a positive surface charge maximum. Above this pH (*e.g.* in the degradation stage I of cement), the surface charge was inversed back to negative due to the increase of hydroxyl groups, which neutralize the positively charged surface in the diffuse layer. This hypothesis was supported by the study of Pointeau and co-workers [71]. In this work, the electrophoretic mobility of colloidal cement particles was determined for Ordinary Portland cement (OPC) in CEM I and OPC with blast furnace slag and fly ash in CEM V. Throughout the measurement, the following stages have been documented: (i) the ζ potential was increased from –17 to +20 mV as the pH dropped from 13.2 to 12.6 and as the Ca(II) concentration raised from $1.1 \cdot 10^{-3}$ to $2 \cdot 10^{-2}$ M. (ii) Afterwards, the ζ potential of the cement particles started decreasing from +20 to –8 mV from pH = 12.6 to 11.0 during the degradation of HCP parallel with the decrease of Ca(II) concentration from $2 \cdot 10^{-2}$ to $4 \cdot 10^{-4}$ M.

In connection with the binding characterization of the OPC (CEM I and CEM V), Pointeau *et* al. studied the sorption of ISA and EDTA with different anionic species (Cl^-, I^-, SeO_3^{2-} and CO_3^{2-}) [93]. From the sorption experiment, the authors calculated the R_d of EDTA ($(1.7 \pm 0.4) \cdot 10^{-4}$ and $(1.1 \pm 0.6) \cdot 10^{-2}$ $m^3 \cdot kg^{-1}$ for pH 13.2 and 11.9) and ISA ($(5 \pm 2) \cdot 10^{-3}$ and $(6.1 \pm 2.1) \cdot 10^{-2}$ $m^3 \cdot kg^{-1}$ for pH 13.2 and 11.9), respectively. These R_d values are lower than measured on degradation stage II cement reported by other researchers [94]. These measurements pointed out that the Ca(II) content within cementitious systems strongly affects the ζ potential (also in connection with the pH), and thereby the uptake of anionic species.

1.4.2 Overview of experimental studies on the cement-M(II)/Ln(III)/An(III/IV) systems.

The quantitative assessment of radionuclide sorption on different cement type surfaces is often described in terms of distribution ratio, as explained in Section 1.4.1, Equation (1). The

uptake or sorption of the radionuclides and therefore the R_d values can be defined by several processes:

1. Adsorption on the free surfaces (adsorption or chemisorption)
2. Precipitation, co-precipitation or surface precipitation (forming new pure solid phase)
3. Solid-solution formation (lattice integration into the cement mineral)
4. Ion-exchange on the surface functional groups

The distribution ratio (R_d) corresponds to the distribution coefficient (K_d) if the precipitation is disregarded from the sorption process. [14, 95]. The uptake of metal cations can proceed in two ways: (i) electrostatic interaction / outer-sphere surface complexation, (ii) surface complexation / inner sphere surface complexation.

In general, the sorption data available in the literature shows clear deficiencies in the understanding of the retention processes at the atomistic scale [95].

The retention of the radionuclides by HCP is affected as well by the degradation stage of cement, the interaction of Cement-Ligand (see Section 1.4.1) and the oxidation state of the radionuclide.

1.4.2.1 Cement-Ni(II) system

Radioactive isotopes of Ni (^{59}Ni and ^{63}Ni) are expected in waste streams to be disposed in repositories for L/ILW. Due to the long half-life of ^{59}Ni ($t_{1/2} = 7.6 \cdot 10^4$ a), it is crucial to properly assess their retention properties in cementitious environments. Several publications have been reported, focusing on the interactions of Ni and cement [96-98]. Noshita *et* al. [99] examined the sorption of four radionuclides on various cement hydrates (*i.e.* brucite, portlandite, tobermorite, C-S-H etc.) in repository conditions of pH = 12.6, T = 298 K, E_h = -600 mV, $CO_3^{2-} = 1.35 \cdot 10^{-4}$ M. The experiments were performed either in NaOH or $Ca(OH)_2$ solutions (unknown concentration) at pH = 12.6, containing 3 g amount of solid phase. The initial concentration of Ni was set to 10^{-8} M. The authors reported the distribution ratios of Ni(II) in NaOH and $Ca(OH)_2$ solutions of 5500 and 3600 $mL \cdot g^{-1}$, respectively. Primarily, it was understood that the sorption of $Ni(OH)_2$ on C-S-H depends on the Ca/Si ratio. The authors proposed two main mechanisms for the retention of Ni by portlandite:

1: Co-precipitation

$n[Ca(OH)_2] + Ni(OH)_2(aq) \rightarrow Ca_nNi(OH)_{2n+2}$

2: Surface complexation

$n[Ca(OH)_2] + Ni(OH)_2(aq) \rightarrow [Ca(OH)_2]_{n-1} \cdot [Ca(OH)_2]_{surface} \cdot Ni(OH)_2$.

Several investigation in the literature indicated that the uptake of Ni(II) is rather solubility-limit controlled in alkaline cementitious system at $[Ni]_{tot} \geq 10^{-8}$ M. The first confirmation was described by Scheidegger and co-workers [100] using various spectroscopy methods. They applied X-ray absorption fine structure (XAS) and diffuse reflectance spectroscopy (DRS) on Portland cement (CPA 55 HTS, Lafarge, France). Ni sorption experiments were carried out by adding aliquots of 0.1 M $Ni(NO_3)_2 \cdot 6H_2O$ solution in artificial cement porewater (concentration of Ni was not given) under alkaline condition of pH = 13.3 in N_2 atmosphere and at S.L = 25 $g \cdot dm^{-3}$. After 150 days of end-over-end sample shaking and centrifugation of the suspensions, the solid pastes were characterized. It was deduced from the assessment that the formation of Ni- and Al-containing hydrotalcite-like layered double-hydroxide (LDH) formulated as $[M^{II}_{1-x}M^{III}_x(OH)_2]^{x+}(A^{n-})_{x/n} \cdot yH_2O$ (M^{II} and M^{III} define the divalent cations *i.e.* Ni(II) and trivalent cations *i.e.* Al(III), whereas (A^{n-}) the various type of anions *e.g.* Cl^-, CO_3^{2-}, SO_4^{2-} and NO_3^-) is responsible maybe not only for immobilization of Ni(II), but probably other di- (*i.e.* Zn(II), Co(II)) and trivalent (*i.e.* Fe(III)) cations in ambient and inert conditions, of which the latter occurs inside the multibarrier repository system. The authors proposed that Ni-Al LDHs and not Ni-hydroxides determine the solubility of Ni in cement materials [100].

On the basis of this information, Wieland and Van Loon [101] investigated the retention of nickel by HCP at variable S:L ratios. The results displayed that the Ni(II) concentration in the range of $5 \cdot 10^{-8} \leq ([Ni]_{in} / M) \leq 2 \cdot 10^{-7}$ remained constant in the aqueous phase regardless of the variable S:L ratio. This can be attributed to the Ni content in the solid cement phase that could dissolve in the liquid phase. This supported the idea that the distribution of Ni could be controlled by the solubility-limiting process, as highlighted by Scheidegger *et* al. [100]. Continuing this train of thought, Wieland *et* al. [102] monitored the ^{63}Ni uptake by HCP in artificial porewater at pH = 13.3 and solid-to-liquid in the range of $10^{-6} - 0.13$ $kg \cdot dm^{-3}$. The study revealed that the uptake at S:L ratio of $2.5 \cdot 10^{-2}$ $kg \cdot dm^{-3}$ was reached in less than 7 days, showing fast kinetics of ^{63}Ni uptake. Although several studies suggested in the past that the sorption can be described as surface binding of Ni on HCP [103, 104], Wieland *et* al. [102] proved that there could be another mechanism in case of ^{63}Ni, namely isotopic exchange between liquid phase ^{63}Ni and natural Ni in the cement phase. This process was specified in the terms of the partition coefficient (α / *dimensionless*), expressed in the Equation (6):

$$\alpha = (n_{s,M^*}/n_{s,M}) / (n_{l,M^*}/n_{l,M}) = R_{d,M^*} / R_{d,M} \quad (6)$$

where n_{s,M^*} and $n_{s,M}$ are the mole number of radioactive ^{63}Ni and non-radioactive Ni in cement paste, whereas n_{l,M^*} and $n_{l,M}$ corresponding to the mole number in liquid phase, which allow the calculation of distribution ratios of active (R_{d,M^*}) and natural ($R_{d,M}$) nickel (in $dm^3\ kg^{-1}$ or $m^3\ kg^{-1}$). The experimental results indicated that the partition coefficient (α) values remained in the range of $(2.8 \pm 0.6)\cdot10^{-2}$ and $(4.5 \pm 1.0)\cdot10^{-2}$, which implied that at most 4.5 ± 1.0 % of the Ni inventory in pristine cement is accessible to isotopic exchange.

Recent literature has emphasized the relevance of C-S-H phases in the uptake of Ni(II) in hyperalkaline system. Missana and co-workers [105] studied the retention of ^{63}Ni in $5\cdot10^{-10}$ M ≤ $[Ni]_{tot}$ ≤ $5\cdot10^{-4}$ M concentration range (in the form of $NiCl_2$) by C-S-H phases with Ca/Si ratios of 0.8 to 1.6 and S:L = 1 and 10 $g\cdot dm^{-3}$ under N_2 atmosphere. In order to obtain higher Ni concentration than 10^{-8} M, stable $NiCl_2$ was applied. The authors observed that the uptake of Ni explicitly depends on the Ca/Si ratio, and modelled their observations in terms of surface complexation applying electrostatic double layer model. Nickel adsorption tended to decrease as the Ca/Si ratio increased, especially when Ca/Si was < 1.2, and then Ca/Si becomes less relevant. It was elucidated that the deprotonated silanol groups (>SiO^-) were good binding sites for Ni(II) on the cement surface. The adsorption region was limited to low final aqueous Ni concentrations (< $5\cdot10^{-8}$ M), and when the Ni concentration exceeded this limit, an increase in the distribution coefficient (K_d) was observed, which could be related to precipitation processes. Hence, next to the isotopic exchange of ^{63}Ni with inactive Ni(II) inside the cement represented by Wieland and co-workers [102] and the incorporation of inactive Ni(II) on LDH solid phase, the surface complexation onto C-S-H phases should be considered as well as mechanism for the uptake of Ni(II) by HCP.

1.4.2.2 Cement-Eu(III) system

The uptake of europium by cement has been extensively studied in the literature under repository relevant conditions [101, 106-108].

Pointeau and co-workers [109] studied the retention of Eu(III) by C-S-H phases, and investigated the retention mechanism utilizing various types of characterization methods *e.g.* XRD, XPS, TRLFS and SEM-EDX. TRLFS pointed to two main sorption sites corresponding to different coordination environments. The first type of C-S-H-Eu(III) species was

characterized by a long life-time (≈ 1 ms), was attributed to a large fraction of Eu(III) being incorporated into the C-S-H structure at Ca/Si ratio of 0.83 via the substitution of Ca. The second species was characterized by a shorter life-time (≈ 0.4 ms), and Eu(III) was found in a highly hydroxylated environment, though less that in europium hydroxide. This second species might be associated to the formation of surface complexes.

A detailed investigation of the uptake of Eu(III) by cement materials was performed by Schlegel and co-workers [110]. They used C-S-H phases with Ca/Si ratios of 1.3, 1.0 and 0.7, and used EXAFS to gain insight on the molecular environment of Eu. During the experiments, the authors realized that the sorption of Eu(III) was taken place in general by co-precipitation with solution containing Ca and Si to generate a mixed hydroxide phase and by diffusion within the hydrated interlayer of C-S-H phase.

Mandaliev and co-workers [111] monitored the sorption of Ln(III) on 11 Å tobermorite and xonolite as crystal analogues of C-S-H phases, providing structural insights by means of TRLFS and EXAFS. All the experiments were performed in N_2 atmosphere and at room temperature (T = (298.15 ± 3) K) using small volume of 10^{-3} M Eu(III) stock solution, either at 5 g·dm^{-3} (TRFLS) and 50 g·dm^{-3} (EXAFS) S:L ratio until 570 days. Mandaliev *et* al. aimed to reach Eu(III) concentration of 0.4 – 7 μmol/g and 7 – 35 μmol/g on solid phase for TRLFS and EXAFS, respectively. After 1 day, Eu(III) was predominantly sorbed on the external surface of the two solid phases through inner-sphere complexes. The incorporation of the Eu(III) into the lattice of the solid phase in both cases took place via the substitution of Ca by Eu, which is the thermodynamically favorable process in long term.

In 1997, Wieland and co-workers [108] monitored the ^{152}Eu and ^{234}Th sorption on the sulphate-resistant Portland cement at S:L ratio of 10^{-5} and 10^{-4} kg·dm^{-3} and pH =13.3 in the time-frame of 130 days. All the measurements were conducted under N_2 atmosphere in ACW with the concentrations of K, Na and Ca of 0.18, 0.114 and $1.7 \cdot 10^{-3}$ M, respectively. The experimental results without the ISA indicated that the distribution ratio in both nuclides were in the range of $10^3 – 10^4$ m^3·kg^{-1}. Also, in both systems, the equilibrium was reached in less than two days, which led the authors to conclude that the processes are adsorption-controlled.

Tits *et* al. studied the interaction of C-S-H phases with ^{152}Eu and ^{248}Cm [112]. The pH of the artificial pore water was set to 13.3, and the batch experiments were performed at 25 °C under N_2 atmosphere inside the glove-box. Utilizing two batch experiments at S:L ratio of $3.8 \cdot 10^{-4}$ and $5.4 \cdot 10^{-4}$ kg·dm^{-3}, and Eu(III) total concentration of $2 \cdot 10^{-9}$ M, the authors determined R_d = $(6.0 \pm 3) \cdot 10^5$ dm^3 kg^{-1}. Moreover, it was observed that the steady state was achieved within 1 day and maintained after 90 days, showing the fast equilibria on the uptake of Eu(III) by

cement, which supports the hypothesis raised in [108]. The authors identified that insufficient phase separation in sorption experiments with trivalent actinides and lanthanides could have a relevant impact on the measured An(III) and Ln(III) concentration in liquid phase as a consequence of the presence of colloids, and accordingly in the distribution ratios [112, 113].

1.4.2.3 Cement-Pu(III/IV) system

Although limited data on the cement-Pu(III) are available in the literature, the An(IV) (including also a few studies on Pu(IV)) have been examined over the years thoroughly [34, 95, 114]. The most comprehensive publication was recently prepared by Ochs *et* al. [34]. Ochs and co-workers summarized the literature about the Pu sorption data along with other radionuclides in cementitious environment (CEM I and CEM V HCP, OPC, Ettringite, C-S-H etc.) in the context of stage I–III cement degradation phases. They also included vital experimental parameters, for instance regarding colloid formation, redox conditions, precipitation, used filtration methods, etc. From the results, the authors provided R_d values of Pu(IV) sorption in stage I to III cement degradation phases, *i.e.* $10 - 1000$ $m^3 \cdot kg^{-1}$. These values are in line with the values previously recommended by Wieland in the context of the PSI-Nagra sorption database [95].

Rojo and co-workers [115] investigated the retention of Pu(IV) and Tc(IV) on Portland cement (CEM I 42.5R/SR, particle size < 1 mm) at pH ≈ 12.45 in the absence and in the presence of ISA under anaerobic conditions (N_2 atmosphere). Batch sorption experiments for binary and ternary systems were conducted at S:L = 20 $g \cdot dm^{-3}$, and the concentration of ^{238}Pu in the liquid phase was measured after centrifugation at 14400 rpm for 45 min. From the sorption kinetics investigation on the Pu-cement system, it was concluded that 7 days were enough for reaching the equilibrium. Under these conditions, the authors reported a strong sorption with $\log (R_d / dm^3 \cdot kg^{-1}) = (5.1 \pm 0.1)$.

Häußler *et* al. [116] studied the uptake of actinides (Am(III), Th(IV), U(VI), Np(V) and Pu(III), at $[An]_0 = 10^{-7}$ and 10^{-8} M by C-S-H phases with S:L = $0.5 - 20.0$ $g \cdot dm^{-3}$ and pH = $12 - 13$. The oxidation state of Pu(III) was monitored by HR-XANES. Pu(III) was generated by electrochemical reduction of a Pu(VI) stock solution [117], but no redox buffers were used to stabilize this oxidation state over time. Phase separation was achieved by ultracentrifugation at 108800 g for 1 hour. The experiments indicated that after 3 days, the R_d value of Pu(III) was around $2 \cdot 10^5$ $dm^3 \cdot kg^{-1}$, which is in good agreement with data reported for Eu(III) and Am(III) in the literature. However, the E_h values and HR-XANES measurement displayed that Pu(III) oxidized to Pu(IV) in the investigated conditions.

In contrast to the redox sensitivity of Pu(III), Pu(IV) displays high stability under cementitious and anaerobic conditions. It was reported for the uptake of Pu(IV) by cement in the degradation stages II and III is the strongest [34], although a large dispersion is also reported between pH = 12 – 12.6. Many authors have investigated the retention of Pu(IV) using different filtration cut-off sizes (0.45 μm, 30000 Da MWCO filters) [118-120]. Reports underlined that the gained R_d values were way lower without employment of appropriate filtration methods.

Regarding the application of different filtration methods and their effect on the uptake processes, Baston and co-workers examined their impact on the uptake of plutonium on concrete, mortar, sand/bentonite, tuff, sandstone and soil in the pH range of 8 – 12.5, where the concrete and mortar were derived from OPC [121]. The whole experiment was conducted in N_2 atmosphere with the radionuclide concentration of $4 \cdot 10^{-11}$ M ≤ $[^{236}Pu]_{in}$ ≤ $8 \cdot 10^{-11}$ M and at S:L ratios of 20 and 200 g·dm^{-3}. In the framework of OPC based concrete and mortar, the solid materials were crushed, sieved (< 250 μm), and mixed with porewater solutions, which resulted batch suspensions at pH = 12.4 containing [Ca] = 8 mM or pH = 12.2 containing [Ca] = 2 mM, respectively. The article gave no hint about the redox conditions of Pu or any applied redox agent used during the experiment, but it could be presumed in accordance with previous reports by the same authors that Pu(IV) was the predominant oxidation state in the aqueous phase. Each sample was systematically centrifuged for 30 minutes at 1500 g and filtrated by 0.45 μm "Millex HV" filters and 30000 MWCO filters. The R_d values of the radionuclide at S:L = 20 g·dm^{-3} on concrete were $(1.4 \pm 0.4) \cdot 10^6$ dm^3·kg^{-1}, and ≈ $(3.4 \pm 1.6) \cdot 10^6$ dm^3·kg^{-1} with the use of 0.45 μm and 30000 MWCO, whilst on mortar these values were R_d >·10^6 dm^3·kg^{-1} and $(1 – 3) \cdot 10^6$ dm^3·kg^{-1} with the same filtration materials, respectively, which are higher values than in former studies. The uptake of plutonium was simulated via a diffuse layer model (DLM) with combination to a surface complexation model. Since in cement degradation stage II phase the calcium concentration is substantially high in the cementitious system, the authors underlined that the surface of C-S-H silanol groups is saturated with the Ca(II) to form different type of surface species, *i.e.* ≡SiOCaOH or ≡Si(OCa)$_2$OH. In this context, the authors proposed that surface complexes involving Ca(II) and Pu(IV) occurred, *e.g.* >SiOH + 2 Ca^{2+} + Pu^{4+} + 6 H_2O ⇌ >Si(OCa)$_2$OH$PuO_2(OH)_2$ + e^- + 9 H^+. The uptake of Pu(IV) determined by Baston and co-workers [121] was higher with the application of filtration methods, which hints towards the possible presence of colloidal particles in the investigated conditions.

Tasi *et* al. [94] investigated the sorption of Pu by Portland cement in the degradation stage II. Experiments were performed under Ar atmosphere and in redox-buffered systems in the presence of HQ, Sn(II) and $Na_2S_2O_4$. The experiments were implemented at log ($[Pu]_{tot}$ /M) = –8.3 and S:L ratio of 0.1 to 50 g·dm^{-3} using 10 kD filters (4020 g, 15 min) and ultracentrifugation (694000 g, 1 h). The authors reported log ($R_{d,in}$ /dm^{-3}·kg^{-1}) = (6.3 ± 0.6), which is relatively in good agreement with other results mentioned above.

1.4.3 Literature review of cement-M(II)/Ln(III)/An(III/IV)-ligand systems

Organic ligands, originated not only from hazardous waste but also contained in the cement itself, may alter the sorption of radionuclides in cementitious environments. In general, the following reactions within cement-radionuclide-organic ligands system(s) can occur [14, 95]:

1. Radionuclide-ligand complex formation
2. Complex formation of cement-radionuclide-organic ligands
3. Precipitation of radionuclides in the presence of organic ligands
4. Surface sorption or precipitation of organic ligands on the mineral-water interfaces
5. Competitive and non-competitive sorption interaction with the organic ligands on the accessible surface site
6. Ion-exchange reactions between the radionuclides and the cations on the mineral surface.

Although the examination and monitoring of ternary complex systems are crucial, only limited reports have dealt with the sorption of di-, tri- and tetravalent cations in the present of water soluble organic molecules containing functional groups with oxygen atom(s) *i.e.* carboxylic or alcoholic groups on cement [14]. Indeed, most of the available studies have targeted ISA and GLU as organic ligands affecting the sorption of radionuclides.

1.4.3.1 Cement-Ni(II)-Ligand system

Van Loon *et* al. [122] probed the effect of α- and β-ISA and degradation products of cellulose materials *e.g.* Aldrich cellulose, Tela tissue, cotton and recycling paper on Ni(II) sorption onto feldspar (particle size d < 63 μm) in artificial cementitious pore water (ACW) containing 0.114 M Na, 0.18 M K and $2.3 \cdot 10^{-3}$ M Ca (pH = 13.3) under N_2 atmosphere and T = (25 ± 2) °C. All the systems were prepared at S:L ≈ 17 $g \cdot dm^{-3}$, 10^{-6} M ≤ $[Lig]_{tot} \leq 10^{-1}$ M and $[^{63}Ni]_{tot} = 3 \cdot 10^{-10}$ M following the order of addition of individual components (Cement + Ligand) + ^{63}Ni. The suspension was equilibrated for 24 h, and then ultracentrifuged for 15 minutes at 27000 g, with the activity of the solutions being measured by LSC. During the analysis of the batch solutions, the uptake of the ^{63}Ni in the presence of ISA, solutions containing degradation products of Aldrich cellulose (DP1) and other cellulose materials (DP2) decreased at [ISA] ≥ 10^{-2} M, [DP1] ≥ 10^{-3} M and [DP2] ≥ 10^{-6} M, respectively. The authors proposed that the more pronounced effect in the Ni retention can be attributed to the fact that the degradation products include other organic molecules with multiple functionalities, which are able to form more stable complexes than ISA itself.

A thorough investigation of ^{63}Ni (along with ^{137}Cs, ^{147}Pm and ^{234}Th) sorption onto cement in the presence of organic ligands was conducted by Holgersson and co-workers [103]. The main objective of this report was to determine the sorption of radionuclides onto crushed cement and their diffusion properties using 2 cm thick concrete disk in N_2 atmosphere, in both cases in the presence of cellulose degradation products. The main degradation product of cellulose was identified as D-gluco-isosaccharinate. The authors generated three types of synthetic organic solutions in pore water: 5 mM ISA, leachate of cellulose powder at 5 $kg \cdot m^{-3}$ and 100 $kg \cdot m^{-3}$. The two latter were equivalent to ISA concentrations of 3 mM and 27 mM, respectively. After 2 months of experiments, the R_d in batch samples of Th and Pm were significantly decreased in ISA media from 10 – 40 $m^3 \cdot kg^{-1}$ to $4 \cdot 10^{-3} – 5 \cdot 10^{-2}$ $m^3 \cdot kg^{-1}$, whereas Cs and Ni remained in the range of $10^{-3} – 0.04$ $m^3 \cdot kg^{-1}$. This observation suggests that ISA has only a weak impact on the sorption of Ni(II).

Under similar boundary conditions, Bruno *et* al. [123] conducted Ni(II) sorption experiments with CEM I 42.5NBV/SR/LA type SKB ordinary Portland cement (d_{av} < 100 μm) in the presence of ISA. The authors applied the following order of addition of the individual components under Ar atmosphere (O_2 < 5 ppm, T = (22 ± 2) °C): (i) (Cement + Ni) + ISA, (ii) (Cement + ISA) + Ni and (iii) (ISA + Ni) + Cement. In all cases, the S:L ratio was 25 $g \cdot dm^{-3}$ and pH = 12.5, with $[^{63}Ni]_{in} = 2.83 \cdot 10^{-10}$ $mol \cdot dm^{-3}$, which is lower than the solubility limit of

Ni(II) at this pH. The solid phase was separated from liquid phase through centrifugation, then aliquots of supernatant filtered with 10 kD filters and the concentration of ^{63}Ni was measured by LSC. Experiments showed that ISA had a greater impact on the Ni sorption on HCP in the order of addition of (ii). At [ISA] ≈ 0.1 M, the uptake of Ni in (i) decreased 75 %, whilst in (iii) almost 100 %. A similar effect was reported by Tasi and co-workers for the cement-Pu-ISA system [94]. The outcome of the desorption experiments reflected similar findings with the study of Van Loon *et* al. [122], *e.g.* decrease in the Ni(II) retention at high ligand concentrations, *i.e.* [ISA] ≥ 10^{-2} M.

Tasdigh conducted batch sorption experiments with Ni under N_2 atmosphere, (1 ≤ (S:L /g·dm^{-3}) ≤ 5) and using UP2W degradation leachates obtained in artificial cement pore water at pH = 12.5 and 13.5, both at room temperature (T = 24 °C) and T = 60 °C. For simulating the effect of the DP on the Ni sorption process, the UP2W organic molecules decomposed in LCPW at ambient room temperature after 6 months of degradation were applied in following the order of addition of (DP + Ni) + Cement. Even though no description was provided of the initial concentration of Ni in the suspensions, the organic fragments of UP2W filter decreased considerably the retention of the radionuclide at S:L = 1 g·dm^{-3} from log (Q_d /m^3·kg^{-1}) 1.8 to 0.6, whereas at higher S:L (≥ 2 g·dm^{-3}), this reduction was approximately a factor of 2 (from log Q_d = 0.4 – 0.6 to 0.1 – 0.3 m^3·kg^{-1}). Consequently, these findings pointed out, that the DP induce only a weak decrease on the uptake of Ni by HCP [16].

1.4.3.2 Cement-Eu(III)-Ligand system

As highlighted in Section 1.4.2.2, Wieland *et* al. investigated the uptake of Eu(III) (and Th(IV)) by sulphate-resistant Portland cement in the presence of ISA [108]. It was apparent that ISA impacts the uptake of Eu(III) at $[ISA]_{tot} \geq 10^{-2}$ M. Besides, Eu(III) is likely complexed with ISA with a stoichiometry of 1:1 under the investigated conditions. Similar complexes and sorption behaviour are expected for other lanthanides and actinides with same oxidation state.

Vercammen [49] investigated the impact of ISA on retention of tri- and tetravalent lanthanides and actinides by feldspar under hyperalkaline conditions in the absence and presence of Ca. The latter conditions resemble those of cementitious environments. A decrease of the Eu(III) sorption was observed at [ISA] ≥ 10^{-6} M both in the absence and presence of Ca, which led the authors to conclude that 1:1 binary complexes without involving Ca prevail in the investigated conditions.

Van Loon and co-workers conducted experiments to assess the impact of α- and β-ISA, as well as degradation products of cellulose materials on the uptake of Eu(III) by feldspar at pH = 13.3 [122]. Batch experiments were performed at S:L = 0.4 g·dm^{-3}, 10^{-6} M ≤ [Lig] ≤ 10^{-1} M and $[^{152}Eu]_{tot}$ = $6.7 \cdot 10^{-10}$ M following the order of addition of individual components (Cement + ^{152}Eu) + Ligand. After phase separation by ultracentrifugation (15 minutes, 27000 g), an aliquot of the sample was characterized by γ-counting. Thermodynamic modelling of the obtained results suggests the formation of Eu(III)-ISA complexes with stoichiometry 1:1, which is in good agreement with the assumption stated in the previous studies [49, 108]. The impact on the Eu(III) sorption was more relevant for α-ISA (effect observed at [ISA] ≥ 10^{-4} M) than β-ISA (effect observed at [ISA] ≥ 10^{-2} M), emphasizing the relevant role of the organic molecule's structure / isomer. On the other hand, the effect of degraded cellulose materials was even more relevant, with an effect on the sorption observed at an equivalent of [Lig] ≥ 10^{-6} M.

Tits and co-workers studied Eu(III) sorption on calcite in hyperalkaline conditions (pH = 13.3) in ISA and GLU solutions at $4 \cdot 10^{-4}$ ≤ (S:L /g·dm^{-3}) ≤ $4 \cdot 10^{-3}$, using of $[Eu]_{tot}$ = 10^{-9} M, $3 \cdot 10^{-6}$ ≤ ($[ISA]_{tot}$ /M) ≤ $7 \cdot 10^{-2}$ and 10^{-7} ≤ ($[GLU]_{tot}$ /M) ≤ 10^{-4} [124]. A clear effect of ISA on the sorption was detected at $[ISA]_{tot}$ ≥ 10^{-5} M, whereas the drop in R_d values in the presence of GLU occurred already at $[GLU]_{tot}$ ≥ 10^{-7} M. The R_d values in the absence of these organic compounds ($10^5 – 10^6$ dm^3·kg^{-1}) were decreased at most 2 – 3 orders of magnitude as the ligand concentration was increased.

Diesen and co-workers conducted Eu(III) sorption experiments on Portland cement in the degradation stage II (pH = 12.5) in the presence of cellulose degradation products [125]. The batch sorption experiments were conducted under N_2 atmosphere with artificial pore water (5 g $Ca(OH)_2$ in 1 L Milli-Q water) and cellulose degradation leachates. The cement material used was crushed and sieved (d_{av} = 63 – 125 μm), and mixed with the artificial pore water at S:L ratios of 0.7 and 3.3 g·dm^{-3}. Solutions were filtered through 0.2 μm cellulose acetate membrane filters to exclude any solid phase or colloid. The authors gave no description of the initial concentration of Eu(III) or any distribution ratio value for the sorption experiments. The comparison of Eu(III) surface coverage in the presence of degradation products (< 0.03 molecules/nm^2) with the coverage in the absence of degradation products (1.4 molecules/nm^2), allowed to obtain a quantitative insight on the effect of such degradation products on the retention of Eu(III). In line with previous observations, the adsorption of Eu(III) is less efficient in the presence of degradation leachates due to the formation of stable complexes in the aqueous phase.

Reports on the effect of UP2W degradation products on the uptake of Eu(III) by HCP are limited. Dario and co-workers [106] examined the uptake of ^{152}Eu by Standard Portland cement and TiO_2 at 1 g·dm^{-3} S:L ratio with/without additional 2 mM Ca(II) in the presence of various complexing ligands such as EDTA, ISA, citric acid, DTPA, NTA, GLU, oxalic acid, thenoyltrifluoroacetone (TTA), fulvic acid (FA) and acetyl acetone (AcAc) at pH = 12.5, T = (20 ± 1) °C and I = 0.3 M. The degradation of the UP2W material was performed at pH = 12.5 and T = 60 °C. The supernatants of the batch sorption samples were systematically analyzed up to t = 420 days. The uptake of Eu(III) in the absence of ligands (with log (K_d /m^3·kg^{-1}) ≈ 4) started to decrease at about 10^{-4} M ligand concentration in cementitious and TiO_2 systems, except for gluconate where the drop in K_d occurred at $[GLU]_{tot} \geq 10^{-5} – 10^{-6}$ M. The UP2W material experienced a fast degradation in alkaline conditions, resulting in 15 % losses of the initial load (in presence and absence of Ca at [TOC] > 120 mM and [TOC] ≈ 80 mM, respectively). In the cement system at pH = 12.5, the log K_d decreased from around 10^{-6} M of degraded UP2W concentration (from log (K_d /m^3·kg^{-1}) ≈ 4 to 0.25), whilst with [Ca] = 0.01 M the decrease in K_d values started at lower organic concentration (from log (K_d /m^3·kg^{-1}) ≈ 4 to –0.5). These results are in line with the work of Duro *et* al., where the interaction of UP2W degradation products on the uptake of Eu(III) by different materials was investigated at pH = 12.5 and 13.4 [17].

Holgersson *et* al. [126] conducted sorption experiments with ^{134}Cs(I), ^{60}Co(II), ^{152}Eu(III) and ^{232}Th(IV) using Ordinary Portland Cement (OPC) at pH = 13.3 and 12.5, and evaluated the role of UP2W degradation products and various organic ligands (ISA among them) on the overall uptake. The leachates of UP2W were obtained after contacting the material for 300 days with fresh and leached cement porewater at 24 g·dm^{-3} S:L ratio. After paper filtration and NPOC measurement, the leachates (or otherwise the selected organic ligands) were spiked to the porewater-cement suspension containing Eu(III) at $4 \cdot 10^{-9}$ M initial concentration. Batch samples were divided into 4 aliquots, which contained approximately $1.7 \leq ([DOC]_{tot}$ /ppm$) \leq 33$. In the case of ^{152}Eu(III), virtually no effect of the degradation leachates on the uptake process was observed, which can be correlated with the low DOC values considered in the aqueous phase.

Tasdigh performed similar experiments at various solid-to-liquid ratio ($1 \leq$ (S:L /g·dm^{-3}) ≤ 5) using only UP2W degradation products (DP) at pH = 12.5, which contained $[Lig]_{tot}$ = 904.7 ppm of TOC (see Section 1.4.2.2) [16]. The authors followed the order of addition of individual components (DP + Cement) + Eu, in contrast to previous studies in the literature [17, 106], where the order (DP + Eu) + Cement was instead used. After 33 days of contact

time, the determined sorption coefficients (Q_d /$m^3 \cdot kg^{-1}$) were in the range of 0.1 – 0.28. This correlates with the results reported in [106] at ligand concentration of log ($[Lig]_{tot}$ /M) = –3 and Ca(II) concentration of [Ca] = 0.01 M. It was proposed that the factors affecting the retention of Eu(III) were (i) the competitive reaction on the cement binding sites between the organic fragments of UP2W and Eu(III), and (ii) the occurred additional depolymerization of the UP2W filter, which can alter the sorption and solubility of radionuclides.

1.4.3.3 Cement-An(III/IV)-Ligand system

Rojo and co-workers studied the effect of ISA on the uptake of Pu(IV) on concrete and mortar at pH = 12.45 (see also Section 1.4.2.3) [115]. Experiments of the ternary system were conducted following the order of addition (Cement + Pu) + ISA, where the ligand concentration was varied in the range of $-6 \leq \log([ISA]_{tot}/M) \leq -2$. The authors reported a decrease of R_d values at $\log([ISA]_{tot}/M) \geq -4$ due to the formation of ternary complexes Pu(IV)-ISA-Ca(II). It was reported that the drop in R_d could be 5 orders of magnitude at the highest ligand concentration.

The effect of the organic ligands and degradation products on the uptake of Pu(IV) on various solid materials at variable pH were investigated by Baston and co-workers. (see also Section 1.4.2.3) [121]. The authors performed their experiments under inert atmosphere (N_2 filled glove-box) with different materials (*e.g.* concrete, mortar, sandstone etc.) in solutions containing degradation products of anion and cation exchange resins, bitumen, polyester, and ISA at S:L ratios of 20 and 200 $g \cdot dm^{-3}$. Two types of phase separation approaches were used, *i.e.* with 0.45 µm and 30000 MWCO filters. The investigated degradation products decreased the Pu sorption in minor ways on concrete, however the uptake of the nuclide was dropped vastly by ISA at most 3 – 4 orders of magnitude *i.e.* from $R_d \approx 10^6$ $dm^3 \cdot kg^{-1}$ to $(7 – 19) \cdot 10^2$ $dm^3 \cdot kg^{-1}$.

Tasi *et* al. [94] studied the influence of ISA on the Pu-ternary system at $0.2 \leq (S:L\ /g \cdot dm^{-3}) \leq 50$ and $-6 \leq \log([ISA]_{tot}/M) \leq -2$ in different redox conditions using of HQ, Sn(II) and $Na_2S_2O_4$. The components were contacted following the orders of addition (i) (Pu + Cement) + ISA and (ii) (Pu + ISA) + Cement for the experiments. The authors monitored the pH, E_h and $[Pu]_{aq}$, after adequate phase separation by centrifugation and ultrafiltration. It is unequivocal that ISA starts hindering the retardation of Pu at $-4.5 < ([Lig]_{tot}/M)$. However, from $-3.5 \leq ([Lig]_{tot}/M)$ a slight increase on the uptake was observed up to $-2 \leq ([Lig]_{tot}/M)$. According to the authors, this observation was interpreted due to the formation of stable

surface complexes with Pu and ISA, also correlating with an inversion of the surface charge at such ISA concentrations from positive to negative.

Th(IV) is often used as redox-inactive analogue of Pu(IV), and many articles provide significant information about its retention in various cementitious systems. The uptake of Th(IV) by sulphate-resistant Portland cement in the presence of ISA has been characterized in corresponding conditions as it was discussed for Eu(III) in Section 1.4.2.2 [108]. Batch sorption experiments were carried out at 0.01 and 0.1 $g \cdot dm^{-3}$ S:L ratio, $-5 \leq \log ([ISA]_{tot} /M) \leq -2$ and pH = 13.3. Phase separation was achieved by ultracentrifugation at 95000 g for 60 minutes. The analysis demonstrated that the ISA was capable of mobilizing the Th(IV) at $([ISA]_{tot} /M) \geq -4$. Based on their observations, the authors proposed also that Th(IV) establishes complexes with ISA with a 1:2 ratio. However, Vercammen [49] expressed at pH = 12.8 and in presence of Ca(II), the complex formed involved the participation of Ca, *i.e* with a stoichiometry Th:ISA:Ca of 1:2:2. Tits and co-workers, similarly to Eu(III) (see Section 1.4.3.2), conducted sorption experiments with Th(IV) and calcite at pH = 13.3, and evaluated the impact of ISA and GLU [124]. Although, ISA and GLU affected the sorption processes of Th(IV) at slightly higher ligand concentrations compared to Eu(III) ($[ISA]_{in} \geq 10^{-5}$ M, $[GLU]_{in} \geq 10^{-6.5}$ M), the effect was still very significant. The authors attributed their observations to the formation of Th(IV)-Ligand-Ca(II) complex, which is in a good agreement with the study by Vercamment [49].

Although no reports are available on the uptake of Pu(IV) by HCP in the presence UP2W degradation products, Holgersson and co-workers [126] investigated the influence of the different type of organic carboxylic acids *i.e.* EDTA, ISA, citric acid as well as UP2W degradation products on the sorption of Th(IV) under alkaline conditions (see also Section 1.4.3.2). Experiments were conducted in porewater conditions representative of the degradation stage II of cement (pH ≈ 12.5) at a ligand concentration of 30 to 500 ppm. Th(IV) concentration was enhanced negligibly in the aqueous phase in the presence of the investigated concentrations of the organic ligands and degradation leachates. From the sorption investigation it was deduced that, under the investigated conditions, they have only a minor impact on the overall retention process of Th(IV).

From the so-far quantified studies of Cement-RN-Ligand ternary systems, where the retention of the radionuclides by HCP occurs parallel with the formation of the different complexes in the solutions, it can be explicitly drawn the conclusion that their assessment is challenging. A number of difficulties have been identified, namely [14]:

1. Maximum R_d that can be quantified in the Cement-RN binary systems. This variable is affected by (i) the total concentration of RN introduced in the solutions, (ii) the chosen phase separation methods and (iii) the applied S:L ratio.
2. Appropriate total organic concentration and S:L have to be utilized in the systems, where the cement solid phase composition is not altered and parallel the free organic concentration is preserved at adequate level in the solution.
3. It is necessary to take into account the solubility reaction of RN under analogous conditions in the ternary systems. This provides upper concentration limits that can be used in the sorption experiments. Surface precipitation in slightly undersaturated systems may occur as well.
4. Equilibration time. The retention of RN on cement in the absence of organic ligands is a relatively rapid process. However, the introduced organic ligands can significantly slow down the sorption process. This effect can be as well strongly dependent on the order of addition of the individual components.

1.5. Main objectives of the PhD thesis

This thesis aims at obtaining an extended knowledge and scientific information on the effect of the UP2W degradation products on the solubility and sorption of radionuclides in cementitious environments, as well as their sorption and impact on the properties of cement in the absence of radionuclides. The whole thesis is built up from bottom-up, starting with (i) solubility experiments with the previously proposed proxy ligands for the degradation products in binary systems M(II)/Ln(III)/An(III/IV)-Ligand, (ii) performing Cement-Ligand sorption experiments with these specified proxy ligands on Portland cement, and (iii) concluding with the Cement-RN-Ligand ternary systems. The methodological approach adopted in this study is briefly outlined in the following paragraphs:

1. **Solubility experiments of Ca(II), Ni(II), Nd(III) and Pu(III/IV) in the presence of proxy ligands for UP2W degradation products under alkaline condition** (Chapter 3.2)

   This part of the thesis is dedicated to monitor the influence of the proposed proxy ligands (see Chapter 1.3.3) on the solubility of Ca(II), Ni(II), Nd(III) and Pu(III/IV) in cement pore water representative of the degradation stage II. Experiments are conducted from undersaturation conditions using well-defined solid phases, *i.e.* $Ca(OH)_2$(cr), β-$Ni(OH)_2$(cr), $Nd(OH)_3$(s) and PuO_2(ncr,hyd). Due to the possible formation of different

oxidation states of Pu, the batch solutions containing this element were adjusted with HQ and $SnCl_2$ redox buffers. Pu(IV) prevails in the mildly reducing environment set by HQ, whereas both Pu(III) and Pu(IV) may co-exist in the strongly reducing conditions imposed by Sn(II). These approaches include the systematic characterization of the pH, E_h and metal ion concentration in aqueous phase under the variation of the ligand concentration. Extensive solid phase characterization and DFT calculations (only in Pu systems) for broader understanding of the M(II/III/IV)-Ligand were implemented. This part of the study aims at gaining insights on the possible complexation of the proxy ligands with the investigated metal ions, as well as to provide upper concentration limits to be considered in the sorption experiments.

2. **Sorption experiments with the proxy ligands onto HCP in the degradation stage II** (Chapter 3.3)

   The main aim of this part of the study was to assess the interaction of the proposed proxy ligands with HCP at various S:L and ligand concentrations. The purpose of these experiments is two-fold: to assess the free-ligand concentration remaining in the cement pore water after interacting with cement, and to characterize the impact of the selected proxy ligands on the surface properties of cement. Sorption experiments were performed using both inactive and C-14 labelled ligands. Sorption data were modelled using conventional sorption isotherms. To gain insight on the effect of the proxy ligands on the surface properties of cement, the electrophoretic mobility of suspended Portland cement colloidal particles was analyzed as a function of the ligands concentration, and this information was used to calculate the zeta potential of the solid phase. The results obtained in this study are compared with data available in the literature, with the aim of deriving general trends in terms of the type and number of functional groups present in the evaluated organic ligands.

3. **Impact of proxy ligands on the uptake of Ni(II), Eu(III) and Pu(III/IV) by HCP in the degradation stage II** (Chapter 3.3)

   In the final and more complex section of this PhD work, the uptake of ^{63}Ni, ^{152}Eu and ^{242}Pu by HCP in the degradation stage II was investigated in the absence and presence of the proxy ligands for the degradation products of UP2W. These experiments were performed

in a step-wise approach: (i) first the binary systems Cement-RN and then (ii) the ternary system Cement-RN-proxy ligands. As in the solubility study, experiments containing Pu were performed both in the presence of HQ and Sn(II) as redox buffers. Experiments in the absence of proxy ligands aimed also at gaining insight on the uptake mechanisms controlling the retention of the investigated radionuclides, especially in the case of nickel, for which the available information is mostly restricted to the degradation stage I of cement. The parameters pH, E_h and metal ion concentration were monitored for periods of up to 125 days, and the sorption process was quantified in terms of distribution ratios, R_d. The results obtained in this work for the proxy ligands of UP2W are compared with literature data available for ISA, a polyhydroxocarboxylic acid sharing some functional groups with the proposed proxy ligands. The study aimed also at providing relevant insights on the impact of UP2W degradation products in the retention of radionuclides under conditions relevant for the disposal of L/ILW.

2. Experimental

Experiments were conducted at INE, KIT; Campus-Nord. All the samples were prepared and stored in glove-boxes at T = (22 ± 2) °C under Ar gas atmosphere containing O_2 < 2 ppm.

2.1 Chemicals

All samples were prepared with cement porewater corresponding to the degradation stage II of cement. This porewater is prepared by equilibrating hardened cement paste (HCP) with ultra-pure water purified with a Milli-Q appliance (Millipore Mill-Q Advantage A10, (18.2 MΩ, (22 ± 2) °C, 4 ppb TOC), Millipore Millipak ® 40 0.22 µm). Before the preparation of the solutions, the Milli-Q water was purged with Ar gas for > 1 hour to remove traces of O_2 and CO_2. $Ni(OH)_2$(cr) was obtained from Acros Organics. $Ca(OH)_2$(cr), glutaric acid ($C_5H_8O_4$, 99%, solid phase), α-hydroxyisobutyric acid ($C_4H_8O_3$, 99%)(s), 3-hydroxybutyric-acid ($C_4H_8O_3$, 99%, liquid phase) and tin(II) chloride ($SnCl_2$, p.a) were purchased from Sigma-Aldrich. NaOH, HCl (both Titrisol), hydroquinone ($C_6H_6O_2$, HQ, p.a.) and concentrated HNO_3 (Suprapur and Ultrapure) were obtained from Merck. $Nd(OH)_3$(s) was generated from Nd_2O_3(cr) (Merck, 99%) with 1.0 M NaOH (Titrisol) in 10 g/100 L following a protocol previously described in the literature [45, 127]. $Eu(NO_3)_3 \cdot 6H_2O$ (99%, solid phase) was obtained from Alfa Aesar.

The solid phase PuO_2(ncr,hyd) had been previously synthesized at KIT-INE with an isotopic composition 99.4 wt.% ^{242}Pu, 0.58 wt.% ^{239}Pu, 0.005 wt.% ^{238}Pu and 0.005 wt.% ^{241}Pu. Further information of synthesis and characterization of the solid phase can be found in the report of Tasi *et* al. [94]. ^{14}C-labelled glutaric acid [1,5-^{14}C-GTA], as solid phase was obtained from American Radiolabeled Chemical. The specific activity of the tracer was 50–60 mCi/mmol, with a total activity of 50 µCi / 1.85 MBq.

^{63}Ni and ^{152}Eu were purchased from Eckert and Ziegler, with total activities of 100 µCi / 3.7 MBq in 1 mL of 0.5 and 0.1 M HCl, respectively.

The hydrated cement paste used in this study was obtained from the Swedish Nuclear Fuel and Waste Management Company (SKB). The representative composition was the mixture of the Swedish Portland cement for civil engineering (CEM I 42.5N BV/SR/LA) and at a water-to-cement weight ratio of 0.5. The HCP monolith was milled and sieved to < 100 µm in a previous study (see Section 2.3 and reference [94]) Chemical composition of the CEM I clinker, provided by the manufacturer, is summarized in the Table 1 [94].

Table 1. *Chemical composition of the cement (CEM I 42.5N BV/SR/LA) used in this work.*

Chemical components	CaO	SiO_2	Al_2O_3	Fe_2O_3	MgO	Na_2O	K_2O	SO_3	Cl
w%	64	22.2	3.6	4.4	0.94	0.07	0.72	2.2	0.1

2.2 Measurement of pH and E_h

The free proton concentration in solution was determined using combination pH-electrodes (type Orion Ross Thermo Scientific) with the calibration of standard pH buffers (pH = 9 – 13, Merck). In solutions containing ionic strength $I \geq 0.1$ mol/kg, the measured pH value (pH_{exp}) is an operational value that can be converted to proton concentration as $pH_c = pH_{exp} + A_c$, where $pH_c = -\log [H^+]$ (in molar units) and A_c is an empirical parameter, which depends on the background electrolyte, ionic strength and temperature. Values of A_c used in this work were obtained from Altmaier *et* al. work [128].

For the determination of the redox potential in systems containing plutonium, the combined Pt and Ag/AgCl reference electrode (Metrohm) was utilized. Measured potentials were transformed to E_h (Standard Hydrogen Electrode: SHE) by correcting for the potential of Ag/AgCl inner-reference electrode with 3 M KCl and T= 22 °C (+207 mV). Equation (7) relates the E_h with the negative logarithm of the electron activity ($pe = -\log a_{e^-}$):

$$E_h = -RT \ln(10)\ F^{-1} \log a_{e^-}, \qquad (7)$$

where the R is the universal gas constant (8.3144 $J \cdot mol^{-1} \cdot K^{-1}$), F is the Faraday constant (96485.3 $C \cdot mol^{-1}$) and a_{e^-} is the activity of the electron. The values of the redox potential (in mV) were collected for 15 min. in every measurement. E_h values of Pu samples in the presence of HQ or Sn(II) were acquired when the absolute drift of the electrode was < 3 mV/min. The uncertainty of E_h was calculated and collected from all the samples showing 2σ of averaged measurements remained in the range of ± 15 and ± 40 mV.

2.3 Initial cement powder and cement porewater

In a previous study [94], the HCP monolith provided by SKB was crushed with a hammer, and a continuous-flow, vibrational sieving mill (®pulverisette 0, Fritsch Gmbh) with stainless steel sifters was used to mill and sieve the cement material. The final fraction with d < 100 µm was used in the experiments.

The resulting cement powder was used to prepare a cement-porewater corresponding to the degradation stage II of cement, in which the alkalis (Na, K) have been washed out. Milli-Q water (V_{total} = 2 L) was mixed with powdered cement solid phase at a solid-to-liquid ratio (S:L) of 50 g·dm^{-3} (or 25 g·dm^{-3} in some cases). The porewater solution was characterized by measuring the pH, as well as minor (Al, Ti, V, Cr, Mn, Fe, Co, Ni, Cu, Rb, Ba, Pt) and major (Na, K, Ca, Mg) elements by ICP-OES or ICP-MS.

The primary leachate after 1 week of contact time was separated after sedimentation of the HCP, and the vessel filled up with new, fresh Milli-Q water in order to acquire the final porewater solution.

In the interest of using the pure porewater, the resulting solution was separated from the main (2 L) stock solution and centrifuged for 15 minute at 2602 g in order to remove the unwanted cement particles. The gained, clear supernatant solutions were used in all solubility and sorption experiments. In every solution prepared, *i.e.* stock solutions, solubility solutions, the pH and concentration of minor/major components were analyzed, together with the measurement of the non-purgeable organic content (NPOC).

2.4 Preparation of (inactive) proxy ligand stock solutions

The glutaric acid (GTA), α-hydroxyisobutyric acid (HIBA) and 3-hydroxybutyric acid (HBA) as chosen "final" degradation products of UP2W (see further details in Section 1.3.3) were weighted under ambient conditions using a Mettler-Toledo Libra balance. GTA and HIBA samples were prepared in Zinsser vials, whereas HBA (as volatile liquid phase) samples were prepared in Nalgene vials.

The prepared materials were transported to a glove-box, with three 25 mL (later 50 mL) volumetric flask and three Kautex plastic flasks. The ligands were transferred with cement porewater (CEM I, degradation stage II) to the volumetric flasks, shaken and poured to the Kautex flasks. Due to acidity of the initial ligand solutions, the pH was adjusted to pH = 12.5 with 1.0 M NaOH (Titrisol).

2.5 Solubility experiments with M(II/III/IV)-GTA/HIBA/HBA systems

Solubility experiments were performed from undersaturation conditions with $Ca(OH)_2$(cr), β-$Ni(OH)_2$(cr), $Nd(OH)_3$(s) or PuO_2(ncr,hyd) solid phases, which were equilibrated with cement porewater before the addition of the proxy ligands solutions to the systems.

Batch solutions were generated in 15 cm^3 PP Sarstedt centrifuge tubes comprising the solutions of cement porewater and proxy ligand ($V_{tot} = 10$ cm^3). Each sample was supplemented approximately with $10 - 20$ mg of $Ca(OH)_2$(cr), β-$Ni(OH)_2$(cr), $Nd(OH)_3$(s), or $0.5 - 1$ mg PuO_2(ncr,hyd). The ligand concentration of GTA, HIBA and HBA was adjusted between 10^{-6} M ≤ $[Lig]_{tot}$ ≤ 0.1 M, except in the case of Pu, where $[Lig]_{tot} = 10^{-3}$ and 10^{-1} M were used instead. Furthermore, in the Pu experiments, redox conditions were buffered with 2 mM HQ or $SnCl_2$. Previous studies confirmed that +IV is the only oxidation state of Pu in HQ systems, whereas both Pu(IV) and Pu(III) may form in the very reducing conditions imposed by Sn(II).

The supernatant of batch solutions was filtered with 10 kD filters ($2 - 3$ nm cut-off, Nanosep® centrifuge tubes, Pall Life Sciences) using centrifugation at 5806 g (and at 3904 g in the case of Pu) for 10 minutes. The filtered solution was diluted in 2% HNO_3 (Suprapur / Ultrapur) and characterized by ICP-OES (for Ca), ICP-MS (for Ni and Nd) and SF-ICP-MS (for Pu). The metal concentration in the aqueous phase was monitored for t_{eq} ≤ 320 days (Ca-system), t_{eq} ≤ 359 days (Ni-system), t_{eq} ≤ 358 days (Nd-system) and t_{eq} ≤ 223 days (Pu-system). The pH (and E_h in Pu samples) was systematically measured after every sampling.

2.6 Sorption experiments

All sorption experiments were conducted with the synthetic cement porewater. The clear, centrifuged porewater was mixed with cement solid phase at variable S:L ratios for getting the final solutions involving RN, proxy ligands or both. The generated sorption experiments can be classified into three groups:

1. Binary, "HCP-Proxy ligands" experiments
2. Binary "HCP-RN" experiments
3. Ternary "HCP-RN-Proxy ligands" experiments

Commercial stock solutions of ^{63}Ni and ^{152}Eu in 0.1 and 0.5 M HCl, respectively, were used for the sorption experiments with Ni and Eu experiments, whereas a $Na_2PuO_7 \cdot xH_2O$ solid phase synthesized and characterized in a previous study at KIT-INE [129], was used for the preparation of the experiments with ^{242}Pu. The resulting concentration of the stock solution was $[^{242}Pu] = 5.6 \cdot 10^{-2}$ M. In the Pu sorption experiments, HQ and Sn(II) redox buffers were used in the ternary systems, whereas only HQ was used for the binary systems. Small

volumes of the radionuclide stock solutions or corresponding dilutions (14−351 µL) were added to the matrix solutions with or without ligands and solid cement.

2.6.1 Binary system "HCP-Proxy ligands"

Batch experiments were conducted inside glove box at room temperature (T = (22 ± 2 °C) under Ar atmosphere. HCP was contacted with mixtures of porewater and the organic compounds GTA, HIBA or HBA as proxy ligands for the degradation of UP2W. The total amount of batch samples was 82. These samples were separated into 5 series as described in Table 2.

Table 2. *Summary of the sorption samples investigated for the binary system HCP-Proxy Ligands.*

Batch experiments	S:L ($g \cdot dm^{-3}$)	$\log([Lig]_{tot}$ /M)	V_{tot} (cm^3)	Batch samples	Measurement
Cement + Ligand I.	1, 2, 4, 6, 10, 20, 50	–3	10	21	pH, NPOC
Cement + Ligand II.	4	–1, –2, –2.5, –3, –3.5, –4, –6	10	21	pH, NPOC
Cement + ^{14}C-GTA	15, 18, 20, 24, 26, 28, 30, 35, 40, 45, 50	–7 (only ^{14}C-GTA)	10	11	pH, LSC [a]
Cement + GTA + ^{14}C-GTA	20	–1, –2, –2.5, –3, –3.5, –4, –4.5, –5	10	8	pH, LSC [b]
Zeta potential	4	–1, –2, –2.5, –3, –3.5, –4	10	21	Electrophoretic measurement via PALS

a: using only ^{14}C labelled GTA in the batch solutions to attain $[1,5\text{-}^{14}\text{C-GTA}]_{tot} = 10^{-7}$ M. No inactive carrier used

b: batch solutions were spiked with ^{14}C-labelled GTA to attain $[1,5\text{-}^{14}\text{C-GTA}]_{tot} = 10^{-7}$ M

The pH was systematically monitored for all samples. The batch solutions containing the inactive proxy ligands have been sampled at given contact times and centrifuged for 10 minutes at 5806 g using 2 cm^3 Sarstedt PP plastic vials. The supernatant was pipetted into 2% HNO_3 solutions, and measured by using Analytik Jena multi n/c 2100 S for NPOC.

Samples containing ^{14}C-labelled GTA were equilibrated for 82 days, centrifuged at 3461 g for 5 minutes and the supernatant was filtered with 10 kD filters at 3461 g for 10 minutes. The filtered samples were characterized via LSC (see Section 2.7.1). The volume removed in the

sampling was replaced with the corresponding ligand stock solutions containing no cement powder, whilst cement porewater was added in the case of the active batch solutions.

Sorption experiments with the binary system HCP-Proxy ligands were complemented with zeta potential measurement. Batch solutions were equilibrated for 14 days and the aliquots of suspended particles were transferred into a pre-washed plastic cuvette. In the final steps, the cuvette was sealed up with measurement cell (Pt electrode) and parafilm under Ar atmosphere. The electrophoretic measurement was carried out with a Nanobrook 90 plus PALS (Brookhaven Instrument Co.) equipment. Zeta potential was quantified from the electrophoretic mobilities applying Smoluchovsky equation implemented in the equipment software. Each sample was analyzed 10 times (for ζ potential), with one datapoint being characterized for 15 cycles run. All datapoints were averaged in the final evaluation. The acquired values were selected according to their smallest value of root-mean-square (RMS) residual and plotted with their uncertainty using 2 times the standard deviation.

2.6.2 Binary system "HCP-RN"

The experimental conditions considered in the sorption experiments with ^{242}Pu, ^{63}Ni and ^{152}Eu onto HCP in the absence of proxy ligands are summarized in the Table 3.

Table 3. *Summary of the sorption samples investigated for the binary system HCP-RN.*

Batch experiments	S:L (g·dm^{-3})	log ([RN]$_{tot}$ /M)	V_{tot} (cm^3)	Batch samples	Measurement
Cement + ^{242}Pu constant [RN]$_{tot}$	0.5, 1, 2, 5	–8	10	4	pH, E_h, SF-ICP-MS [a]
Cement + ^{242}Pu constant S:L	1	–7.8, –8, –8.2	10	5	pH, E_h, SF-ICP-MS [a]
Cement + ^{63}Ni constant [RN]$_{tot}$	1, 2, 4, 10, 20	–8	10	5	pH, LSC [b]
Cement + ^{63}Ni constant [RN]$_{tot}$	1, 2, 4, 10, 20	–9	10	5	pH, LSC [b]
Cement + ^{152}Eu constant [RN]$_{tot}$	0.5, 1, 2, 3, 4	–8	5	5	pH, γ-counter [c]

a: buffered by HQ; **b**: ^{63}Ni stock solution contains also log [^{nat}Ni]$_0$ = = (1.6 ± 0.8)·10^{-7} M in the cement pore water, as assessed in this work, **c**: batch solutions comprise additional [^{nat}Eu]$_0$ = 3.1·10^{-8} M, which comes from the ^{152}Eu commercial stock solution

After the 7 days of contact time, the Sarstedt vessel containing HCP + RN was centrifuged for 5 minutes at *ca*. 3400-3904 *g*. The supernatant solution was transferred and filtered with 10 kD filters for 10 minutes at *ca*. 3400-3904 *g* in order to remove any cement particle or colloid from the liquid phase (phase separation at 3904 *g* was applied for Pu; 3461 *g* was used for Ni and Eu samples). In the case of Eu, ultracentrifugation was also applied as phase separation method (Beckman XL-90, rotor type 90Ti, 694000 g, 1 h). The colloid-free solutions of Pu, Eu and Ni were diluted with 2% HNO_3 in 5 cm^3 ICP tubes (Pu), empty ICP tubes (Eu) and Zinsser vials containing LSC cocktail (Ultima Gold XR, PerkinElmer, for Ni). Pu, Ni and Eu samples were analysed by SF-ICP-MS (type Element XR, Thermo Fisher), LSC (Section 2.7.1) and gamma counting (Section 2.7.2), respectively. The solutions in the HCP-Ni system were additionally quantified for total nickel concentration by ICP-MS. After some preliminary attempts with Suprapur HNO_3, Ultrapure 2% HNO_3 was used for the dilution of the samples. Besides the measurement of the metal concentrations, batch samples were systematically characterized for pH (and in the case of Pu also E_h). Their volumes were restored with cement porewater after each sampling.

Since radionuclides at such trace concentrations are able to sorb onto the walls of the vessel, the Sarstedt vessels containing the suspension were rinsed with Milli-Q and filled with 2% HNO_3 (Suprapur). After one day of waiting, the activity of the solutions was characterized. It was indicated that 30% of ^{63}Ni and 4% of ^{152}Eu sorbed on the vessel's wall.

2.6.3 Ternary system "HCP-RN-Proxy ligands"

Table 4 summarizes the experimental conditions considered in the investigation of the ternary system HCP-RN-Proxy ligands, with RN = ^{242}Pu, ^{152}Eu, ^{63}Ni and Proxy ligands = GTA, HIBA, HBA.

Table 4. *Summary of batch experiments within the ternary system of (Cement + RN) + Ligand, where the Ligand = GTA, HIBA and HBA*

Batch experiments	S:L ($g \cdot dm^{-3}$)	log ($[RN]_{tot}$ /M)	log($[Lig]_{tot}$ /M)	V_{tot} (cm^3)	Batch samples	Measurement
(Cement + ^{242}Pu) + Ligand	1	–8	–1, –1.5, –2, –2.5, –3, –4	10	36	pH, E_h, SF-ICP-MS [a]
(Cement + ^{63}Ni) + Ligand	1	–8	–1, –1.5, –4	10	9	pH, LSC [b]
(Cement + ^{152}Eu) + Ligand	1	–8.67	–1, –1.5, –2, –2.5, –3	5	15	pH, γ- counter [c]

a: buffered by HQ and $SnCl_2$

b: ^{63}Ni stock solution contains also log $[^{nat}Ni]_0 = (1.6 \pm 0.8) \cdot 10^{-7}$ M in the cement pore water, as assessed in this work,

c: All batch solutions contain natural Eu ($[^{nat}Eu]_0 = 1.1 \cdot 10^{-7}$ M), which comes from $Eu(NO_3)_3 \cdot 6H_2O$ as inactive carrier ($[^{nat}Eu]_{in} = 10^{-7}$ M) and commercial ^{152}Eu stock solution ($[^{nat}Eu] = 6.6 \cdot 10^{-9}$ M).

All batch samples were prepared according to the following additional order: (i) proper concentrations of radionuclides were added to the cement and cement porewater suspension. The Pu samples were buffered by HQ and Sn(II) redox buffers. (ii) After 2 d equilibration, the batch solutions were spiked with 0.2, $5 \cdot 10^{-2}$ and $5 \cdot 10^{-3}$ M of GTA, HIBA and HBA stock solutions to reach $-4 \leq \log([Lig]_{tot}/M) \leq -1$. Additional ligands solutions with corresponding organic concentration and cement S:L ratio were generated in order to restore the original volume of the batch solutions after each sampling.

Likewise in the binary systems, the aqueous phases containing Pu, and Ni and Eu were first centrifuged at 3904 and 3461 *g* for 5 minutes. In a second step, the supernatant was filtered through 10 kD filters at 3904 and 3461 *g* for 10 minutes, respectively. The filtered solution was diluted with 2% HNO_3 and characterized as described in Section 2.6.2. Batch solutions were further characterized with pH (and E_h in the case of Pu).

Similarly in Section 2.6.2, the "sorption onto the vessel wall" effect was considered in the evaluation.

2.7 Characterization of the aqueous phase

2.7.1 Liquid scintillation counting

This method was applied for the determination of ^{14}C (1,5-^{14}C-GTA) and ^{63}Ni activity in liquid phases. After proper solid-liquid phase separation, a given volume of the resulting solution was mixed with 2% HNO_3 in PE plastic Zinsser vials (Zinsser Analytic GmbH), 10 cm^3 LSC cocktail (Ultima Gold XR, PerkinElmer) were added and the sample measured by LSC (Tri-Carb 3110TR, PerkinElmer) for 30 minutes using a 0 – 100 keV energy window. Uncertainties are reported as 2 times the standard deviation. The counting rate of 2% HNO_3 blank was also determined getting 20 cpm.

2.7.2 Gamma counting

Counting rates of $[^{152}Eu]_{tot}$ solutions were systematically measured with a Wizard^2 10-2480 Detector Gamma Counter (PerkinElmer, USA) equipped with a Na(Tl) crystal. After the filtration of the supernatant of batch sorption samples with 10 kD or ultracentrifugation, the clear solution was diluted in 2% HNO_3 Suprapur solutions. The radioactive samples were transported to test tube racks and arranged to the automatic controlled conveyor belt. Data was collected in regards of a preliminary established protocol (*i.e.* 30 minutes measurement time per sample, termination of the sample analysis at maximum count rate of 10^6 cpm, multichannel analysis in the energy window of 15 – 2000 keV), which were recognized by using a bar code read on the side of the sample rack. The results were presented as cpm after the offset by the acquisition time. The count rate of 2% HNO_3 blank was ~ 20 cpm.

2.8 Characterization of solid phase

The solid phase of $Ca(OH)_2$(cr), β-$Ni(OH)_2$(cr) and $Nd(OH)_3$(s) from the solubility experiments were separated from the suspension using centrifugation and filtration (10 kD filters). After getting the optimal weight (1 – 2 mg), they were left to be dried on the filter for a week inside the glove-box. In the case of PuO_2(ncr,hyd), subsequently the centrifugation of the batch solutions, the solid phase was dried on the analyzing plate (see below in Section 2.8.1).

2.8.1 X-ray diffraction

For standard analysis of β-$Ni(OH)_2$(cr), $Nd(OH)_3$(s), $Ca(OH)_2$(cr), and Pu-hydrous-oxide (i) before and (ii) after the complexation with organic ligands, few mL of a suspension containing 0.5 − 1 mg were pipetted to 10 kD filters, centrifugation at 5806 g for 10 minutes, dried at room temperature inside an Ar-glove-box, and placed on a crystal silicon plate covered with an air-tight dome. In regards of solid Pu-hydrous-oxide, the suspension within the original vessel was centrifuged (3904 g, 10 minutes) and dried directly on the silicon plate. Due to the low background electrolyte concentration employed in the solubility studies and to avoid washing away possibly forming secondary phases with the proxy ligands, solid samples were not washed. The solid phases were analyzed with a D8 Advance (Bruker AXS) diffractometer (Cu Kα radiation) equipped with an energy-dispersive detector. The XRD patterns were recorded in the range of $5° \leq 2\Theta \leq 105°$, with step size of 0.011° and 0.5 second per step counting time. The data gathered were evaluated with the Bruker AXS Diffrac^{Plus} EVA software. The evaluated diffractograms were compared to XRD patterns of reference solid phases included in the JCPDS database [130]. The evaluation of Rietvald refinement was carried out with Bruker DiffracPlus TOPAS software package (Bruker AXS, Germany, version 4.2).

2.9 Theoretical methods for Pu(IV)-OH-Ligand systems

Further investigations of the Pu(IV)–OH–Ligand system (where Ligand = GTA, HIBA and HBA) were performed by R. Polly of KIT-INE via density functional theory (DFT) calculations [131, 132]. The evaluation were carried out using TURBOMOLE (version 7.0, 2015) [133-138] with BP86 functional [139] and def2-SVP basis set [136] as it was conducted in the report of Tasi *et* al. [19]. We employed the 5f-in core pseudo potentials (PP) for Pu(IV) for the DFT calculations (see Tasi *et* al. [19] for further information) and the accompanying basis set of double zeta (ecpIVmwb-avdz). Computations performed for the Pu(IV)–OH–GTA system were compared with the bigger def2-TZVPP basis sets for the lighter atoms and the triple zeta (ecpIVmwb-avtz) basis set for Pu to ensure that the used basis sets provide accurate results and do not vary strongly with the basis set anymore.

DFT calculations were done without the use of any solvent in the first stage, resulting in a computation of the gas phase. In order to consider molecular structures in the presence of aqueous media, the first shell (six molecules) of H_2O entities were included and the structure

further approximated with the conductor-like screening model (COSMO) [140, 141]. Using COSMO to deal with additional solvation effects and specifically considering the first water shell gives an acceptable way to investigating species structures in aqueous solutions.

3. Result and discussion

3.1 Characterization of cement porewater

Table 5 shows the concentration of minor and major constituents of the cement pore water as analyzed by ICP-OES and ICP-MS techniques. The table includes as well the results of pH measurements. In addition, Table 5 provides the results of previous literature studies.

The determined pH value in present work (12.48 ± 0.13) is in good agreement with pore water from former articles (pH ≈ 12.5) [14, 15]. The concentration of alkali metal ions (Na, K) is significantly decreased compared to degradation stage I ([Na] ≈ 0.38 M, [K] ≈ 0.11 M) indicating that the washing step described in chapter 2.3 was very efficient, even though measured concentrations are slightly higher than those reported in Tasi *et* al. [94], who used a similar procedure. Low concentrations of Si and Al were determined in the pore water used in this work, in line with generally low concentrations reported in the literature [142]. The measured Ca concentrations and pH values support that the generated cement pore water represents well the degradation stage II of cement.

Table 5. *Composition and pH of the generated cement pore water in aqueous phase at S:L = 25 g·dm^{-3} after $t_{eq} \geq 7$ d of contact time with Milli-Q. Uncertainty was calculated as twice the standard deviation of mean values. Obtained results were compared to former reports of pore water in degradation stage II [14, 15, 115, 142].*

Porewater	Ca(II) [M]	Na(I) [M]	K(I) [M]	Si(IV) [M]	Al(III) [M]	pH
p.w.	$(1.9 \pm 0.2)\cdot10^{-2}$	$(5.4 \pm 0.2)\cdot10^{-3}$	$(2.6 \pm 0.3)\cdot10^{-3}$	$(1.7 \pm 0.6)\cdot10^{-4}$	$(6.0 \pm 0.8)\cdot10^{-5}$	(12.48 ± 0.13)
Tasi *et* al. [14]	0.02	$7\cdot10^{-5}$	$3\cdot10^{-4}$	$< 10^{-5}$	$2\cdot10^{-6}$	(12.55 ± 0.08)
SKB report [15]	0.02	$3\cdot10^{-3}$	10^{-4}	$3\cdot10^{-6}$	$2\cdot10^{-6}$	12.5
Pointeau *et* al. [142][a]	0.01	$2\cdot10^{-4}$	$1.4\cdot10^{-4}$	$8.3\cdot10^{-5}$	$2.6\cdot10^{-5}$	12.36
Pointeau *et* al. [142][b]	0.01	–	–	$4.9\cdot10^{-5}$	–	12.5
Rojo *et* al. [115][c]	0.01	$2\cdot10^{-4}$	$9.3\cdot10^{-4}$	$2\cdot10^{-5}$	$1.2\cdot10^{-5}$	12.45

a: CEM I in Ca/Si = 1.3

b: C-S-H in Ca/Si = 1.3

c: CEM I 42.5R/SR Portland cement sulphate resistant type I

3.2 Solubility study

The produced result of radionuclides solubility studies can be separated into several sections, where the solubility behaviour of the chosen radionuclides was investigated under alkaline conditions and inert Ar-atmosphere. In the case of Pu, experiments were performed in the presence of reducing chemicals (see Experimental section):

1. Ca(II) solubility
2. Ni(II) solubility
3. Nd(III) solubility
4. Pu(III/IV) solubility

3.2.1 Ca(II) solubility

The interaction of Ca(II) with GTA, HIBA and HBA was investigated under alkaline conditions and it is displayed in the Figure 7. Red solid and dashed lines denote the solubility of $Ca(OH)_2(cr)$ and its uncertainty in the absence of organic ligands applying thermodynamic data from NEA-TDB and ThermoChimie databases [64, 143]. Black crosses illustrate the Ca concentration in cement pore water characterized in the present work. For comparison, the black solid line shows the solubility of $Ca(OH)_2(cr)$ in the presence of ISA.

After a contact time of 8 days, the values determined are consistent with the calculated solubility, indicating that thermodynamic equilibrium was reached. Although Ca concentration remains within the uncertainty of the calculated solubility, measured concentrations in the HBA system are slightly decreased at the highest ligand concentrations, as compared to GTA and HIBA.

Several experimental studies dealing with Ca-Ligand complexation (where Ligand = GTA, HIBA and HBA) were previously reported, even though up to now these measurements were performed only in acidic or close to neutral pH conditions. The first study was conducted by Canaan and Kibrik, who investigated the complexation of divalent cations (*e.g.* Ca, Sr, Zn, and Ba) and mono-, di-carboxylic acids via potentiometric technique in ~ 0.2 M KCl solutions. The equilibrium constants for the reactions $Ca^{2+} + (GTA)^{2-} \rightleftharpoons Ca(GTA)(aq)$ and $Ca^{2+} + (GTA)^{-} \rightleftharpoons Ca(GTA)^{+}$ are log β = 1.06 and 0.5, whilst for $Ca^{2+} + (HIBA/HBA)^{-} \rightleftharpoons Ca(HIBA/HBA)^{+}$ the log β values are 0.51 / 0.60, respectively [144]. Schubert and Lindenbaun investigated the complexation of Ca^{2+} and Sr^{2+} with various dicarboxylic acids at T = 25 °C, in near-neutral solutions of 0.16 M NaCl using the ion exchange method. The

authors reported the formation of 1:1 complexes, with log β = 0.55 for Ca(II)-GTA [145], which is in good agreement with results of Canaan and Kibrik [144]. Veerbek and Thun characterized the alkaline earth metals (Ba, Sr, Ca, Mg) complexation in the presence of lactose and α-hydroxybutyric acid with cation-exchange chromatography method.

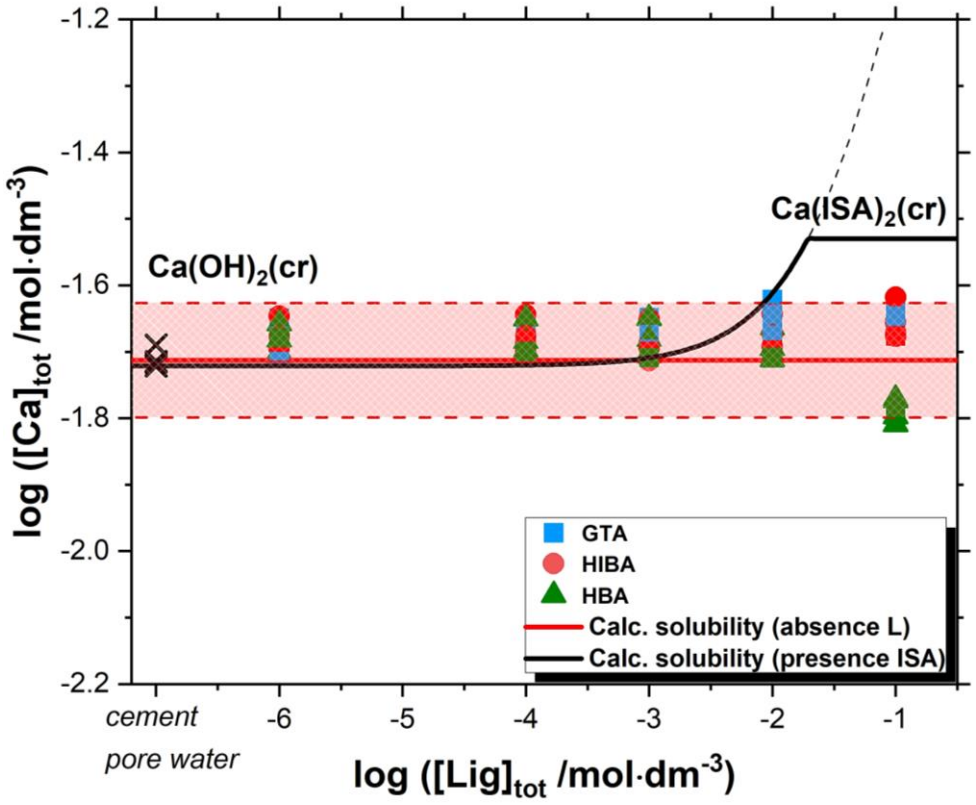

Figure 7. *Solubility measurement of $Ca(OH)_2$(s) in cement pore water at pH = 12.5 and $[Ca]_{tot}$ = 20 mM with 10^{-6} M ≤ $[Lig]_{tot}$ ≤ 0.1 M in glutaric acid (■); α-hydroxyisobutyric acid (●) and 3-hydroxybutyric acid (▲) after 340 days. Black cross symbols illustrate the Ca(II) concentration in the absence of any ligands. Red solid and dash lines represent solubility limit and uncertainty of $Ca(OH)_2$(cr). Black line correspond to the solubility of $Ca(OH)_2$(cr) in the presence of ISA. Thermodynamics calculations conducted using the NEA-TDB and ThermoChimie databases [64, 143]*

By various characterization methods *e.g.* Bjerrum's half n method, Fronaeus graphical technique etc., it was quantified that the first stability constant of Ca(II)-HBA is in the range of 0.92 ≤ log β_1 ≤ 1.11, whilst the stability constant for 1:2 complex is between 1.16 ≤ log β_2 ≤ 1.29 [146]. Experiments investigating the complexation of HIBA and Ca(II) (and Mg(II)) were carried out with the help of potentiometric titration in 0.5 M $NaClO_4$ by Piispanen and Lajunen [147]. The authors reported the equilibrium constant of $Ca(HIBA)^+$ as log β = (1.09 ±

0.03), which is in line with the value in the previous study of Veerbek and Thun [146]. The discussion above emphasizes the weak complexation between Ca(II) and the investigated proxy ligands. Although these measurements were conducted in acidic-neutral pH conditions, the weak complexation is in line with the outcome of this work gained from the solubility of $Ca(OH)_2$(cr) at pH ≈ 12.5.

Figure 7 shows the calculated solubility of $Ca(OH)_2$(cr) in the presence of ISA for comparison (see black solid and dashed lines in the figure). It is apparent from the Figure 7 that above $[ISA]_{tot} \geq 10^{-3}$ M the Ca(II) solubility increase is more relevant than in GTA/HIBA/HBA systems. The formation of the complex $Ca(ISA)^+$ has been reported as weak (log β = 1.7 ± 0.3), nevertheless in alkaline pH, the complex $Ca(ISA_{-H})$(aq) becomes dominant as one of the alcohol groups in ISA deprotonates, which contributes to the increased stability of the complex and the solubility increase [64, 143]. In addition, the calculated ISA concentration at $[ISA]_{tot} \geq 10^{-2}$ M becomes constant due to the predicted precipitation of $Ca(ISA)_2$(cr) (see black solid line).

Since the HIBA comprises carboxylic groups in C1 and alcoholic groups in C2 (α-position) such as in the ISA, analogous complexation could be expected. Dudás and co-workers study of Ca(II) reaction with ISA denoted the carboxylic oxygen on C1 carbon and alcoholic groups on C2 carbon generate five-membered chelate ring [148]. Despite the fact that similar complex reactions are anticipated in the case of Ca(II)-HIBA, due to the weak acidity of hydroxyl groups in the investigated ligand, this kind of formation might be detected only at higher pH milieu than in the present work (pH ≈ 12.5).

3.2.2 Ni(II) solubility

Slight but systematic enhancement in the solubility of β-$Ni(OH)_2$(cr) in the presence of GTA, HIBA and HBA was observed at pH = 12.5 and $[Ca]_{tot} = 10^{-2}$ M, as shown in Figures 8 – 10. Red solid and dashed lines show the solubility limit of β-$Ni(OH)_2$(cr) and its uncertainty in the absence of any ligand [23]. Black crosses correspond to the nickel concentration in the cement porewater (without any addition of β-$Ni(OH)_2$(cr) solid phase) as quantified within the present work. Figures 8 – 10 also display the experimental and calculated solubility data points of Ni(II) in the presence of increasing ISA concentrations, as reported by González-Siso and co-workers [23].

The noticeable increase of the Ni concentration in all three system was observed from the $[Lig]_{tot} \leq 10^{-2}$ M, albeit not as intensively as in Ni(II)-ISA system [23]. Furthermore, it is

evident from Figures 8 – 10 that GTA contributes more to a solubility increase than HIBA or HBA. This solubility increase at high ligand concentration suggests minor complex formation in the reaction of Ni(II)-Ligand under alkaline conditions. The Ni(II) concentration in the absence of proxy ligands and β-$Ni(OH)_2$(cr) solid phase in cement porewater (CEM I, pH ≈ 12.5) fits well with previous results of scientific articles, *i.e.* $[Ni(II)]_{aq} \approx 10^{-7} - 10^{-8}$ M as reported by Wieland *et* al. [102]. Within similar pH conditions but in the absence of Ca, González-Siso and co-workers [23] pointed out the formation of the species of $Ni(OH)_2ISA^-$ and $Ni(OH)_3ISA^{2-}$, which are responsible for the enhanced solubility in the presence of ISA. Due to the moderate solubility changes and the fact that the crucial parameters (*e.g.* pH, ionic strength) were not varied, which can affect the Ni-GTA/HIBA/HBA systems, no chemical and thermodynamic models can be accomplished. However, it can be presumed that the complexation occurs in the metallic cation and organic ligand ratio of 1:1 on the basis of mild increase in solubility. Reports on Ni(II) and organic ligands containing carboxylic and hydroxyl functional groups *e.g.* malonic acid, succinic acid, HIBA/HBA etc. complexation are scarce [149-152]. Based on the stated conclusions in these studies, the complexation occurs in ratios 1:1, 1:2 and 1:3 under acidic or neutral pH milieu between the Ni(II) and the organic molecules. Thermodynamic calculations with these equilibrium constants indicate that these binary complexes are not capable of overcoming the Ni(II) hydrolysis under hyperalkaline conditions. Therefore, the minor increase in the present work cannot be aligned to the formation of $Ni(Ligand)^+$ (HBA/HIBA) or Ni(Ligand)(aq) (GTA). Taking into consideration, again the report of González-Siso and co-workers [23], the complex formation in the current study can be hypothetically described with the formation of $Ni(OH)_xGTA^{-x}$ and $Ni(OH)_x(HIBA/HBA)_{-yH}^{1-y-x}$ (y = 0 or 1) complexes, where the hydroxyl group(s) has/have to be taken into consideration as further ligands. These recommended formulas however remain theoretical, because in order to derive the thermodynamic stability and stoichiometry of the Ni complexation reactions, the essential parameters (*e.g.* pH, ionic strength) should be varied in the solubility experiments. This was not in the scope of this PhD project.

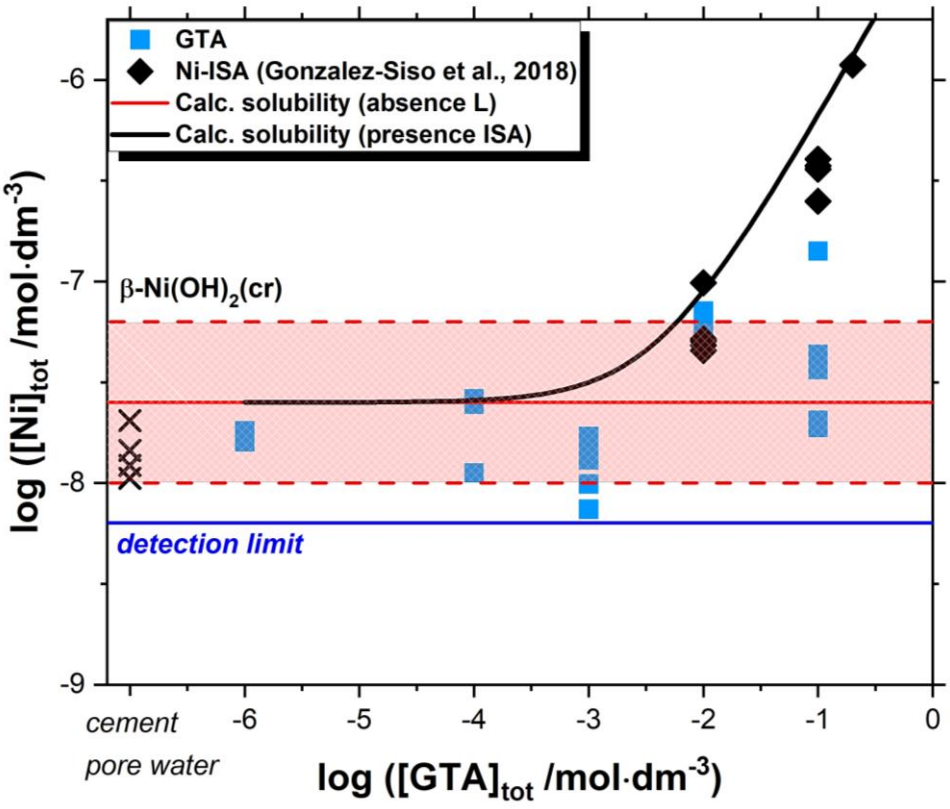

Figure 8. *Solubility measurement of β-Ni(OH)$_2$(cr) in cement porewater at pH = 12.5 with 10^{-6} M ≤ [Lig]$_{tot}$ ≤ 0.1 M in glutaric acid (GTA) for the contact time ≤ 359 days. No typical trend was indicated with time for each ligand concentration. Red lines (solid and dashed lines) represent solubility limit of β-Ni(OH)$_2$(cr) calculated by González-Siso et al. [23]. The blue solid line corresponds to the detection limit, while black crosses show the concentration of Ni(II) determined in cement porewater. The black averted squares and solid line represent obtained datapoints and evaluated solubility of Ni-ISA, reported by González-Siso et al. [23].*

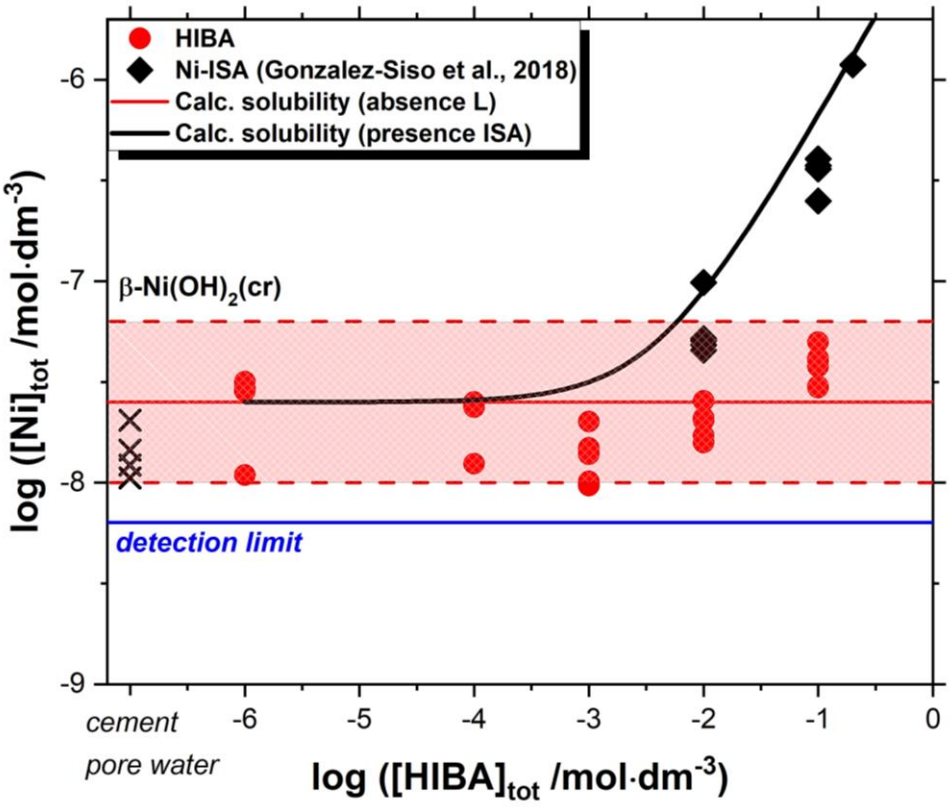

Figure 9. *Solubility measurement of β-Ni(OH)$_2$(cr) in cement porewater at pH = 12.5 with 10^{-6} M ≤ [Lig]$_{tot}$ ≤ 0.1 M in α-hydroxyisobutyric acid (HIBA) for the contact time ≤ 359 days. No typical trend was indicated with time for each ligand concentration. Red lines (solid and dashed lines) represent solubility limit of β-Ni(OH)$_2$(cr) calculated by González-Siso et al. [23]. The blue solid line corresponds to the detection limit, while black crosses show the concentration of Ni(II) determined in cement porewater. The black averted squares and solid line represent obtained datapoints and evaluated solubility of Ni-ISA, reported by González-Siso et al. [23].*

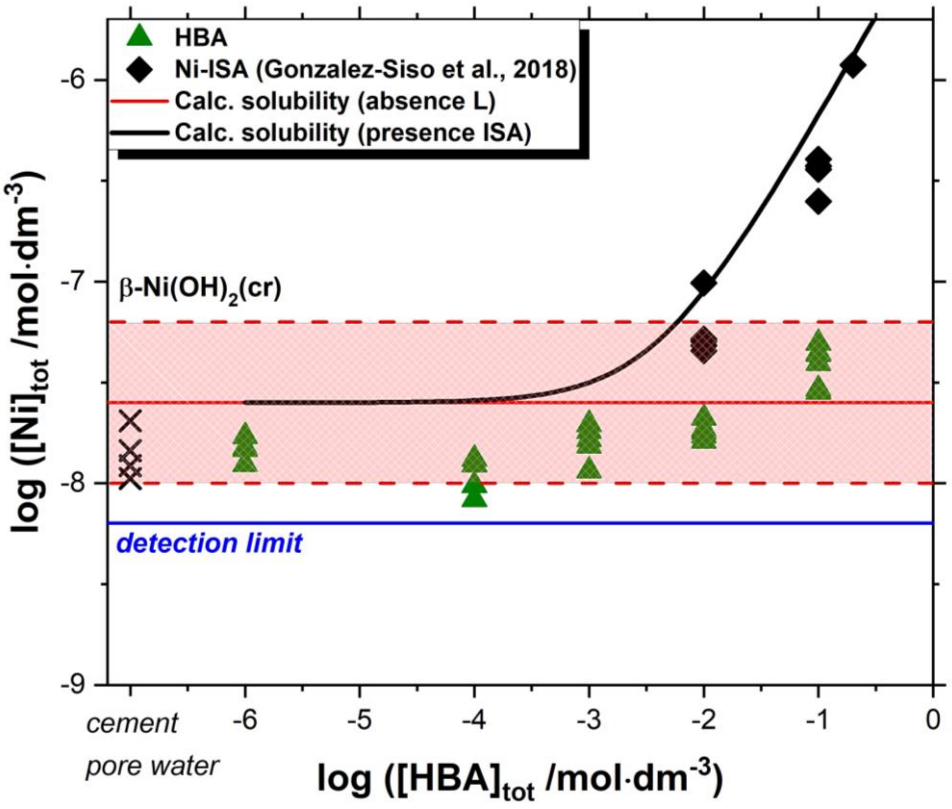

Figure 10. *Solubility measurement of β-Ni(OH)$_2$(cr) in cement porewater at pH = 12.5 with 10^{-6} M ≤ [Lig]$_{tot}$ ≤ 0.1 M in 3-hydroxybutyric acid (HBA) for the contact time ≤ 359 days. No typical trend was indicated with time for each ligand concentration. Red lines (solid and dashed lines) represent solubility limit of β-Ni(OH)$_2$(cr) calculated by González-Siso et al. [23]. The blue solid line corresponds to the detection limit, while black crosses show the concentration of Ni(II) determined in cement porewater. The black averted squares and solid line represent obtained datapoints and evaluated solubility of Ni-ISA, reported by González-Siso et al. [23].*

3.2.3 Nd(III) solubility

The effect of the 3 investigated proxy ligands on the solubility of Nd(OH)$_3$(s) is shown in the Figures 11 – 13. Red solid and dashed lines represent the calculated solubility of the Nd(OH)$_3$(s) in ligand-free systems and the respective data uncertainty [45]. For comparison purpose, the impact of ISA on the solubility of Nd(OH)$_3$(s) is illustrated as black symbols and black solid line, as reported by Gugau [50].

From the Figure 11 – 13 it is apparent that no increase in the Nd(OH)$_3$(s) solubility can be detected in the presence of the proxy ligands. A large dispersion in all 3 systems was noted in the concentration of Nd at log [Nd(III)]$_{tot}$ ≈ –(9 ± 1.5). This observation is consistent with previous publications on the An(III)/Ln(III) and An(IV) systems in the absence of complexing

ligands [19, 45, 153]. Such dispersion is often assigned to the prevalence of neutral species $An/Ln(OH)_3(aq)$ and colloids in solution, which may sorb on the vessel walls and / or filters. Moreover, insufficient separation *e.g.* ultrafiltration or ultracentrifugation can inflict increase the Nd(III) concentration in aqueous phase as well. The large data dispersion observed also at high ligand concentrations can be related to the absence of complexation, as corroborated by Gugau for the Nd-ISA systems (Figure 11 – 13). The authors reported huge deviation in Nd(III) concentration until $\log [ISA]_{tot} \approx -3$. As a matter of fact, as the ligand concentration increased, visible increase in Nd(III) concentration and more accurate solubility measurement were detected [50]. This phenomenon was interpreted with the formation of $Nd(OH)_3ISA^-$ at $pH_m \geq 12$ at $\log [ISA]_{tot} \geq -3$.

The interaction of the lanthanides (including Nd) with GTA, HIBA and HBA have been investigated in various articles in acidic to near-neutral pH conditions [154-157], but not under (hyper-)alkaline conditions. In the experiments of Giroux *et* al., the behaviour of Pr(III) in the presence of butyric acids (2-hydroxy and 3-hydroxy butyric acids) was monitored from acidic to mild alkaline conditions ($2 \leq pH \leq 8$) [48]. The authors reported the equilibrium constants in the range of $\log \beta = 2 - 4$. These complexes however fade away in alkaline to hyperalkaline conditions, where (just like in Ni-Ligand complexation, Section 3.2.2) the hydrolysis outcompetes complexation. Kim and co-workers investigated complexation under mild acidic conditions, and concluded that the GTA forms 1:1 complexes with the Ln(III) by end-on bidentate binding of single carboxylic group [158]. This might serve as a basic information on the Nd(III)-Ligand complex formation. In summary, considering also the available thermodynamic data for Nd(III)-Ligand complexes in acidic conditions, the present work shows that these defined proxy ligands have only minor influence on the solubility of Nd(III) under cementitious conditions.

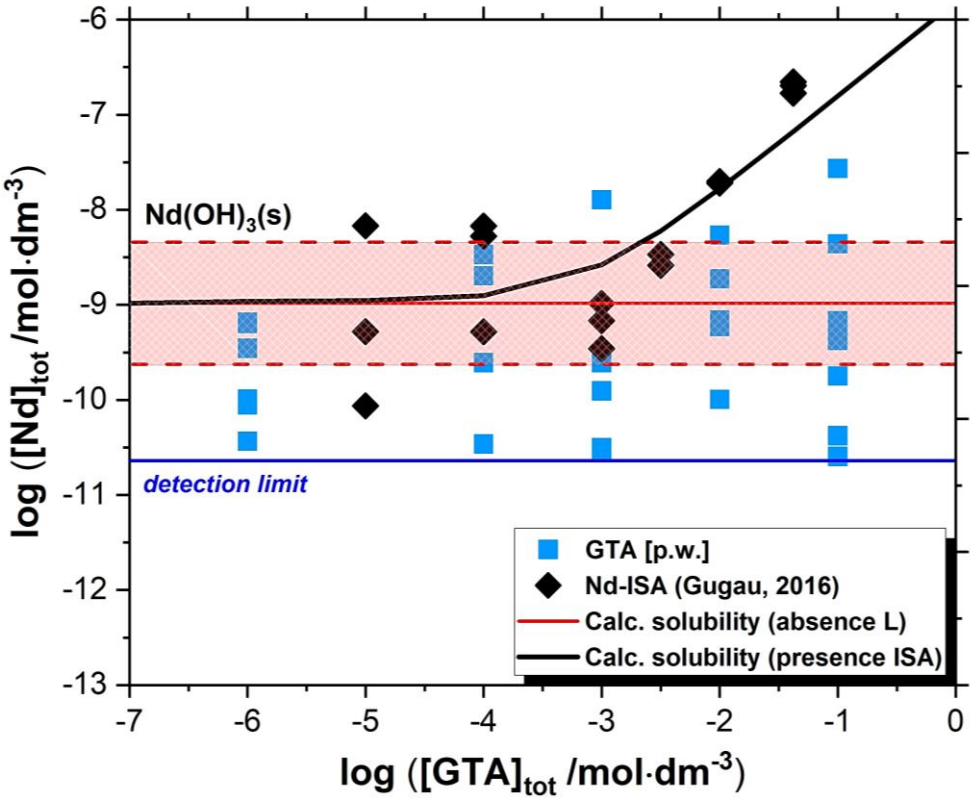

Figure 11. *Solubility measurement of $Nd(OH)_3(s)$ in cement pore water at pH = 12.5 and $[Ca]_{tot}$ = 20 mM with 10^{-6} M ≤ $[Lig]_{tot}$ ≤ 0.1 M in glutaric acid (GTA) at t_{eq} ≤ 358 days. Data dispersion is due to scattering and does not represent a trend with time. Red lines (solid and dashed lines) show the solubility limit of $Nd(OH)_3(s)$ in the absence of any ligand as reported by Neck et al. [45]. The blue solid line illustrate the detection limit of Nd(III) in the investigated conditions. The black symbols and solid line correspond to the experimental and calculated solubility of $Nd(OH)_3(s)$ in ISA media, as reported by Gugau [50].*

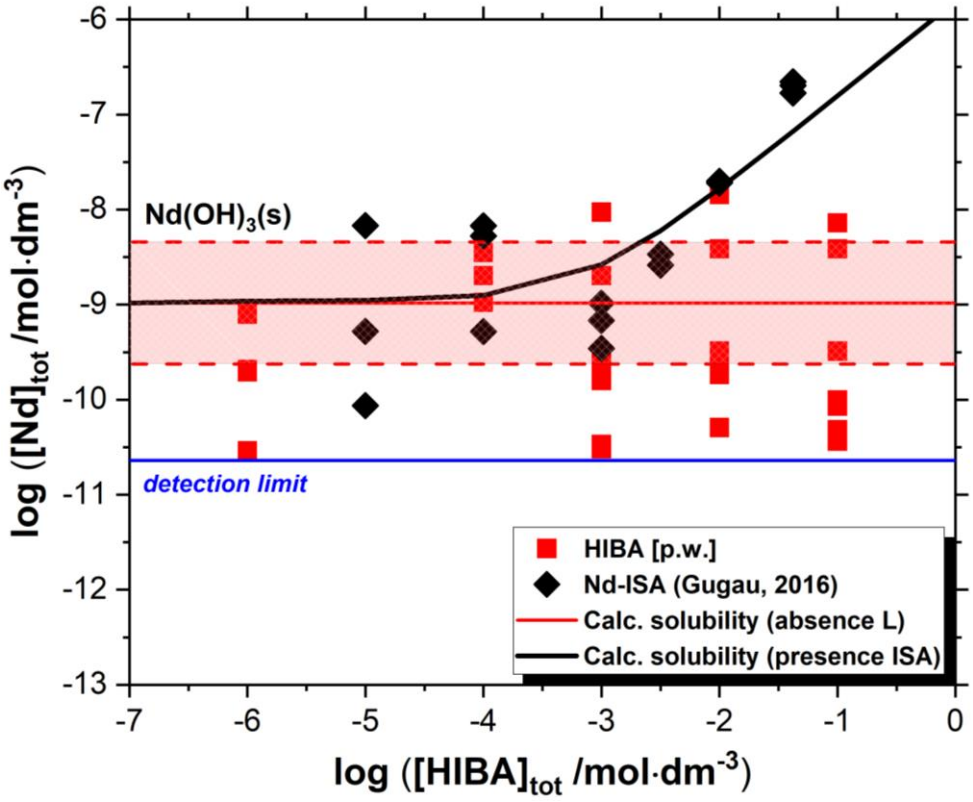

Figure 12. *Solubility measurement of $Nd(OH)_3(s)$ in cement pore water at pH = 12.5 and $[Ca]_{tot}$ = 20 mM with 10^{-6} M ≤ $[Lig]_{tot}$ ≤ 0.1 M in α-hydroxyisobutyric acid (HIBA) at t_{eq} ≤ 358 days. Data dispersion is due to scattering and does not represent a trend with time. Red lines (solid and dashed lines) show the solubility limit of $Nd(OH)_3(s)$ in the absence of any ligand as reported by Neck et al. [45]. The blue solid line illustrate the detection limit of Nd(III) in the investigated conditions. The black symbols and solid line correspond to the experimental and calculated solubility of $Nd(OH)_3(s)$ in ISA media, as reported by Gugau [50].*

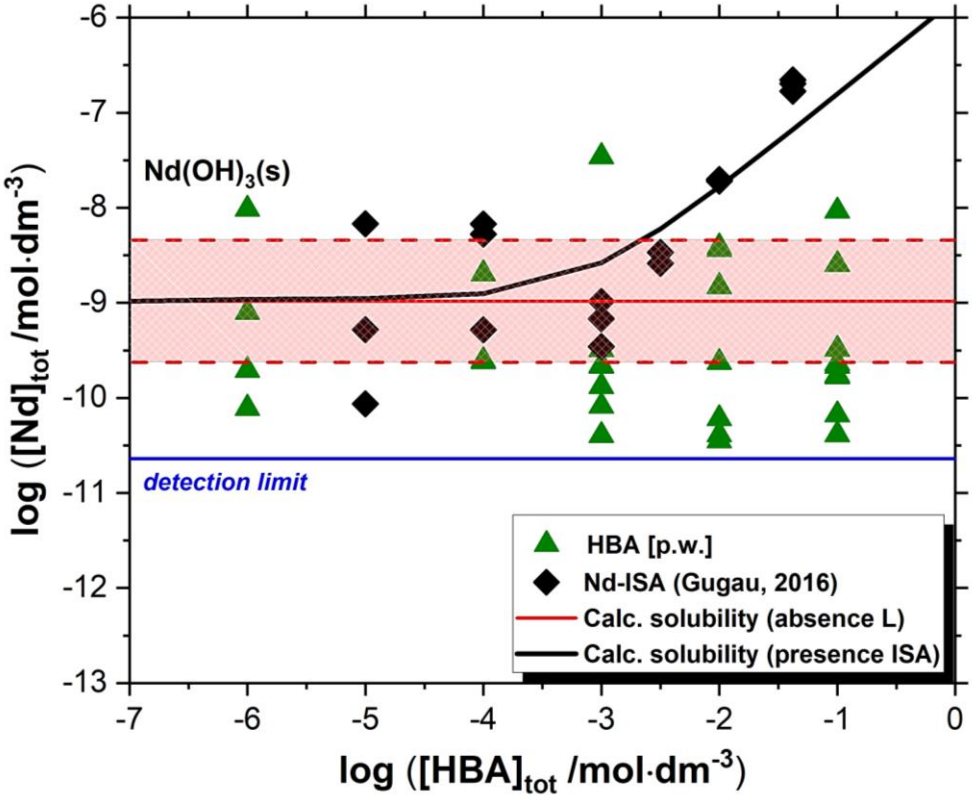

Figure 13. *Solubility measurement of $Nd(OH)_3(s)$ in cement pore water at pH = 12.5 and $[Ca]_{tot}$ = 20 mM with 10^{-6} M ≤ $[Lig]_{tot}$ ≤ 0.1 M in 3-hydroxybutyric acid (HBA) at t_{eq} ≤ 358 days. Data dispersion is due to scattering and does not represent a trend with time. Red lines (solid and dashed lines) show the solubility limit of $Nd(OH)_3(s)$ in the absence of any ligand as reported by Neck et al. [45]. The blue solid line illustrate the detection limit of Nd(III) in the investigated conditions. The black symbols and solid line correspond to the experimental and calculated solubility of $Nd(OH)_3(s)$ in ISA media, as reported by Gugau [50].*

3.2.4 Pu(III/IV) solubility

Figures 14 and 15 summarize the influence of GTA, HIBA and HBA on the solubility of PuO_2(ncr,hyd) buffered by HQ (pe + pH ≈ 9, Figure 14) and Sn(II) (pe + pH ≈ 2, Figure 15). The red area defined by solid and dashed lines represent the solubility limits for PuO_2(ncr,hyd) in absence of any organic ligand, calculated using thermodynamic data reported in Appendix, Table A-2 [63, 64], and the related data uncertainties. Black diamonds and solid lines show the experimental and calculated solubility of PuO_2(ncr,hyd) in the presence of ISA, according to the study of Tasi *et* al. [19].

Both redox buffered systems (HQ and Sn(II)) show no increase in the Pu concentration in the presence of proxy ligands. As in the case of Nd(III) solubility experiments, the organic ligands cannot overcome the Pu(IV) strong hydrolysis in HQ buffered systems. Even though there is no evidence that the investigated Pu in Sn(II) buffered media is in oxidation state +III, both +IV (as observed for HQ) and +III (as observed for Nd(III)) oxidation states are expected to remain unaffected in the presence of proxy ligands.

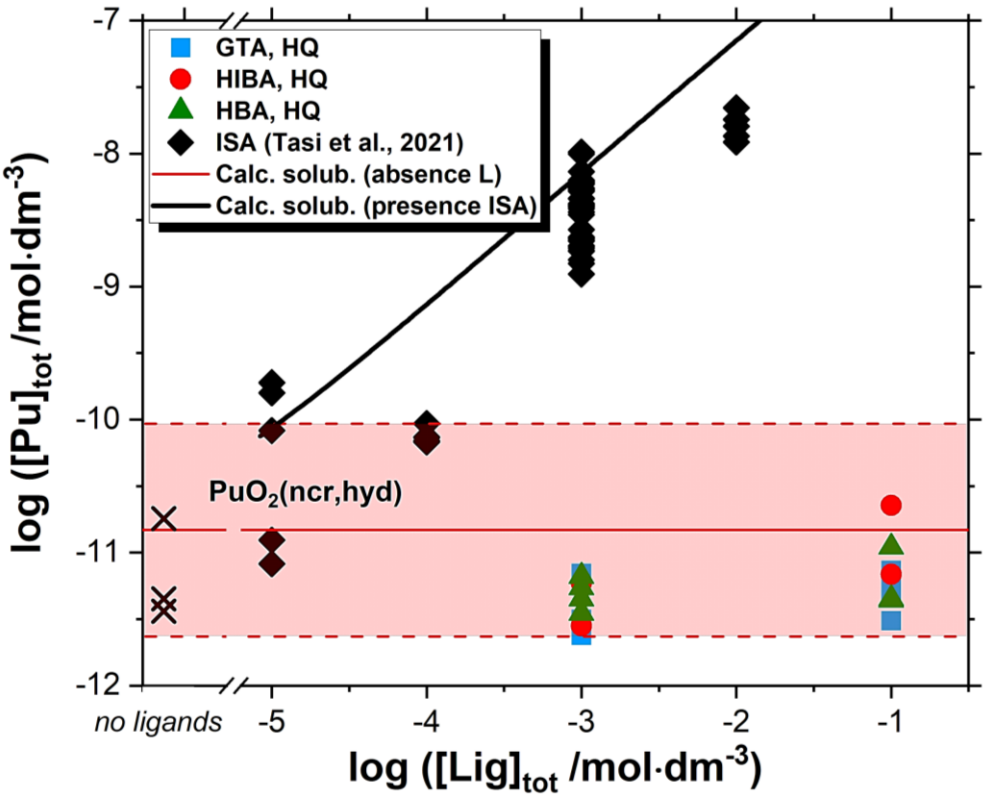

Figure 14. *Solubility of PuO_2(ncr,hyd) in the presence of GTA(■), HIBA(●) and HBA(▲) in the contact time of $t_{eq} \leq 223$ days. Redox condition was adjusted by HQ (pe + pH ≈ 9). Red solid and dashed red lines represent the solubility limit of PuO_2(ncr,hyd) and its uncertainty as calculated with thermodynamic data reported in the NEA-TDB and Neck et al. [63, 64]. Black crosses show the Pu concentration in ligand-free systems. Black diamonds and solid line illustrate the experimental and calculated solubility of PuO_2(ncr,hyd) in the presence of ISA [19].*

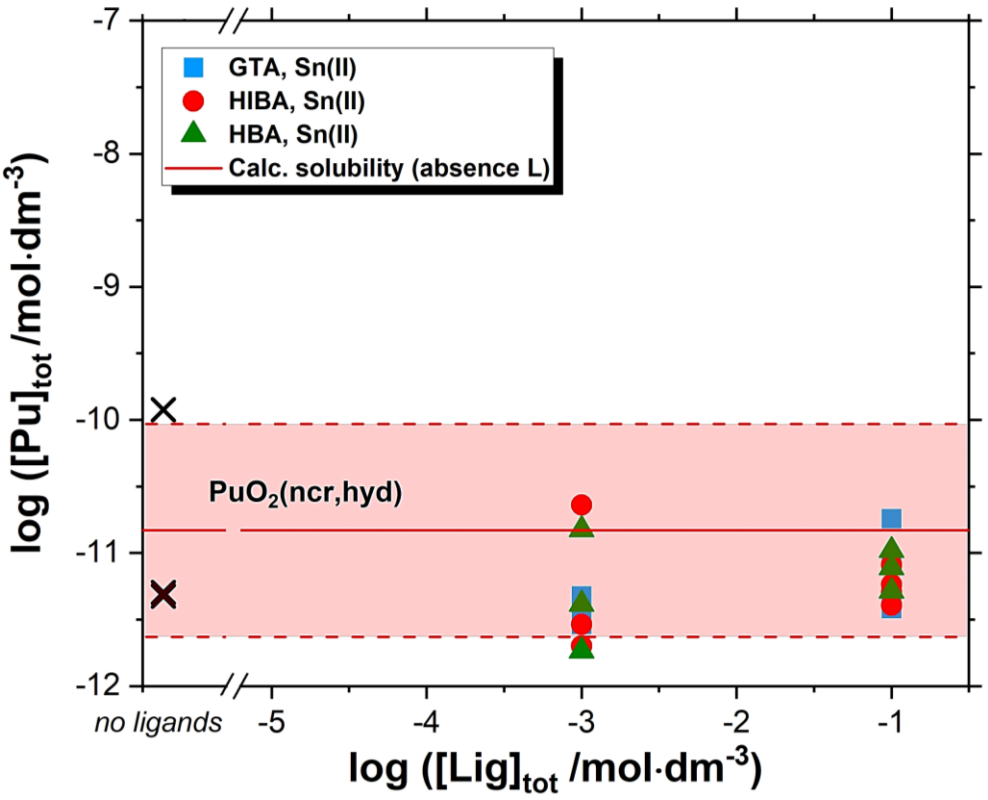

Figure 15. *Solubility of PuO_2(ncr,hyd) in the presence of GTA(■), HIBA(●) and HBA(▲) in the contact time of $t_{eq} \leq 223$ days. Redox condition was adjusted by $SnCl_2$ ($pe + pH \approx 2$). Red solid and dashed red lines represent the solubility limit of PuO_2(ncr,hyd) and its uncertainty as calculated with thermodynamic data reported in the NEA-TDB and Neck et al. [63, 64]. Black crosses relate to the Pu concentration in free-ligand system.*

No literature studies are available focusing on the complex reactions between Pu(IV) and the 3 assigned proxy ligands. Considering analogies in the oxidation state, some data are available for Th(IV). Tomat *et* al. investigated the Th(IV) interaction with various types of dicarboxylic acids (*e.g.* malonic acid, succinic acid, phthalic acid, maleic acid and glutaric acid) in acidic conditions (T = 20 °C, 1 M $HClO_4$ and $NaClO_4$) analyzed by potentiometric titration [159]. It was observed that the first four organic molecules establish chelate type complexes with the actinide, whereas glutaric acid forms 1:1 and 1:2 complexes ($Th(GTA)^{3+}$ and $Th(GTA)_2^{2+}$) as a monodentate ligand. Chelate formation was thus proposed for dicarboxylic acids $C_nH_{2n+2}(COOH)_2$ with $n \leq 3$. Complexation of Th(IV) with HIBA/HBA under acidic conditions in 1 M $NaClO_4$ and T = 20 °C were studied by Magon and co-workers via potentiometric titrations [160]. From their calculations, the authors stated that in the presence of HIBA, Th(IV) formed 1:1, 1:2, 1:3 and 1:4 complexes, whilst only 1:1, 1:2 and

1:3 complexes could be formed with HBA. These observations implied that the strength of the complex depends on the position of mono alcoholic groups in the carbon-chain. It was deduced that a mono hydroxyl group in α-position can participate in the chelation of the metal ion, whereas –OH in β-(and even γ-) position cannot [160]. Kobayashi and co-workers examined the Th(IV) and Zr(IV) complexation with various dicarboxylic acids in the pH range 1 – 10 in 0.5 M $NaClO_4$ solutions [161]. The authors proposed that GTA (as well as succinic and adipic acids) may coordinate Th(IV) as monodentate ligands, which is in good agreement with the report of Tomat *et* al. [159].

The studies discussed above underline the possible complex formation of the 3 proxy ligands with An(IV) under acidic media. However, similarly to the case of Nd(III), these complexation reactions cannot overcome the hydrolysis effect in alkaline conditions.

Similar solubility experiments with Pu(IV) (cement porewater in the degradation stage II) were conducted in the presence of ISA, where the solubility of PuO_2(ncr,hyd) considerably increased above log $[ISA]_{tot} \approx -5$ (see Figure 14, black diamonds) [19]. Drawing the conclusions from their observations, the authors determined that this enhancement was the consequence of the quaternary complex $CaPu(IV)(OH)_3(ISA_{-2H})(aq)$ formation. By using DFT in the same study, it was underlined that the deprotonated α- and δ-OH functional groups in ISA are able to contribute to the formation of stable chelate complex with Pu(IV). Considering that HIBA and HBA contain only one –OH group, it underpins that the number of hydroxyl groups on the organic molecule is a key factor in the context of generating stable complexes. On the other hand, since the acidity of the alcoholic groups of the aforementioned two organic ligands is relatively weaker than in the case of ISA, this could be another explanation that their complexation with hard Lewis acids like Pu(IV) will be most likely minor.

3.2.5 Solid phase characterization by XRD after solubility experiments

This section focuses on the characterization of $Ca(OH)_2$(cr), β-$Ni(OH)_2$(cr), $Nd(OH)_3$(s) and PuO_2(ncr,hyd) solid phases before and after the equilibration with cement pore water containing $[Lig]_{in}$ = 0.1 M. The equilibrated solid samples were characterized by XRD and are presented in Figures 16 – 19.

Figure 16 represents the XRD patterns of $Ca(OH)_2$(cr). The GTA and HIBA diffractograms are in excellent agreement with the initial $Ca(OH)_2$ reference (PDF 44-1481, in the JCPDS database [130]). However, next to the main peaks of $Ca(OH)_2$, the presence of a small fraction

of calcite ($CaCO_3$(cr), with main peaks at 2Θ = 29.4° and 31.7°; PDF 17-0763) was observed in all systems. A small new peak at 2Θ ≈ 28.35° emerged in the diffractogram of the Ca(II)-HBA system, which suggests the possible formation of a secondary phase as impurity. This hypothesis is in line with the slight decrease in solubility observed at $[HBA]_{tot}$ = 0.1 M (see Figure 7).

Figure 17 illustrates the XRD pattern for β-$Ni(OH)_2$(cr) before and after the equilibration with GTA, HIBA and HBA in 0.1 M ligand concentration. In general, main patterns show a good agreement with the original β-$Ni(OH)_2$(cr) (PDF 14-0117). The pattern collected for the Ni(II)-GTA system shows an additional peak at 2Θ = 31.7°, which was not reported in any previous article involving Ni(II)-organic compounds. The crystal formation of Ni(II) in the presence of various dicarboxylic acids (glutaric acid, oxalate) were examined via XRD [162-164]. New solid phases are expected to form by the aforementioned organic molecules, although the preparation of the Ni(II)-Ligand solid phases were performed in acidic media and under hydrothermal conditions. The signal peak of 2Θ = 31.7° in the Ni(II)-GTA system may correspond to a solid phase comprising the organic ligand but not Ni(II), although this hypothesis remains to be further validated.

The XRD diffractograms of the $Nd(OH)_3$(s) displayed in the Figure 18 correspond to the solid phases equilibrated in 0.1 M GTA, HIBA and HBA. Figure 18 shows that XRD patters are generally in good agreement with the reference solid phase $Nd(OH)_3$(cr) (PDF 83-0235), although in case of HIBA and HBA another peak at 2Θ = 19.24° is manifested. This intense signal in both systems could not be identified in any scientific report. Böszörményi *et* al. [165] studied the formation of Nd(III)-GLU solid phases in alkaline conditions, and proposed the formation of the following solid structures: $Nd(GLU_{-H})(OH)\cdot 2H_2O$(cr) and $CaNd(GLU_{-H})(OH)_3\cdot 2H_2O$(cr). However, these observations cannot be compared to the interaction of Nd(III)-HIBA/HBA in the present work, because GLU forms stronger complexes thanks to various –OH groups, in contrast to the HIBA and HBA (both with only one –OH group). Also, the authors prepared the solid phases in largely oversaturated conditions, for instance $[NaGLU]_0$ = 0.5 M and $[Nd(III)]_0$ = 0.5 M. In an experimental study with Nd(III)-GLU in 0.1 – 5.0 M NaCl and 0.1 – 3.5 M $CaCl_2$ with 9 ≤ pH ≤ 13 and –6 ≤ log ($[GLU]_{tot}$ /M) ≤ –2, Rojo and co-workers analyzed solid structure of Nd(III)-GLU at $[GLU]_{tot}$ = 10^{-2} and 10^{-3} M in 0.1 M NaCl and 0.25 M $CaCl_2$ solutions [127]. Based on the solubility increase in the presence of Ca content, it was speculated that this enhancement can be attributed to the formation of Ca(II)-Nd(III)-GLU aqueous complexes in $CaCl_2$ media. Rojo and co-workers confirmed the XRD pattern of $Nd(OH)_3$(s) is predominated in all systems.

The authors speculated as well that even though the formation of amorphous solid phase (Ca(II)-Nd(III)-GLU) cannot be affirmed by XRD, it may have formed similarly to the one reported by Böszörményi *et* al. [165].

The XRD patterns of PuO_2(ncr,hyd) solid phases, separated from batch solubility experiments containing log $[Lig]_{tot}$ = 0.1 M and HQ, are shown in the Figure 19. The figure shows also the patterns reported for the same solid phase PuO_2(ncr,hyd) in ligand-free systems, as reported by Tasi *et* al. XRD (see Figure 19, black diffractogram) [19]. Due to the similar solubility impact observed for both HQ and Sn(II) buffered systems (see Section 3.2.4), no characterization of the solid phase was conducted for Sn(II) systems. Besides the well-defined patterns of PuO_2(cr), reflections of $Ca(OH)_2$(cr) were noted in all 3 proxy ligand systems. This can be argued by the use of cement pore water in the degradation stage II, where the pore water composition is controlled by the solubility of portlandite (saturation index (SI) ≈ 0). Therefore, the precipitation of $Ca(OH)_2$(cr) under various minor changes in the boundary conditions (*e.g.* temperature, pH etc.) can occur. Moreover, next to the pattern of PuO_2(ncr,hyd) and $Ca(OH)_2$(cr), additional reflections emerged in all systems, which could not be assigned to any inorganic Pu / Ca solid phase. XRD analysis of the dried supernatant (5 mL) in Ar environment showed almost identical patterns (see Appendix, Figure A-1 − A-3). Considering the given Ca and Pu concentrations in the supernatant ($[Ca]_{tot}$ ≈ 20 mM and $[Pu]_{aq}$ ≈10^{-11} M), the patterns may correspond to binary solid phases of Ca with the individual organic ligands.

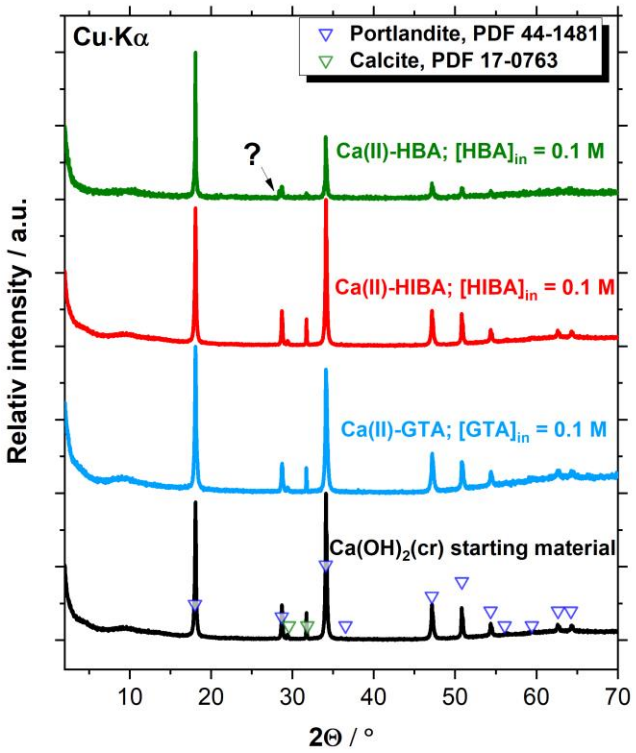

Figure 16. *XRD patterns of Ca(II) in the absence and the presence of organic ligands after equilibration at* $[Lig]_{in}$ *=0.1 M. Purple and green inverted triangles represent the peak positions of* $Ca(OH)_2$ *(PDF 44-1481) and Calcite (PDF 17-0763), respectively.*

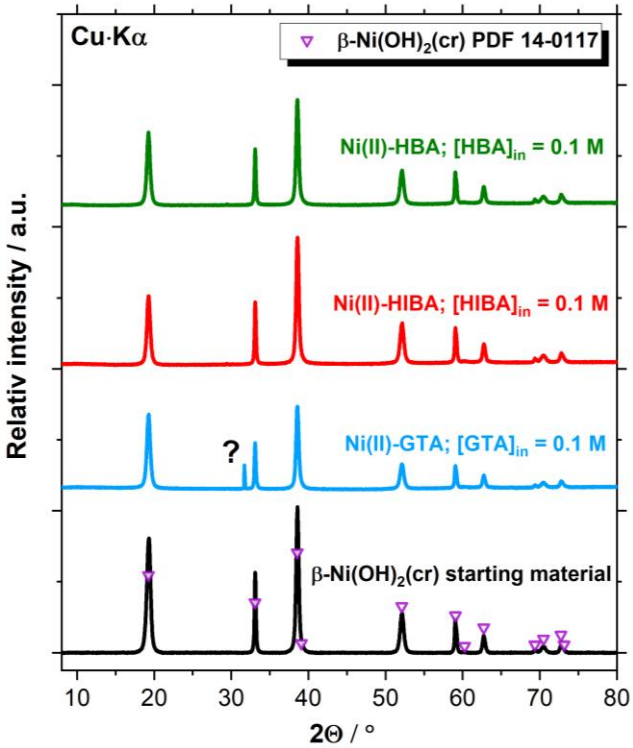

Figure 17. *XRD patterns of Ni(II) in the absence and the presence of organic ligands after equilibration at* $[Lig]_{in}$ *=0.1 M. Purple inverted triangles represent the peak positions of β-*$Ni(OH)_2$*(cr) (PDF 14-0117).*

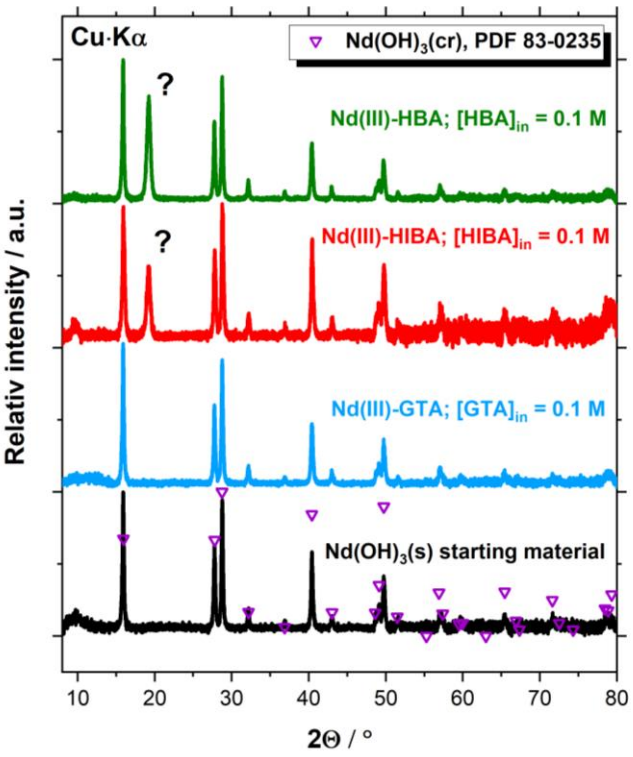

Figure 18. *XRD patterns of Nd(III) in the absence and the presence of organic ligands after equilibration at* $[Lig]_{in}$ *=0.1 M. Purple inverted triangles represent the peak positions of* $Nd(OH)_3(s)$ *(PDF 83-0235).*

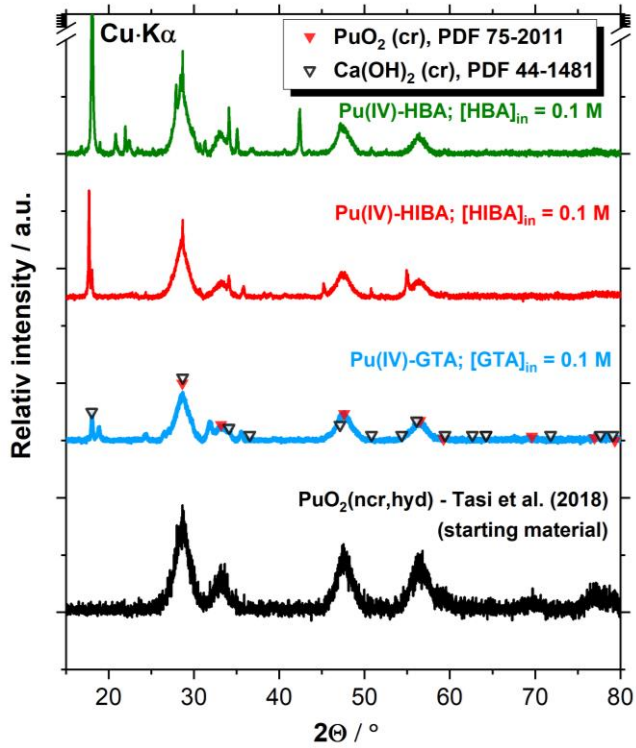

Figure 19. *XRD patterns of Pu(IV) in the absence (reported by Tasi et al. [65]) and the presence of organic ligands after equilibration at* $[Lig]_{in}$ *=0.1 M., in all cases containing HQ as redox buffer. Red and black inverted triangles represent the peak positions of* $PuO_2(cr)$ *(PDF 75-2011) and portlandite* $(Ca(OH)_2(cr)$*, PDF 44-1481).*

3.2.6 Quantum chemical evaluations for the Pu(IV)-OH-Ligand systems

In order to better understand the interaction of the proxy ligands with Pu(IV), DFT calculations were conducted by Robert Polly of KIT-INE to assess the structures of the Pu(IV)-OH-Ligand ternary complexes (Ligand = GTA, HIBA and HBA). For comparative purposes, structural data collected using similar theoretical calculations for the system Pu(IV)-OH-ISA [18] are also summarized in this chapter. The Ca^{2+} ion was ignored during calculations due to the incapacity or the proxy ligands to increase the solubility of Pu(IV) (Figure 15), and thus the unlikely formation of ternary complexes Ca(II)-Pu(IV)-OH-Ligand. Considering the lack of information about the stoichiometry of the hypothetical Pu(IV)-OH-Ligand complexes, these complexes were tentatively proposed as $[Pu(OH)_4Ligand]^{n/m}$ (with n = –2 for GTA and m = –1 for HIBA and HBA). When considering the deprotonated alcoholic functional groups of HIBA and HBA within the structural optimization, spontaneous protonation of alcohol groups by adjacent water molecules occurred, which resulted in the formation of hydroxide. This outcome, obtained for HIBA and HBA but not observed for ISA, suggests that two or more alcoholic functional groups are required for the formation of stable complexes with Pu(IV) under alkaline conditions [18]. The optimized structures of $[Pu(OH)_4Ligand]^{n/m}$ are illustrated in Figure 20, whilst the calculated Pu-O distances obtained by using DFT and DFT + COSMO in the present work or in the report of Tasi and co-workers [19] are summarized in Table 6. The comparison of def2-SVP/ecpIVmwb-avdz and def2-TZVPP/ecpIVmwb-avtz basis sets for $[Pu(OH)_4GTA]^{2-}$ resulted only in minor differences. Meaning, that the small def2-SVP basis set provides already almost converging results.

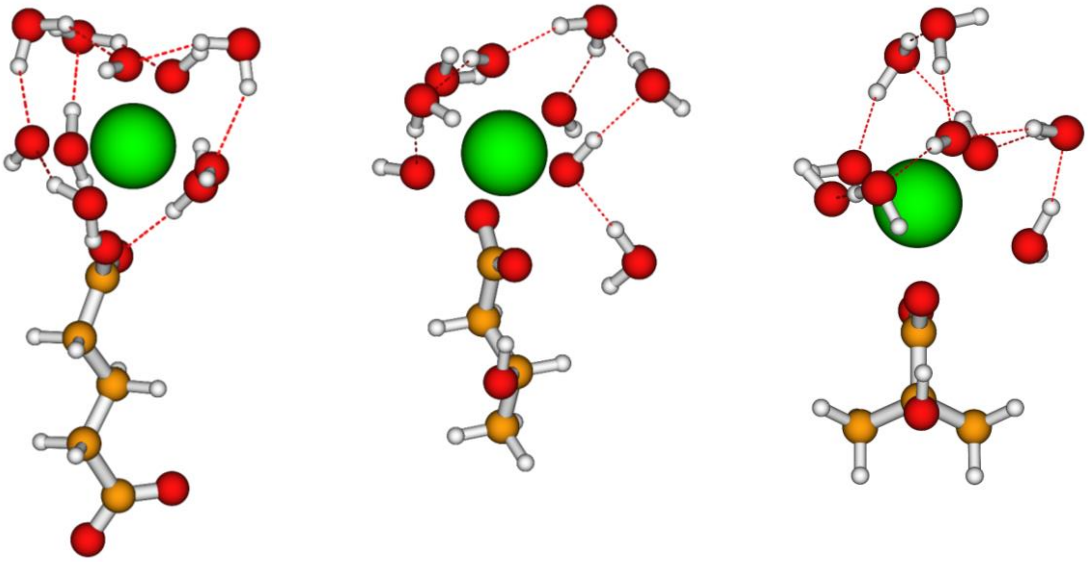

Figure 20. *Theoretical structure of* $[Pu(OH)_4Ligand]^{n/m}$ *complexes (Ligand = GTA (left), HBA (middle) and HIBA (right)) by DFT with n = –2 for GTA and m = –1 for HIBA and HBA. Green, red, orange and grey orbs represent Pu, C, O and H atom, respectively.*

Table 6. *DFT(BP86/de2-SVP/ecpIVmwb-avdz) estimation of Pu-O distances (in pm) for the complexes $[Pu(OH)_4Ligand]^{n/m}$ (with n = –2 for GTA and m = –1 for HIBA and HBA) and $[Pu(OH)_3ISA_{-H}]^-$, as optimized in present work or in the literature [18]. Column 2 (in brackets) shows the corrected results for $[Pu(OH)_4GTA]^{2-}$ using the def2-TZVPP(H, O, C) and ecpIVmwb-avtz (Pu) basis sets.*

$[Pu(OH)_4GTA]^{2-}$		**$[Pu(OH)_4HBA]^-$**		**$[Pu(OH)_4HIBA]^-$**		**$[Pu(OH)_3ISA_{-H}]^-$**	
Bond	DFT / DFT + COSMO	Bond	DFT / DFT + COSMO	Bond	DFT / DFT + COSMO	Bond	DFT + COSMO
Pu-OH^-	223 (223) / 225	Pu-OH^-	219 / 222	Pu-OH^-	225 / 225	Pu-OH^-	226 / 227
Pu-OH^-	231 (231) / 230	Pu-OH^-	225 / 224	Pu-OH^-	225 / 227	Pu-ISA(–C_2O^-)	231 / 230
Pu-OH^-	233 (233) / 234	Pu-OH^-	229 / 226	Pu-OH^-	228 / 228	Pu-OH^-	233 / 233
Pu-OH^-	240 (239) / 238	Pu-OH^-	229 / 231	Pu-OH^-	228 / 229	Pu-OH^-	236 / 234
Pu-GTA (–COO^-)	247 (247) / 243	Pu-HBA (–COO^-)	255 / 252	Pu-HIBA (–COO^-)	248 / 253	Pu-ISA (–COO^-)	239 / 240
Pu-OH_2	259 (259) / 253	Pu-HBA (–COO^-)	263 / 259	Pu-HIBA (–COO^-)	266 / 257	Pu-OH_2	250 / 251
Pu-OH_2	259 (261) / 263	Pu-OH_2	274 / 266	Pu-OH_2	268 / 258	Pu-OH_2	260 / 259
Pu-OH_2	275 (268) / 269	Pu-OH_2	377 / 378	Pu-OH_2	369 / 369	Pu-OH_2	267 / 267

Short distances were noticed in the $[Pu(OH)_4Ligand]^{n/m}$ complex for the Pu(IV)-OH^- bond (average 228/228 pm), compared to the longer distance for the Pu-Ligand(-COO^-) binding (249/250 pm) and Pu-OH_2 (260/255 pm) in $[Pu(OH)_4GTA]^{2-}$. Analogous observation was made during the comparison between the data points of Pu(IV)-OH^- and averaged distances of Pu-OH_2 (271/262 and 372/373 pm) in $[Pu(OH)_4HIBA/HBA]^-$. This decrease can be attributed to the increased electron density around Pu^{4+} by O-groups (*e.g.* hydroxide ions: –OH, alcoholate groups: –C*n*-O^- and carboxylic functional groups: –COOH), which was validated in previous study of Pu-OH-ISA system [18].

As shown in Table 6, the complexation of GTA, HIBA and HBA to Pu(IV) takes place with one carboxylate functional group, whereas the alcoholic functional groups do not participate, neither in the deprotonated nor in the protonated form. This supports the weak complexation capacity of both HIBA and HBA as compared to ISA. In addition, the Table 6 illustrates that the distance between Pu and (–COO^-) in the case of Pu-ISA [18] is significantly shorter than in the complexes with GTA, HIBA and HBA. These DFT (+ COSMO) calculations confirm the weak complexation behaviour of the proxy ligands, in line with the results obtained in the solubility experiments with PuO_2(ncr,hyd), but also with ($Ca(OH)_2$(cr), β-$Ni(OH)_2$(cr) and $Nd(OH)_3$(s). These organic molecules form mostly (weak) binary complexes in acidic to weakly alkaline pH conditions.

3.3 Sorption studies

This section of the PhD project was dedicated to provide experimental results about different type of sorption experiments with corresponding Portland cement under hyperalkaline conditions (*i.e.* $[Ca]_{tot} \approx 20$ mM, pH = 12.5).

Therefore, these different uptake experiments can be separated into 3 main parts:

1. Experimental results and data evaluation of the sorption in the binary system cement-proxy ligands (Section 3.3.1)
2. Experimental results and data evaluation of the sorption in the binary system cement-RN (Section 3.3.2 – 3.3.4)
3. Experimental results and data evaluation of the sorption in the ternary system cement-RN-proxy ligands. (Section 3.3.2 – 3.3.4)

3.3.1 Sorption experiments in the binary system cement-proxy ligands

The sorption of proxy ligands (GTA, HIBA, and HBA) onto cement was investigated by measuring the evolution of the total organic content (NPOC) in the aqueous phase. Additional sorption experiments were conducted with ^{14}C-labelled GTA.

For the experiments with inactive ligands, the leaching of organic impurities from HCP can increase the NPOC concentrations in the porewater at various S:L ratio. For this reason, all the raw NPOC data were corrected according to the recommendation of Tasi and co-workers [14] by utilizing Equation (8). This expression was derived using the same HCP powder as in the present study.

$$NPOC_{impurities}\,(ppm) = 0.036 \cdot S{:}L\ ratio\ (g \cdot dm^{-3}) + 1.22\ (ppm) \quad (8)$$

3.3.1.1 Sorption experiments with inactive GTA, HIBA and HBA

Figure 21 shows the uptake of the GTA, HIBA and HBA ligands by HCP at $-6 \leq \log([Lig]_{in}/M) \leq -1$ and S:L = 4 g·dm^{-3}. The figure shows sorption data either with or without applying filtration of the samples. The red area represents the uncertainty of the NPOC values, calculated as 2σ at each ligand concentration. After 306 days of monitoring, the measured ligand concentrations in the aqueous phase are in agreement with the initial concentrations, suggesting no or only weak sorption of the investigated proxy ligands at S:L = 4 g·dm^{-3} on HCP.

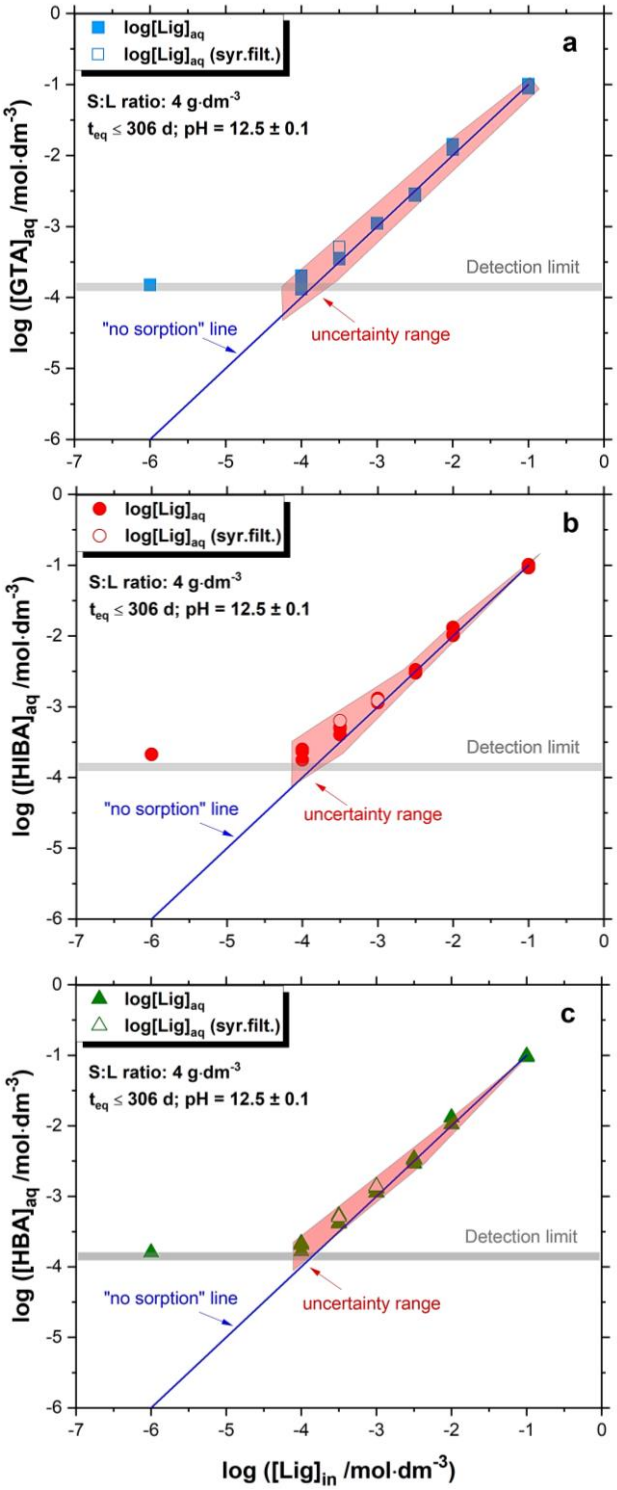

Figure 21. *Experimentally measured concentration of glutaric acid (GTA, a), α-hydroxyisobutyric acid (HIBA, b), 3-hydroxybutyric acid (HBA, c) as a function of initial ligand concentration. Sorption experiments at S:L = 4 g·dm^{-3} have been studied for $t_{eq} \leq 306$ days. Grey solid line represents the detection limit of the NPOC method for the specific conditions of the experiment. The blue solid line named as the "no sorption" line depicts identical initial and aqueous phase concentration of the ligand. The red shaded area shows the associated uncertainty range, calculated as two times the standard deviation of the data points (2σ) at each concentration level.*

Figure 22 summarizes the results using fixed $[Lig]_{in}$ concentrations (10^{-3} M) and increasing S:L ratio from 1 to 50 g·dm^{-3}. The red area in the figures illustrates the initial concentration and its uncertainty, calculated as two times the standard deviation of the average value. Figure 22 includes also data on the uptake of acetate by hardened cement paste as reported by Wieland *et* al [87] (black solid line). For GTA, the blue line shows the sorption calculated using the one-site Langmuir isotherm described below. The results show that the concentration of HIBA and HBA in the aqueous phase decreases only at S:L = 50 g·dm^{-3}, whereas in case of GTA a decrease is observed already at S:L ≈ 10 g·dm^{-3}. This indicates that the latter organic molecule has the highest affinity for the HCP surface.

The distribution ratios (R_d /m^3·kg^{-1}) of the 3 proxy ligands were calculated by using the Equation (1), from which the R_d values of GTA, HIBA and HBA were quantified as (1.0 ± 0.5)·10^{-2}, (2.2 ± 1.3)·10^{-3} and (1.6 ± 0.9)·10^{-3} m^3·kg^{-1}, respectively. These values are higher than those reported by Wieland *et* al. for formate and acetate (R_d(formate) = 10^{-3} m^3·kg^{-1}, R_d(acetate) = 3.3·10^{-4} m^3·kg^{-1}) at pH = 13.3 and S:L = 333.3 g·dm^{-3} [87]. Such differences can be correlated with the differences in the surface charge of HCP at pH = 12.5 (this work) and pH = 13.3 [87], but also with the presence of a second functional group in all the proxy ligands investigated in this work.

As a consequence of the weak retention of HIBA and HBA, only the sorption data determined for GTA were fitted with the one-site Langmuir isotherm as described in Equation (3). Langmuir isotherms (one or two sites) have been frequently used to model the uptake of ISA by HCP [26, 89, 94, 166], providing a satisfactory empirical description of the uptake at various $[Lig]_{aq}$ and S:L ratios. The different datasets available for GTA were simultaneously fitted using Equation (9), which is the combination of the Equation (2) and (3).

$$[Lig]_{ads}(\text{mol kg}^{-1}) = ([Lig]_{in} - [Lig]_{aq})\cdot V(\text{porewater, dm}^3)\cdot m(\text{cement, kg})^{-1}$$
$$= K\cdot q\cdot[Lig]_{aq}\cdot(1 + K\cdot[Lig]_{aq})^{-1} \quad (9)$$

Using the calculated $[Lig]_{ads}$ and the measured $[Lig]_{aq}$, one-site Langmuir isotherm was fitted using of nonlinear regression.

The calculated adsorption affinity constant (K) and adsorption capacity (q) for GTA at constant inactive ligand concentration of $[GTA]_{tot}$ ≈ 10^{-3} M, active ligand concentration of $[^{14}C\text{-GTA}]_{in}$ ≈ 10^{-7} M (see Section 3.3.1.2) and various solid-to-liquid ratio (1 ≤ (S:L /g·dm^{-3}) ≤ 50) are

$$K = (22.5 \pm 6.1)\ \mathrm{dm^3 \cdot mol^{-1}}$$
$$q = (0.45 \pm 0.12)\ \mathrm{mol \cdot kg^{-1}}$$

The one-site Langmuir isotherm with the independent variable was fitted on the datapoints of GTA (blue solid line, Figure 22).

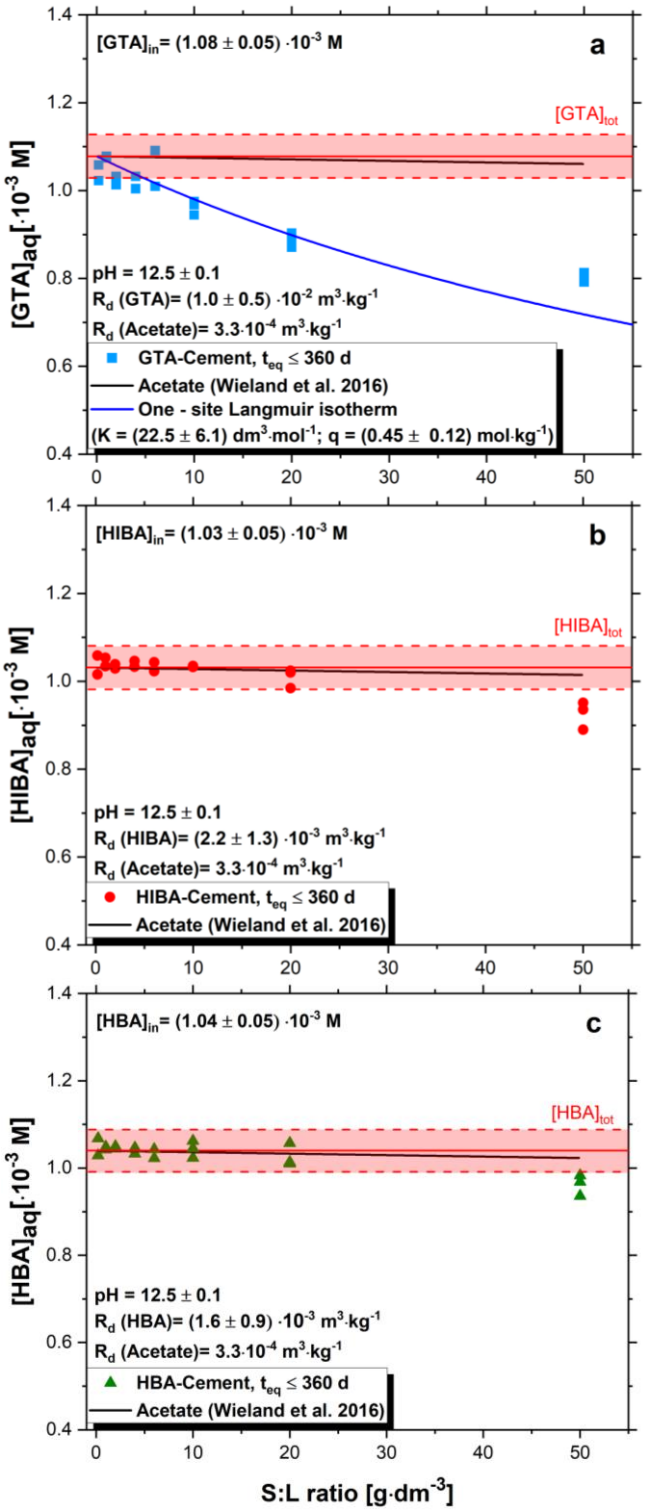

Figure 22. *Uptake of (a) GTA, (b) HIBA and (c) HBA by HCP at the initial ligand concentration of* $[Lig]_{in} \approx \cdot 10^{-3}$ *M with S:L ratio: 0.2, 1, 2, 4, 6, 10, 20 and 50* $g \cdot dm^{-3}$ *after contact time of 360 days. Red solid and dash line represent the initial concentration of the proxy ligands along with their uncertainty (2σ). Black curve illustrate the sorption line of the acetate by cement reported by Wieland et al. [87] and blue curve of one-site Langmuir isotherm calculated by Equation (9).*

3.3.1.2 Sorption experiments with ^{14}C-labelled and GTA

The uptake of ^{14}C-labelled GTA at $[^{14}C\text{- GTA}]_{in} = 10^{-7}$ M and $15 \leq (S{:}L\ /g{\cdot}dm^{-3}) \leq 50$ for $t_{eq} \leq 82$ days is shown in Figure 23. The measured values remain constant after the first sampling at $t_{eq} = 69$ days, which suggests that the equilibrium was reached within this timeframe. The Figure 23 includes the fitted one-site Langmuir isotherm, with $K = (22.5 \pm 6.1)$ $dm^3{\cdot}mol^{-1}$ and $q = (0.45 \pm 0.12)$ $mol{\cdot}kg^{-1}$ as calculated from Equation (9) in Section 3.3.1.1. The corresponding R_d value was estimated according to Equation (1), and resulted as $R_d = (1.3 \pm 0.5){\cdot}10^{-2}$ $m^3{\cdot}kg^{-1}$.

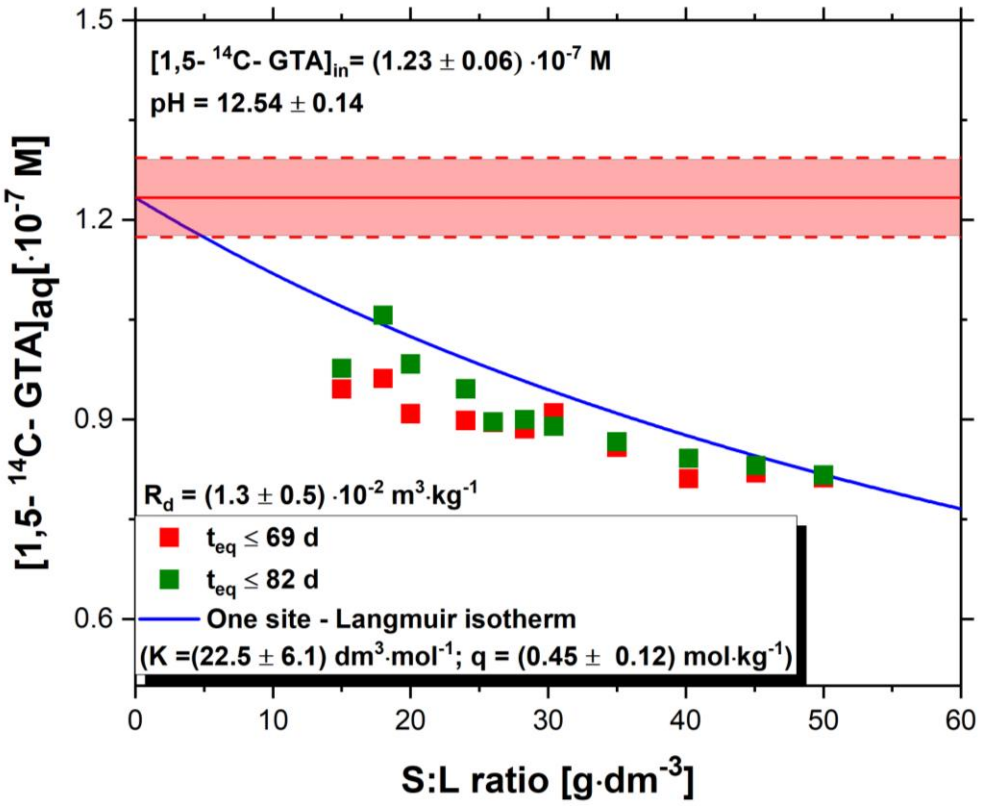

Figure 23. *^{14}C labelled GTA-cement sorption reaction at $[1,5\text{-}^{14}C\text{-GTA}]_{in} = 1.23{\cdot}10^{-7}$ M ligand concentration with S:L ratio: 15, 18, 20, 24, 26, 28, 30, 35, 40, 45 and 50 $g{\cdot}dm^{-3}$ in contact time of 69 and 82 days. Red solid and dash line represent the initial concentration of the organic molecule along with it is uncertainty (2σ) and the blue curve the calculated one-site Langmuir isotherm derived from Equation (9).*

In order to prove that evaluated one-site Langmuir-isotherm is sufficient to describe the uptake of GTA onto cement paste, additional sorption experiments (Figure 24) in the combination of inactive and ^{14}C-labelled GTA at S:L = 20 $g{\cdot}dm^{-3}$ were implemented. In this

case, inactive GTA solutions were systematically spiked with ^{14}C-labelled GTA at [^{14}C-GTA]$_{tot}$ ≈ 10^{-7} M. Furthermore, datapoints from inactive (Figure 22) and radioactive (Figure 23) GTA sorption measurement were added to Figure 24 of log [Lig]$_{ads}$ as the function log [Lig]$_{aq}$. Figure 24 shows that the calculated sorption isotherm is in excellent agreement with the three datasets obtained in this work.

Comparing the gained *K* and *q* for GTA in the present work with those reported for polyhydroxycarboxylic acids (ISA and GLU), the adsorption capacity of cement paste for GTA is slightly higher than the binding capacity of HCP for ISA considering the two sorption sites, *i.e.* q_{tot}(ISA) = q_1 + q_2 = (0.35 ± 0.02) mol·kg^{-1} [94] (HCP in degradation stage II, pH ≈ 12.5) and q_{tot}(ISA) = (0.27 ± 0.02) mol·kg^{-1} [89] (HCP in degradation stage I, pH ≈ 13.3). In the study of Glaus *et* al. [167], higher adsorption capacity was reported for the system HCP-GLU (q_{tot}(GLU) = (0.7 ± 0.3) mol·kg^{-1}), which however overlaps with the value determined in this work considering the corresponding uncertainties. The adsorption affinity constant determined for GTA is unequivocally lower than the values reported for ISA and GLU on the stronger binding sites of [89] (pH ≈ 13.3), K_1(ISA) = (2510 ± 500) dm^3·mol^{-1} [94] (pH ≈ 12.5) and K_1(GLU) = (2 ± 1)·10^6 dm^3·mol^{-1} [167] (pH ≈ 13.3). Nonetheless, the *K*(GTA) value is moderately higher than *K*(ISA) for the weaker binding site of HCP (K_2(ISA) = (12 ± 4) dm^3·mol^{-1} [89], K_2(ISA) = (12 ± 2) dm^3·mol^{-1} [94]). Yet again, these results corroborate the weak sorption of GTA, HIBA and HBA onto HCP as compared to ISA and GLU.

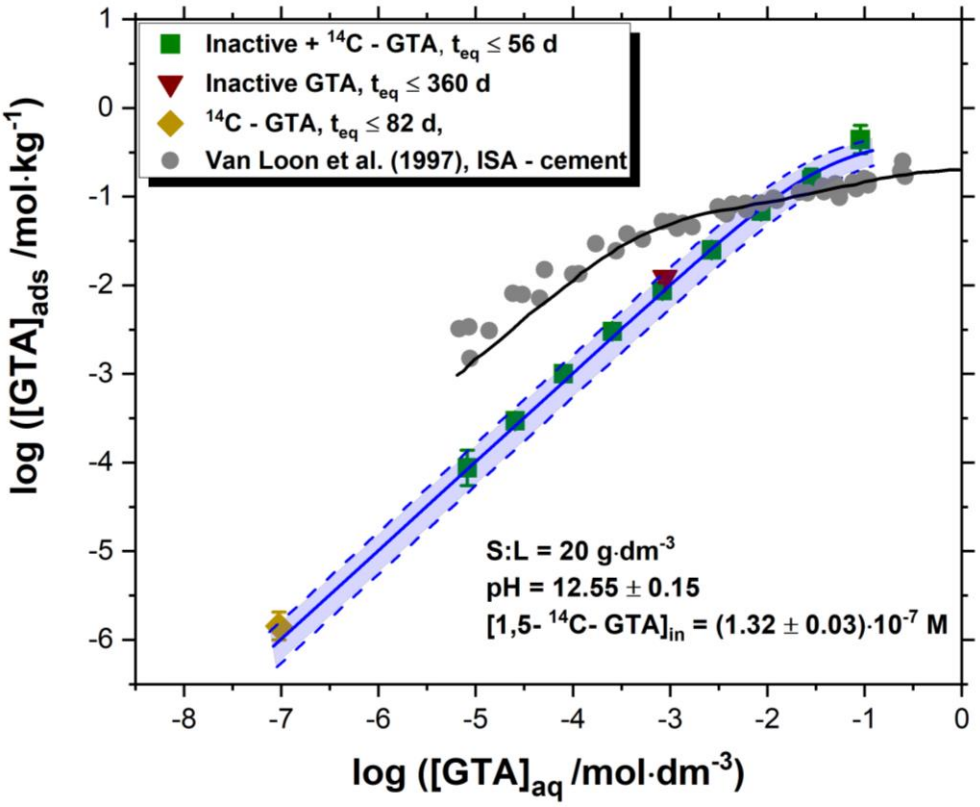

Figure 24. *Uptake of ^{14}C labelled GTA in the presence of inactive GTA as carrier by cement in equilibrium at [1,5-^{14}C-GTA]$_{in}$ = 1.32·10^{-7} M ligand concentration after the contact time of 56 days is shown along with the results of inactive GTA (brown triangle) and active GTA (yellow diamond) from previous experiments at given S:L ratio. Blue solid and dashed lines corresponding to the calculated one-site Langmuir isotherm and its uncertainty of 2 times standard deviation, respectively. Sorption datapoints and evaluated two-site Langmuir isotherm of HCP-ISA in greyish circle and black line are shown regarding the study of Van Loon et al. [89].*

3.3.1.3 Measurements of the zeta potentials

The evolution of the zeta potential (ζ) of suspended colloidal cement particles with increasing ligand concentration was quantified via electrophoretic mobility in the range –4 ≤ log ([Lig]$_{tot}$ /M) ≤ –1 at S:L = 4 g·dm^{-3} (see Figure 25). The grey area in the figures illustrates the range of zeta potentials measured for cement CEM I in the degradation stage II [71, 92, 94]. Black symbols show the evolution of the zeta potentials in the presence of ISA for an analogue system as measured by Tasi and co-workers [94]. Solid yellow line shows the surface coverage of cement surface calculated using the sorption isotherm described above.

For HIBA and HBA systems, a slight decrease of ζ potentials can be noticed only at $[Lig]_{tot} \geq 10^{-1.5}$ M. This observation can be correlated with the weaker sorption observed for these ligands (see Figure 22). In the case of GTA, the ζ potential starts decreasing from log $([GTA]_{tot}$ /M) ≥ –3, and attains the isoelectric point (IEP) at log $([GTA]_{tot}$ /M) ≈ –1.5. Zeta potentials further decreased to ζ ≈ –3.55 mV until log $([GTA]_{tot}$ /M) = –1. These outcomes confirm that the GTA has a stronger affinity to sorb onto the cement than the HIBA and HBA. The evolution of surface charge in GTA system correlates with the evolution of the surface coverage of cement with increasing GTA concentration, which was calculated with the one-site Langmuir isotherm using Equation (9) from Section 3.3.1.1.

Comparing the results obtained for all 3 proxy ligands with the ISA, it is quite obvious that the decrease of zeta potential is more significant in the presence of ISA than with the proxy ligands (IEP is reached in the presence of ISA at log $([ISA]_{tot}$ /M) = –2.5). Consequently, it is evident that the sorption of GTA, HIBA and HBA on Portland cement is weaker than ISA.

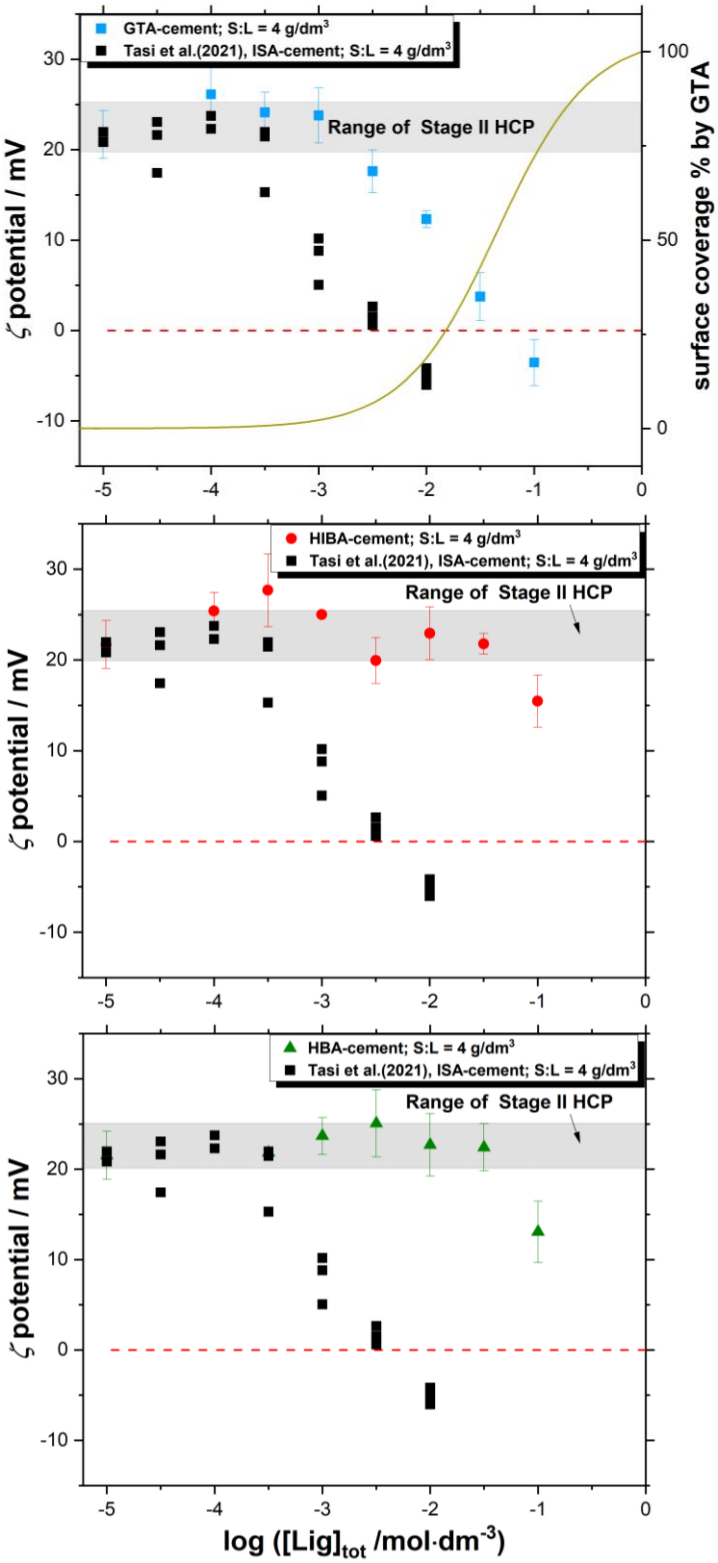

Figure 25. *Zeta potential on suspended colloidal cement particles in the presence of GTA (■) HIBA (●) and HBA (▲) at cement powder of S:L = 4 g·dm^{-3} after contact time of t_{eq} = 14 d. Uncertainty was calculated according to standard deviation 2σ. Grey area presents the Portland cement zeta potential range in ligand-free systems [71, 92]. Black squares represents datapoints of Cement-ISA as reported by Tasi et al. [94]. Solid yellow line in GTA plot depicts the surface coverage of the cement solid phase by GTA calculated from the one-site Langmuir isotherm.*

3.3.1.4 Comparison of the experimental R_d values with the literature data.

The Table 7 summarizes the R_d values determined in this work for GTA, HIBA and HBA, including also R_d values reported in the literature for other organic ligands containing different functional groups, such as EDTA, GLU, ISA, formic acid, acetic acid, ethanol and methanol. The table provides also information on the cement degradation stage that was studied in the given publication. Currently, only limited sorption reports with low molecular weight organic molecules are available under alkaline conditions [6, 87, 89, 167-169]. On the basis of the R_d values summarized in Table 7, the influence of various fundamental experimental parameters *i.e.* S:L, $[Lig]_{tot}$ etc. is considered. This brief summary provides also insight on the strength of Cement-Ligand bonding according to the type and number of functional groups.

Wieland and co-workers [87] studied the uptake of methanol, ethanol, formic acid, acetic acid, formaldehyde and acetaldehyde by Portland cement under alkaline conditions. The pH of the pore water after 1 h of hydration was in the range of 12.4 – 12.7, whilst after 28 and 390 d ranged within 12.7 – 13.3. The increase of the pH within 28 and 390 d was attributed to the release of NaOH and KOH from the cement to aqueous phase. The authors reported also the increase in Ca concentration, which was not found in the present work. Wieland *et* al. suggested that the increase of Ca concentration in the pore water occurred due to the dissolution of Portland cement. The uptake of the organic compound investigated by these authors followed the order: formate > acetate ~formaldehyde ~acetaldehyde > methanol > ethanol. Table 7 highlights that GTA, HIBA and HBA sorb stronger on the cement surface than formate, methanol, acetate and ethanol, yet not as strongly as ISA or GLU [89, 94]. For instance, in the sorption of ISA reported by Tasi and co-workers [94], a decrease in the ligand concentration at $[ISA]_{tot} = 10^{-3}$ M was observed already at the lowest S:L ratio (2 $g \cdot dm^{-3}$). Even compared to EDTA, which is a strong chelating agent, ISA shows a significantly stronger uptake by HCP in the degradation stages I and III [93]. From this observation, it can be concluded that the number of alcoholic and carboxylic functional groups have a big impact on sorption of the organic materials on HCP. Furthermore, previous studies showed that the sorption of the organic ligands was enhanced in the cement degradation stage II compared to the degradation stage I. This observation is likely related to the positively charged surface in the cement degradation stage II, where the negatively charged organic functional groups expectedly sorb stronger than on the negatively charged surface of stage I. Considering the high concentration of Ca(II) in the pore water of the degradation stage II of cement (≈ 20

mM) as well as in the surface of C-S-H, the uptake of anionic species by cement is expected to occur through Ca bridges.

Considering the relevance of Ca in cementitious systems, several studies have attempted to assess the role of Ca as bridge between HCP / C-S-H phases and organic molecules [93, 170]. In this context, it was suggested that the strength of the uptake or organic ligands might be linked to the stability of corresponding complexes with Ca, *i.e.* Ca(II)-Ligand (see Table 8).

Table 7. *Summary of the R_d values and sorption conditions as investigated in this work for GTA, HIBA and HBA or reported in the literature for EDTA, ISA, GLU, formic acid, acetic acid, methanol, and ethanol with HCP (CEM I and degradation stage I-III).*

Organic ligand	**Functional groups (number of groups)**	**Cement /deg. phase (pH)**	**R_d [$m^3 \cdot kg^{-1}$]**	**log ($[Lig]_{tot}$ /M); S:L /$g \cdot dm^{-3}$**	**Reference**
GTA	-COOH (2)	CEM I / stage II (pH = 12.5)	$\sim(1.0 \pm 0.5) \cdot 10^{-2}$ $\sim(1.3 \pm 0.5) \cdot 10^{-2}$	–3; 10 – 50 [a] –7; 15 – 50 [b]	present work
HIBA	-COOH (1); -OH (1)	CEM I / stage II (pH = 12.5)	$\sim(2.2 \pm 1.3) \cdot 10^{-3}$	–3; 10 – 50 [a]	present work
HBA	-COOH (1); -OH (1)	CEM I / stage II (pH = 12.5)	$\sim(1.6 \pm 0.9) \cdot 10^{-3}$	–3; 10 – 50 [a]	present work
EDTA	-COOH (4)	CEM I / stage I (pH = 13.2) CEM I / stage III (pH = 11.9)	$(1.7 \pm 0.4) \cdot 10^{-4}$ $(1.1 \pm 0.6) \cdot 10^{-2}$	–3; 940 –3; 1 – 7	Pointeau *et* al. [93]
ISA	-COOH (1); -OH (4)	CEM I / stage II (pH = 12.5) CEM I / stage I (pH = 13.4) CEM I / stage I (pH = 13.2) CEM I / stage II (pH = 12.5) CEM I / stage III (pH = 11.9)	$6.4 \cdot 10^{-2}$ – 0.1 $1 \cdot 10^{-3}$ – 0.5 $(5 \pm 2) \cdot 10^{-3}$ (0.10 ± 0.03) $(6.1 \pm 2.1) \cdot 10^{-2}$	–3; 0.2 – 50 –5 – –0.5; 25 – 500 –3.1; 1 –3.1; 1 –3.1; 1	Tasi *et* al. [94] Van Loon *et* al. [89] Pointeau *et* al. [93] Pointeau *et* al. [93] Pointeau *et* al. [93]
GLU	-COOH (1); -OH (5)	CEM I / stage I (pH = 13.4) CEM I / stage II (pH = 12.5)	$8 \cdot 10^{-4}$ – $2 \cdot 10^{2}$ $4 \cdot 10^{-2}$ – 5.4	–7 – –4; 17 – 50 –8 – –3; 20	Glaus *et* al. [167] Androniuk *et* al. [6]
Formic acid	-COOH (1)	CEM I / stage I (pH = 12.92)	$1.1 \cdot 10^{-3}$	–0.07; 333	Wieland *et* al. [87]
Acetic acid	-COOH (1)	CEM I / stage I (pH = 12.74)	$1.75 \cdot 10^{-4}$	–0.08; 333	Wieland *et* al. [87]
Methanol	-OH (1)	CEM I / stage I (pH = 13.21)	$6.25 \cdot 10^{-5}$	–0.33; 333	Wieland *et* al. [87]
Ethanol	-OH (1)	CEM I / stage I (pH = 13.26)	$1.16 \cdot 10^{-5}$	–0.33; 333	Wieland *et* al. [87]

a: characterized inactive GTA via NPOC; **b**: ^{14}C labelled organic ligand, defined by LSC

Table 7 provides a meticulous overview of the sorption affinity of these organic ligands under conditions relevant in cement-based repositories. Comparing the R_d results of ethanol (R_d =

$1.16 \cdot 10^{-5}$ $m^3 \cdot kg^{-1}$) to the R_d of GLU ($R_d = 2 \cdot 10^2$ $m^3 \cdot kg^{-1}$), a difference of more than 7 orders of magnitude was detected. Table 7 allows the classification of the strength of the uptake as a function of the type and number of functional groups as follows:

[weak uptake] -OH (1) < -COOH (1) < -COOH (1) + -OH (1) < -COOH (2) ≈ -COOH (4) < -COOH (1) + -OH (4) < -COOH (1) + -OH (5) [strong uptake]

Table 8. *pK_a and log β of Ca-Ligand in the present work and literature (Ligand = GTA, HIBA, HBA, EDTA, ISA, GLU, formic acid, acetic acid, methanol, and ethanol). The formation constants of Ca(II)-Ligand is described from the presumed reaction of Ca^{2+} + $Ligand^{x-} \rightleftharpoons CaLigand^{(2-x)}$.*

Organic ligand	pK_a	log β(Ca-Ligand)	Reference
GTA	pK_{a1} = (4.345 ± 0.006) pK_{a2} = (5.422 ± 0.002)	(1.09 ± 0.03) (I = 0.5 M $NaClO_4$)	Smith *et* al. [171]
HIBA	(3.760 ± 0.006) (*I* = 0.5 M $NaClO_4$)	0.6 (*I* ≈ 0.2 M KCl)	Piispanen *et* al. [147]
HBA	4.39 (*I* ≈ 0.2 M KCl)	1.18 (*I* = 0.1 M)	Cannan *et* al. [144]
EDTA	pK_{a1} = (2.23 ± 0.05) pK_{a2} = (3.15 ± 0.02) pK_{a3} = (6.80 ± 0.02) pK_{a4} = (11.24 ± 0.03)	(12.69 ± 0.06)	Hummel *et* al. [172]
ISA	pK_{a1} = (4.0 ± 0.5) pK_{a2} = 14.5 (*I* = 1 M NaCl)	(1.7 ± 0.3)	Dudás *et* al. [148] Hummel *et* al. [172]
GLU	pK_{a1} = (3.9 ± 0.1) pK_{a2} = 13.7 (*I* = 1 M NaCl) pK_{a2} = 13.9 (*I* = 4 M NaCl) pK_{a3} = 14.7 (*I* = 4 M NaCl)	(1.73 ± 0.05)	Giffraut *et* al. [143] Kutus *et* al. [173]
Formic acid	(3.744 ± 0.009)	1.43	Smith *et* al. [171]
Acetic acid	4.76	(1.12 ± 0.02)	Giffraut *et* al. [143]
Methanol	15.5	–	Ballinger *et* al. [174]
Ethanol	~ 15.9 (estimated)	–	Ballinger *et* al. [174]

For the four ligands having just one functional group (formic acid, acetic acid, methanol and ethanol), there is a qualitative inverse correlation between R_d values listed in Table 7 and pK_a values presented in Table 8. Note however that higher R_d values were determined for

HIBA/HBA than for formate / acetate, in spite of the similar pK_a's values. One possible reason for this is the contribution of HIBA's and HBA's alcoholic groups to the binding on the HCP via surface complexation, although differences could also arise by the stronger uptake expected for the degradation stage II (Cement-HIBA/HBA, this work) than the negatively charged surface in the degradation stage I (Cement-formate/acetate, [87]).

Table 8 gives evidence that the equilibrium constant for the complexes Ca(II)-Ligand does not represent accurately the tendency of the given ligand adsorption on the HCP. For instance, GTA (2–COOH functional groups, log β = 1.18) and EDTA (4–COOH along with two nitrogen groups, log β = 12.69) show very similar R_d values. This suggests that for EDTA only two carboxylic functional groups contribute for the sorption on the cement paste. Based on this fact, the steric aspects have to be taken into account when assessing the uptake process of ligand onto cement materials. Stronger interaction was observed in the context of Cement-ISA/GLU, although their binary complexes with Ca ($Ca(Lig)^+$) are rather weak. Nevertheless, numerous publications have confirmed that the complexation of ISA and GLU with Ca under hyperalkaline environments is strong, and involves at least the deprotonation of one of the ligand's alcoholic groups [148, 173, 175]. Sorption experiments with HIBA and HBA pointed out that their alcoholic groups do not play any role for the R_d increase, unlike ISA and GLU. Although no thermodynamic data related to the complex formation of HIBA and HBA with Ca under alkaline conditions (pH = 12.5 – 13.3) are available in the literature, yet in the solubility of $Ca(OH)_2(cr)$ with the corresponding ligands at 10^{-6} M $\leq [Lig]_{tot} \leq$ 0.1 M (Section 3.2.1) underpins the generated Ca-Ligand including the deprotonated alcoholic functional groups are considerably weak or no formation is expected.

It was expressed in various publications that the C-S-H phases participate extensively in the uptake mechanism of low molecular weight organic molecules [6, 93, 176], just like C-A-S-H phases. It was determined by using ISA as sorbate on the latter cementitious phase that it contains distinct sorption sites [26, 94]. Wieland and co-workers have undertaken significant efforts to quantify the uptake of organic ligands by different cement phases, *i.e.* C-S-H, AFt and AFm. The latter two phases were defined as anion exchangers of cement, particularly SO_4^{2-} / $HCOO^-$ in AFt-SO_4 and CO_3^{2-} / $HCOO^-$ in AFm-CO_3. Nonetheless, Wieland *et* al. reported lower R_d values on AFt and AFm than C-S-H phases [87]. As it was noted in this work, the linear sorption trend of GTA (Figure 24) provided interpretation about only one sorption site takes part on the uptake of the proxy ligand. These so-far specified experimental

outcomes emphasized the possibility that different sorption sites and cement phases contribute in the retardation of organic molecules with various functional groups, charge and/or size.

As a short summary of this section of the study, it is clear that more experiments and thermodynamic evaluation are required due to lack of datasets, yet the above compiled experimental results establish a fundamental knowledge on how the organic molecules and degradation products of disposed organic materials containing carboxylic and hydroxyl functional groups interact with the cementitious materials. Alcohol groups contribute considerably to a strong sorption when several of them are present together with at least one carboxylic group. In these conditions, some of these alcohol groups may deprotonate, thus actively participating in the formation of surface complexes. Other conditions, which have the ability to influence the uptake of the organic compounds, are pH, equilibrium constant of the Ca-Ligand (not in all organic molecules) and steric features of the organic ligands (see EDTA).

3.3.2 Ni(II) sorption studies

The main focus of this chapter is to monitor the ^{63}Ni uptake processes on Portland cement at pH = 12.5 in absence and presence of the proxy ligands. These experiments have been investigated under the following parameters:

1. log ($[Ni]_{in}$ /M) = –8 and –9; S:L = 1, 2, 4, 10 and 20 g·dm^{-3}
2. log ($[Ni]_{in}$ /M) = –8; S:L = 1 g·dm^{-3}; $[Lig]_{in}$ = 10^{-1}, $10^{-1.5}$ and 10^{-4} M
   where Lig = GTA, HIBA and HBA

3.3.2.1 Cement-Ni(II) binary system

Figure 26 represents the uptake of ^{63}Ni by Portland cement as log (R_d /m^3·kg^{-1}) *vs.* S:L ratio from 0.5 ≤ (S:L /g·dm^{-3}) ≤ 20 using different initial ^{63}Ni concentrations as $[^{63}Ni]_{in}$ = 10^{-8} and 10^{-9} M. The figure includes also log R_d values reported in the literature [34, 101, 177].
Figure 26 shows that the R_d values are mostly independent of S:L ratio for both $[^{63}Ni]_{in}$ = 10^{-8} and 10^{-9} M batches. The sorption of nickel on the vessel wall was quantified and has been considered for the calculation of the reported R_d values.

Slightly enhanced R_d values were observed for $[Ni]_{in} = 10^{-8}$ M. The calculated R_d values are in a range of 0.5 – 7 m^3 kg^{-1}, which are in line with data reported in the literature for the same degradation stage of cement [99, 104, 119, 178]. However, previous studies observed the decrease of R_d values of ^{63}Ni with increasing S:L ratios [95, 101], which is not clearly observed in the current work. Figure 26 shows that the retardation of ^{63}Ni in the current study is higher than at pH = 13.3 [101]. Such differences are possibly related to the different surface charge of cement at pH = 12.5 and 13.3, as well as differences in the aqueous speciation of Ni(II).

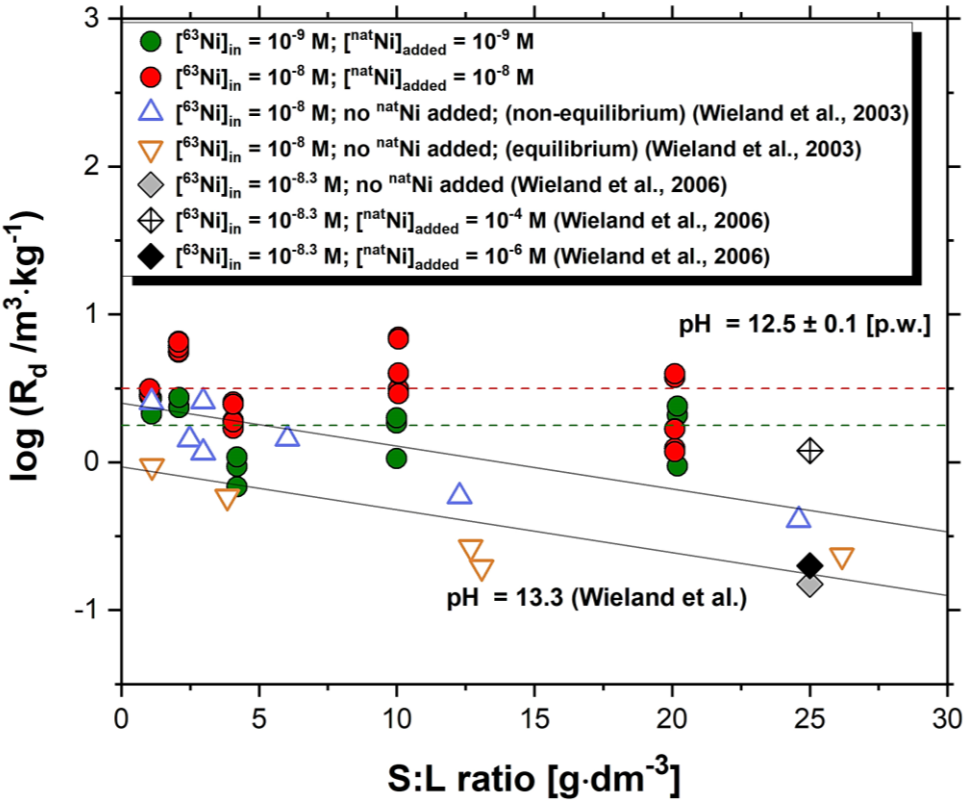

Figure 26. *Uptake of ^{63}Ni by HCP at $[^{63}Ni]_{in} = 10^{-8}$ M (red circle) and 10^{-9} M (green circle) applying cement powder – cement porewater systems at 1 ≤ (S:L /g·dm^{-3}) ≤ 20 after contact time of t_{eq} = 113 d and 81 d, respectively. Triangles and diamonds corresponding to experimental datapoints of log R_d values determined in various articles [101, 102]. Solid and dashed lines illustrate the trend of R_d values with increasing S:L ratios as assessed in the report of Wieland et al. [101] and this study, respectively.*

Previous studies have indicated that the retention of Ni(II) in cementitious systems is controlled by solubility phenomena, with nickel being present as Ni and Al hydrotalcite-like solid phase (LDH) on the cement surface [100, 102]. Moreover, the uptake of ^{63}Ni is proposed

to take place primarily through isotopic exchange between the radioactive Ni in solution and non-radioactive Ni within the original cement matrix [102].

Wieland *et* al. [102] evaluated the extent of the isotopic exchange in their experiments at pH = 13.3 through partition coefficients (α / *dimensionless*), which are compared in the Table 10 with values determined (R_d values of ^{63}Ni and ^{nat}Ni) in the present work using Equation (6). Partition coefficients (α) were calculated with the following R_d values of natural nickel as analyzed by ICP-MS in the solid and liquid phase:

Table 9. *R_d ($m^3 \cdot kg^{-1}$) of natural nickel in batch suspension at various S:L and ^{63}Ni concentration. Uncertainties were calculated as 3 times the standard deviation.*

S:L ($g \cdot dm^{-3}$)	**$[^{63}Ni]_{in} = 10^{-8}$ M**	**$[^{63}Ni]_{in} = 10^{-9}$ M**
1	(1.4 ± 0.7)	(1.4 ± 0.7)
2	(1.9 ± 0.9)	(1.9 ± 0.9)
4	(2.1 ± 1.0)	(2.1 ± 1.0)
10	(2.3 ± 1.1)	(2.3 ± 1.1)
20	(2.3 ± 1.1)	(2.3 ± 1.1)

Table 10. *Partition coefficients (α / dimensionless) determined in this work for $[^{63}Ni] = 10^{-8}$ M and 10^{-9} M at variable S:L and pH = 12.5. Uncertainties were calculated as 3 times the standard deviation. For comparison purposes, the results of Wieland et al. [102] at pH = 13.3, $[^{63}Ni]_{in} = 5 \cdot 10^{-9}$ M and S:L = 25 $g \cdot dm^{-3}$ are also shown. Authors used $[^{nat}Ni]_{add} = 0$; 10^{-4} and 10^{-6} M as carrier in each batch solution.*

S:L ($g \cdot dm^{-3}$)	**$[^{63}Ni]_{in} = 10^{-8}$ M (p.w.)**	
	t_{eq} =29 d	**t_{eq} =113 d**
1	(2.3 ± 1.1)	(2.4 ± 1.2)
2	(3.4 ± 1.7)	(3.6 ± 1.8)
4	(0.9 ± 0.5)	(1.2 ± 0.6)
10	(1.8 ± 0.9)	(3.2 ± 1.6)
20	(0.8 ± 0.4)	(1.7 ± 0.9)
S:L ($g \cdot dm^{-3}$)	**$[^{63}Ni]_{in} = 10^{-9}$ M (p.w.)**	
	t_{eq} =68 d	**t_{eq} =81 d**
1	(1.6 ± 0.8)	(1.5 ± 0.8)
2	(1.3 ± 0.6)	(1.5 ± 0.8)
4	(0.5 ± 0.2)	(0.5 ± 0.3)
10	(0.8 ± 0.4)	(0.9 ± 0.5)
20	(0.9 ± 0.5)	(1.1 ± 0.5)
$[Ni]_{add}$ /M	**Wieland *et* al. (S:L = 25 $g \cdot dm^{-3}$; $[^{63}Ni]_{in} = 5 \cdot 10^{-9}$ M; pH = 13.3)**	
	t_{eq}=7 d	**t_{eq} =30 d**
-	(3.3 ± 1.0) 10^{-2}	(2.9 ± 0.6) 10^{-2}
10^{-4}	(4.5 ± 1.0) 10^{-2}	(4.5 ± 1.0) 10^{-2}
10^{-6}	(2.8 ± 0.6) 10^{-2}	-

Table 10 shows that significantly higher values of α are determined in this work, compared with the values reported by Wieland and co-workers [102]. In line with the measured log $R_{d,^{63}Ni}$ values shown in Figure 26, the values of α calculated for $[^{63}Ni]_{in}$ = 10^{-9} and 10^{-8} M remain nearly constant. The average values determined for both datasets are α = (1.0 ± 0.5) and (1.9 ± 1.0) for experiments conducted at $[^{63}Ni]_{in}$ = 10^{-9} and 10^{-8} M, respectively. The values of α ≥ 1 suggest that all ^{nat}Ni in the HCP is available for isotopic exchange (α = 1). It has been recently studied by Missana *et* al. [105] that the uptake of Ni(II) by C-S-H phases appears as a feasible uptake mechanism complementary to isotopic exchange. Missana and co-workers [105] investigated the interaction of ^{63}Ni in different nuclide concentration at either various Ca/Si ratio of C-S-H suspensions or S:L in inert atmosphere. The authors observed that the uptake of Ni depends on the Ca/Si ratio. At high Ca/Si ratio (1.6 at pH = 12.36), Ni has lower tendency to sorb on the cement materials than at 0.8 Ca/Si (pH = 9.5). Stronger sorption at lower pH occurred by the interaction of deprotonated silanol (SiO^-) groups with the positively charged $Ni(OH)^+$ and Ni^{2+}. On the other hand, under high alkaline conditions (pH = 12.36) and high Ca/Si (1.6), the authors proposed the formation of the surface complex $SiOCa^+ + Ni(OH)_3^- \rightleftharpoons SiOCaNi(OH)_3$.

Differences between the extent of the isotopic exchange observed in Wieland *et* al. and in this work are probably related with the different pH used in this work (pH = 12.5, degradation stage II) and in Wieland *et* al. (pH = 13.3, degradation stage I).

3.3.2.2 Cement-Ni(II)-Ligand ternary system

The effect of the proxy ligands on the uptake of Ni by HCP following the order of addition (Cement + ^{63}Ni) + Ligand is summarized in Figure 27, for systems with S:L = 1 g·dm^{-3}, log ($[Ni]_{in}$ /M) = –8 and –4 ≤ log ($[Lig]_{tot}$ /M) ≤ –1. The figure includes also the experimental results for the sorption of ISA (with S:L = 25 g·dm^{-3}) as reported by Bruno and co-workers [123]. The values of log R_d in the absence of proxy ligands are included also as reference.

The distribution ratio at $[Lig]_{tot} \geq 10^{-4}$ M remains in the range of 0.4 ≤ log (R_d /m^3·kg^{-1}) ≤ 1 in line with R_d values in ligand-free system. A slight decrease in the retention is only observed at $[Lig]_{tot} \geq 10^{-1.5}$ M. This confirms the weak character of the proxy ligands for the complexation of Ni(II). This observation is consistent with the slight solubility increase of Ni(II) at $[Lig]_{tot} \geq 10^{-2}$ M (Section 3.2.2), which could be attributed to the formation of Ni(II)-OH-Ligand ternary complexes. In the case of ISA, the concentration of Ni in aqueous phase

starts increasing at $[ISA]_{tot} \approx 10^{-3}$ M [123], which supports the weaker influence of GTA, HIBA and HBA on the Cement-Ni(II) sorption reactions.

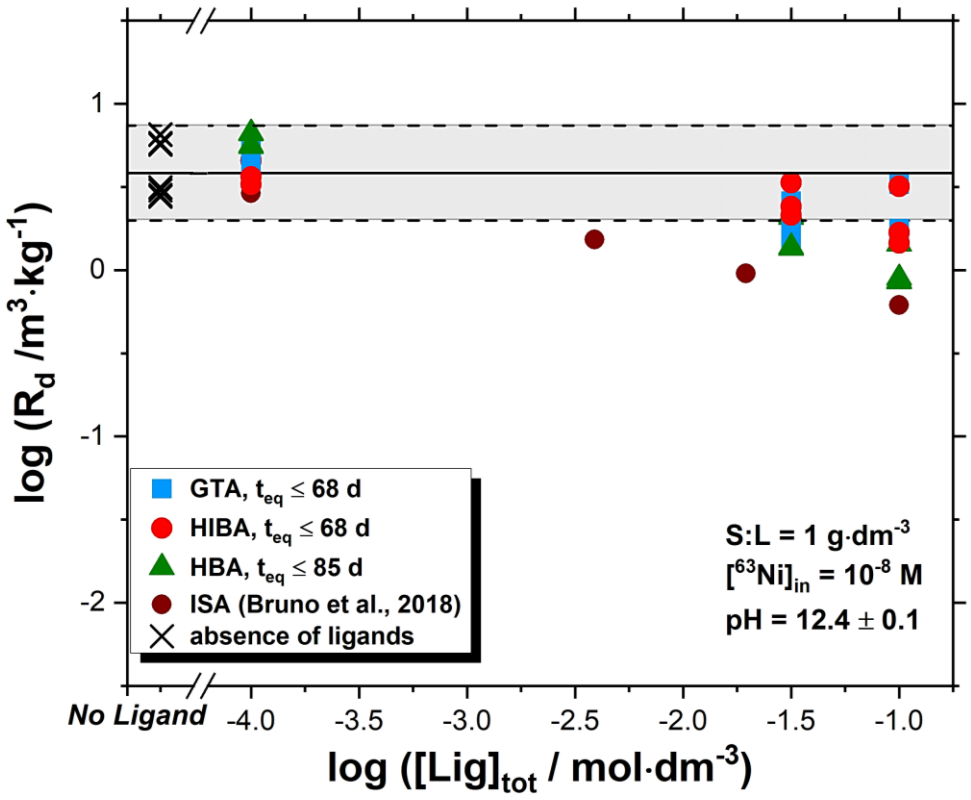

Figure 27. *Distribution ratio (R_d, in $m^3 \cdot kg^{-1}$ units) of Ni sorption reaction in the presence of GTA(■), HIBA(●) and HBA(▲) equilibrium with cement powder-porewater system with $\log([Ni]_{in}/M) = -8$, $-4 \leq \log([Lig]_{tot}/M) \leq -1$ and S:L = 1 g·dm^{-3} in the order of addition of the components: (Cement + Ni) + Ligand. Black cross represents the log R_d values in the absence of organic ligands, quantified within Section 3.3.2.1. Black solid and dashed lines illustrate the expected distribution ratio of Ni in ligand-free system. Brown circles display the calculated values of (Cement + Ni) + ISA as expressed by Bruno et al. [123].*

3.3.3 Eu(III) sorption studies

The next section of the ternary systems is dedicated to present the retardation of Eu(III) onto HCP in the absence and presence of the proxy ligands. This section can be separated into two sub-groups in accordance with experimental details:

1. log ($[^{152}Eu]_{in}$ /M) = –8; S:L = 0.5, 1, 2, 3, 4 g·dm^{-3}
2. log ($[Eu]_{in}$ /M) = –7 radiolabelled with log ($[^{152}Eu]_{in}$ /M) = –8.67; S:L = 1 g·dm^{-3};
   log ($[Lig]_{in}$ /M) = –1, –1.5, –2, –2.5, –3
   where Lig = GTA, HIBA and HBA

3.3.3.1 Cement-Eu(III) binary system

The uptake of Eu(III) by HCP was investigated in suspensions (log ($[Eu]_{tot}$ /M) = –8 at 0.5 ≤ S:L ≤ 4 g·dm^{-3}) for contact times of up to 125 days. In order to assess the possible presence of colloids, phase separation was conducted using centrifugation (with standard lab centrifuge at 3461 g) and ultracentrifugation (694000 g, 1 h). In addition to the experimental data points, Figure 28 shows the log $R_{d,max}$ calculated on the basis of the detection limit of the quantification method and the corresponding S/L ratio. The figure includes also as grey zone the sorption data reported by Wieland and co-workers [108] at pH = 13.3. In the current study, the sorption of europium on the vessel wall was quantified and has been considered for the calculation of the reported R_d values.

Figure 28 shows a significant difference between samples where phase separation was conducted with standard lab centrifuge and with ultracentrifuge, which suggests that colloids might be present in the system. The results in the current study are in line with the upper sorption limits of Eu(III)-HCP reported in [108], notwithstanding that experiments in the literature were performed at pH = 13.3 and at pH = 12.4 in the present work.

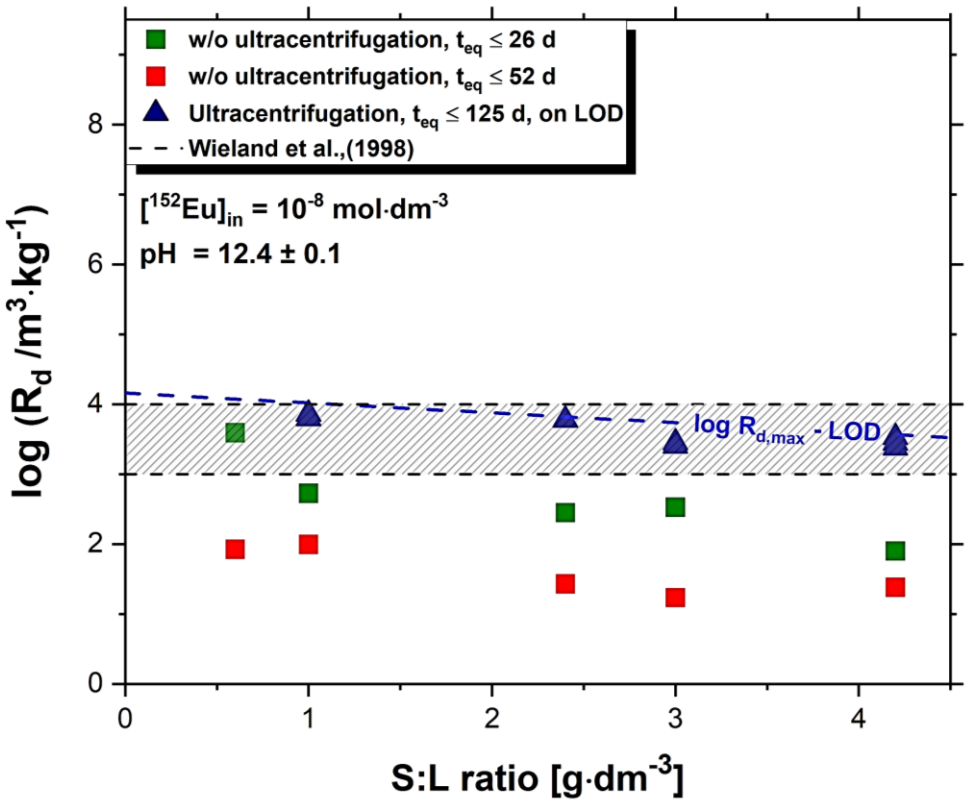

Figure 28. *Distribution ratio (R_d in $m^3 \cdot kg^{-1}$ units) of Eu at 0.5 $g \cdot dm^{-3} \leq$ S:L $\leq$ 4 $g \cdot dm^{-3}$ and $[^{152}Eu]_{in} = 10^{-8}$ M. Green and red squares represent the values with phase separation using a laboratory centrifuge, while blue triangles corresponding to the distribution ratio using additional ultracentrifugation. Blue dash lines corresponding to the maximal R_d values at given S:L. Grey shaded area presents estimated uncertainty range of sorption values as reported by Wieland et al. [108] at pH = 13.3.*

3.3.3.2 Cement-Eu(III)-Ligand ternary system

Figure 29 shows the effect of the proxy ligands on the uptake of Eu(III) at S:L = 1 g·dm^{-3}, log ($[Eu]_{in}$ /M) = –7 and –3 $\leq$ log ($[Lig]_{tot}$ /M) $\leq$ –1. The results are expressed as log (R_d /m^3·kg^{-1}) *vs.* log ($[Lig]_{tot}$ /M). All batch solutions were spiked with ^{152}Eu stock solutions. The purple triangles and green stars represent the impact of ISA and GLU on the retention of Eu(III) at pH = 13.3, respectively. The greyish region shows the upper and lower limits reported by Wieland *et* al. for the uptake of Eu(III) in the absence of organic ligands [95].

The steady state of the systems was reached at $t_{eq} \leq 7$. Almost all datapoints are situated close to limit of detection (log ($R_{d,max}$ /m^3·kg^{-1}) $\approx$ 4) and are in line with the sorption values of Wieland *et* al. [95], concluding strong uptake of Eu(III) occurred on the cement. In line with

the negligible effect of the proxy ligands on the solubility of Nd(III) (see Section 3.2.3), these proxy ligands have no impact on the Cement-Eu(III) sorption process. In contrast to these proxy ligands, polyhydroxocarboxylic acids like ISA and GLU [95] show a significantly stronger influence on the uptake of Eu(III) by HCP.

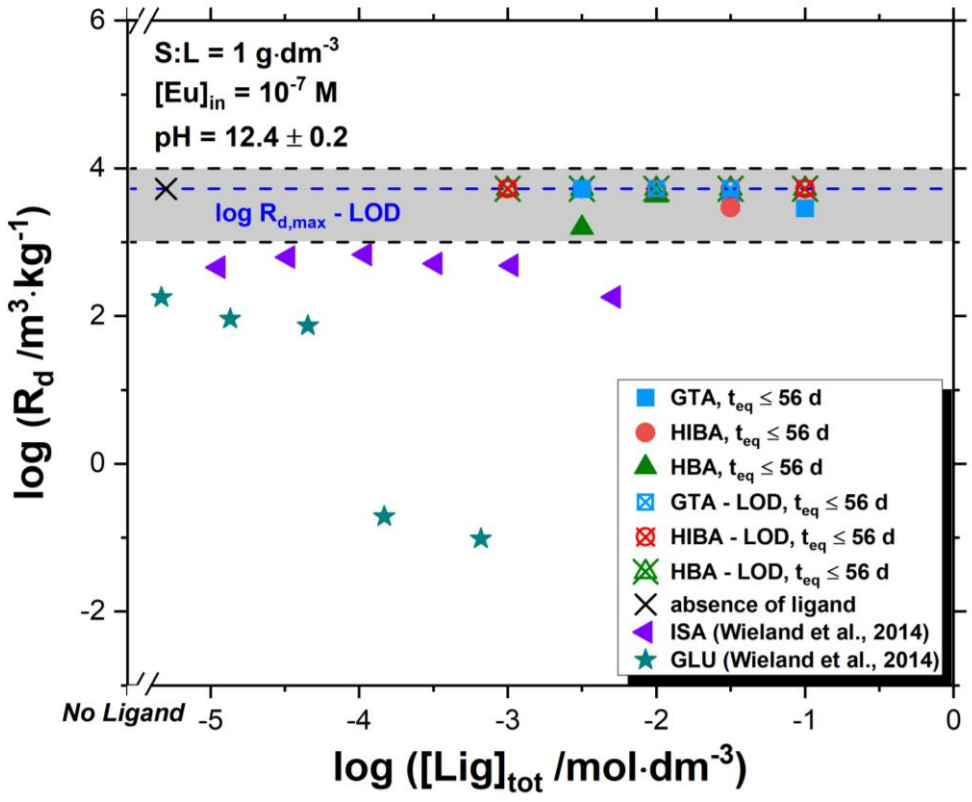

Figure 29. *Sorption of Eu(III) on HCP in the presence of GTA, HIBA and HBA equilibrium with cement powder-porewater system with* $[Eu]_{in} = 10^{-7}$ *M,* $-3 \leq \log ([Lig]_{tot}/M) \leq -1$ *and* $S:L = 1\ g \cdot dm^{-3}$ *in the order of addition of individual components: (Cement + Eu) + Ligand. The batch solutions were spiked with* ^{152}Eu*, which concentration in the samples corresponding to* $[^{152}Eu]_{in} = 2.2 \cdot 10^{-9}$ *M. Purple triangle, green star and black dashed line are the experimental Eu sorption results with the interaction of ISA, GLU and estimated uncertainty range of sorption values as reported by Wieland et al. [95, 108]. Black cross symbolizes the* R_d *values of Eu(III) in the absence of any organic ligands portrayed in the Figure 28. Blue dash line displays the limit of detection described as log* $R_{d,max}$*.*

3.3.4 Pu(III/IV) sorption studies

3.3.4.1 Cement-Pu(IV) binary system

The binary system of Pu with Portland cement has been investigated at various RN concentration and S:L ratio. As the Table 5 in Section 2.6.2 displays, the following batch series were monitored:

1. log ($[Pu]_{in}$ /M) = –8; S:L = 0.5, 1, 2, 5 g·dm^{-3}; with 2 mM HQ
2. S:L = 1 g·dm^{-3}; log ($[Pu]_{in}$ /M) = –7.8, –8, –8.2, with 2 mM HQ

Figure 30 shows the log R_d values determined for the uptake of Pu by HCP at $t_{eq} \leq 80$ days. The strong sorption observed in this work is in line with log $R_{d,in}$ = (3.3 ± 0.6) m^3·kg^{-1} reported by Tasi and co-workers for the uptake of Pu(IV) by HCP under analogous boundary conditions [94]. Similar values are obtained for the uptake of Pu at S:L = 1 g·dm^{-3} and log ($[Pu]_{in}$ /M) = –7.8, –8, –8.2 (data not shown).

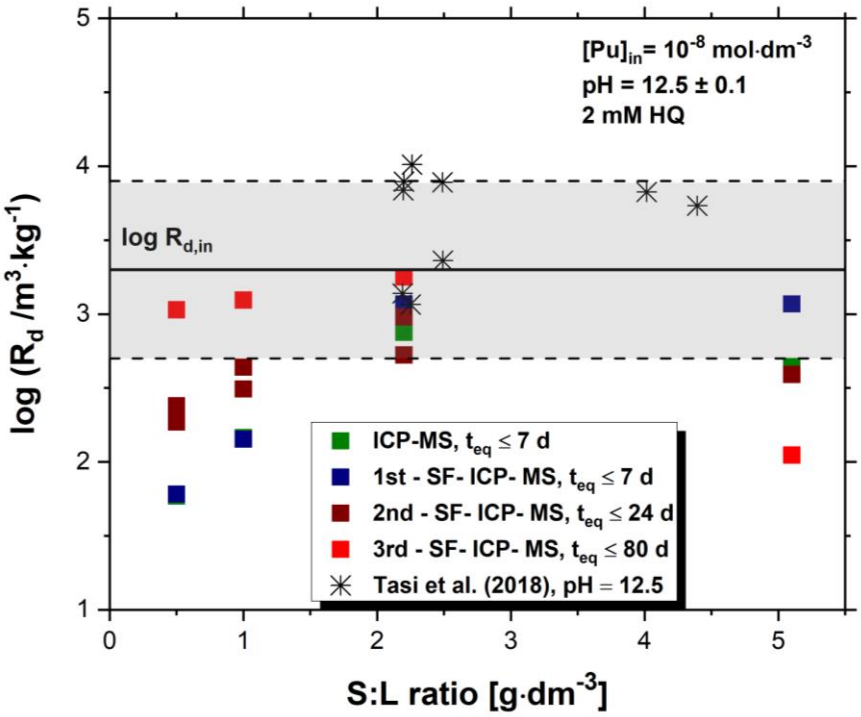

Figure 30. *Distribution ratios (R_d in m^3·kg^{-1} units) of Pu sorption reaction in equilibrium at $[Pu]_{in} = 10^{-8}$ M, buffered by hydroquinone with cement S:L ratio: 0.5, 1, 2 and 5 g·dm^{-3} at t_{eq} = 7 d (green and blue), 24 d (brown) and 80 d (red). The first sampling was performed in ICP-MS (green) and SF-ICP-MS (blue) for comparison. Solid black lines and grey shades the distribution ratio of Pu and its uncertainty in the absence of organic ligand (log ($R_{d,in}$ /m^3·kg^{-1}) = (3.3 ± 0.6). Black asterisk represents the R_d values of Tasi et al. [94].*

3.3.4.2 Cement-Pu(III/IV)-Ligand ternary system

In total, 36 batch solutions were prepared inside the glove-box. The samples were generated according to the following parameters:

1. $[Pu]_{in}$ = 10^{-8} M; S:L = 1 g·dm^{-3}; $[Lig]_{in}$ = 10^{-1}, $10^{-1.5}$, 10^{-2}, $10^{-2.5}$, 10^{-3} and 10^{-4} M with 2 mM HQ
2. $[Pu]_{in}$ = 10^{-8} M; S:L = 1 g·dm^{-3}; $[Lig]_{in}$ = 10^{-1}, $10^{-1.5}$, 10^{-2}, $10^{-2.5}$, 10^{-3} and 10^{-4} M with 2 mM Sn(II)
   where Lig = GTA, HIBA and HBA

After a week of equilibration, the samples were centrifuged for 5 minutes at 3904 g, and a small portion of supernatant was filtered through 10 kD filters by centrifugation for 12 minutes at 3904 g. The aliquots were acidified with 2% HNO_3, and characterized by (SF-)ICP-MS.

In order to confirm the predominant Pu oxidation states and species in aqueous phase, the pH_c, pe and (pH_c + pe) of supernatant were measured and are summarized in Table 11 for all Pu sorption experiments in the presence of the proxy ligands, which were buffered with either HQ or Sn(II). These values are in good agreement with data previously reported by Tasi *et* al. for similar experiments in the presence of ISA (HQ (pe + pH ≈ 9) and Sn(II) (pe + pH ≈ 2)) [94]. It is worth to note that the authors found that the Pu(IV) was the dominating species both in HQ and Sn(II) redox buffered systems containing ISA.

Table 11. *Determined pH_c, pe and (pH_c + pe) in HQ and Sn(II) buffered solutions in the presence of GTA, HIBA and HBA. Uncertainty was calculated as twice the standard deviation of mean values.*

HQ	**pH_c**	**pe**	**(pH_c + pe)**
GTA	(12.48 ± 0.13)	–(2.17 ± 0.25)	(10.31 ± 0.32)
HIBA	(12.49 ± 0.12)	–(2.23 ± 0.32)	(10.25 ± 0.24)
HBA	(12.48 ± 0.15)	–(2.21 ± 0.33)	(10.27 ± 0.36)
Pu-ISA	(12.54 ± 0.16)	–(3.50 ± 1.0)	(9.2 ± 0.8)
Sn(II)	**pH_c**	**pe**	**(pH_c + pe)**
GTA	(12.50 ± 0.14)	–(10.0 ± 0.6)	(2.47 ± 0.71)
HIBA	(12.54 ± 0.06)	–(10.5 ± 0.6)	(2.03 ± 0.66)
HBA	(12.54 ± 0.09)	–(10.6 ± 0.6)	(1.89 ± 0.62)
Pu-ISA	(12.50 ± 0.16)	–(11.6 ± 1.1)	(1.00 ± 0.70)

Figure 31 shows the results of the sorption experiments for the ternary system (Cement + Pu) + Ligand at S:L = 1 $g \cdot dm^{-3}$, $[Pu]_{in} = 10^{-8}$ M and $10^{-4} \leq ([Lig]_{tot}\ /M) \leq 10^{-1}$ in the redox-buffered system of HQ and Sn(II). Results are illustrated in terms of log ($R_d\ /m^3 \cdot kg^{-1}$) *vs.* ($[Lig]_{tot}\ /mol \cdot dm^{-3}$). For comparison purpose, the highest log R_d values (dash blue line), representing the limit of detection in each redox media, were included in the figure. The surface coverage (green solid line) of HCP by GTA calculated by one-site Langmuir isotherm using the Equation (9) was also depicted in the Figure 31.

In both HQ and Sn(II) systems, in spite of high dispersion due to the low concentration of Pu and the formation of neutral Pu(IV) complex (*i.e.* $Pu(OH)_4(aq)$) in the solutions, most of the log R_d values remain close to log R_d values in the absence of proxy ligands. A slight decrease in R_d values might be suggested for log ($[Lig]_{tot}\ /M$) ≥ –2, although overall this effect could be considered within the uncertainty of the measurements. Due to the increase in Na concentration introduced by the increasing Na-L salts, the possible effect of sodium on the uptake of Pu was also evaluated. For this purpose, additional batch solutions were prepared under analogous conditions using NaCl and $NaClO_4$ of the same concentration as those inserted by the proxy ligands (Appendix, Figure A-4). In line with the results obtained in the presence of proxy ligands, Figure A-4 shows dispersed R_d values within $1 \leq \log (R_d\ /m^3 \cdot kg^{-1}) \leq 4$. It can be thus concluded that Na has no significant effect on the retention of Pu by C-S-H phases, at least within the upper concentration values considered in this study, *i.e.* 0.1 – 0.2 M. In summary, the observations obtained for the uptake of Pu by HCP in the presence of

proxy ligands are consistent with the negligible effect observed in the solubility experiments (see Section 3.2.4).

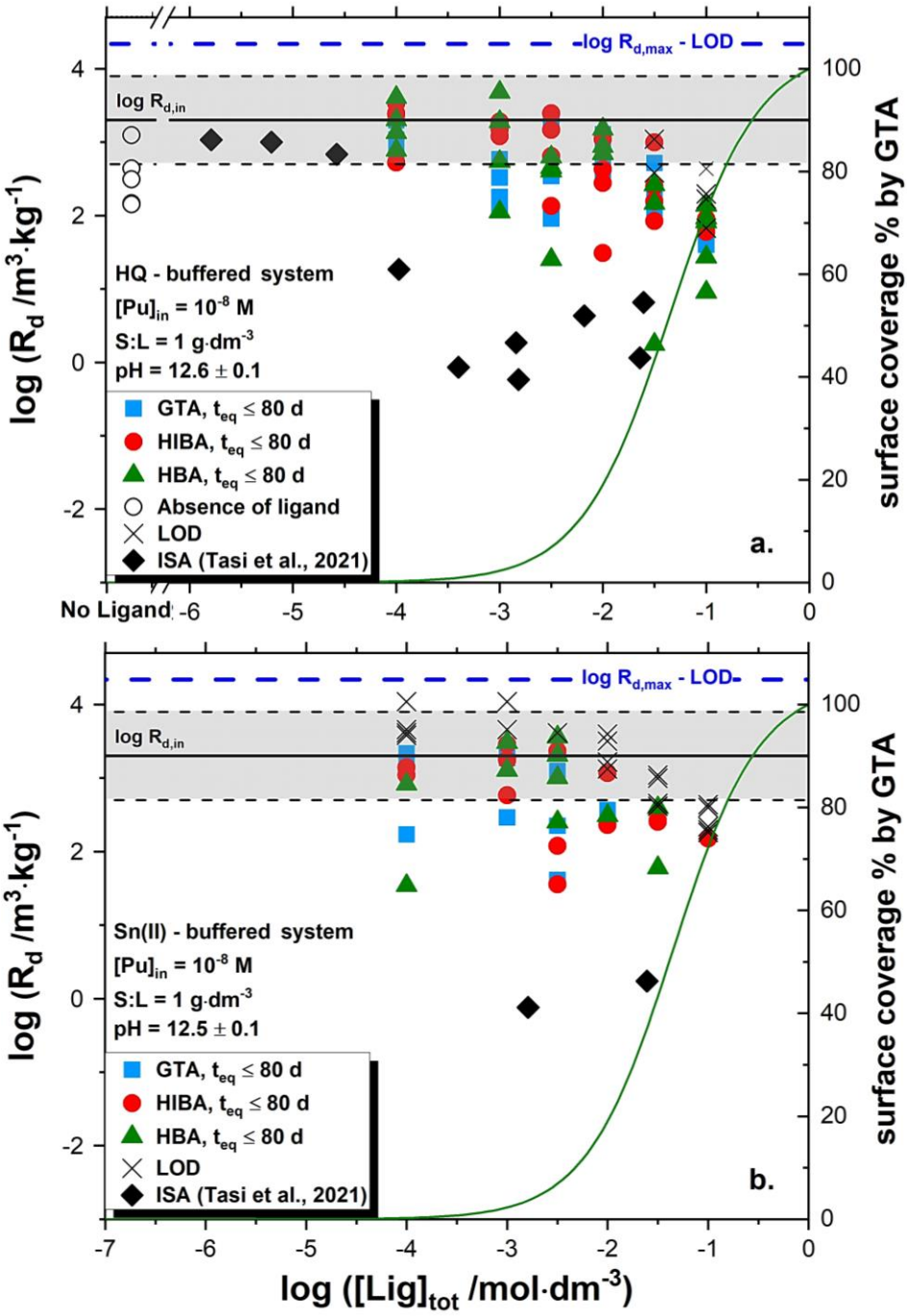

Figure 31. *Distribution ratios (R_d in $m^3 \cdot kg^{-1}$ units) of Pu sorption reaction in equilibrium at $[Pu]_{in} = 10^{-8}$ M, $10^{-4} \leq ([Lig]_{tot}/M) \leq 10^{-1}$ and S:L ratio: 1 $g \cdot dm^{-3}$, buffered by (a) HQ and (b) Sn(II) in the sequence of addition of individual components: (Cement + Pu) + Ligand in the contact time of $t_{eq} \leq 80$ days. Experiment shows no typical trend with time after long period of sampling. The blue dash line represents the highest log R_d that can be quantified, based on the detection limit of SF-ICP-MS for [Pu]. Solid black lines and grey shades are the distribution ratio of Pu and its uncertainty in the absence of organic ligand (log ($R_{d,in}$ /$m^3 \cdot kg^{-1}$) = (3.3 ± 0.6) [94]. Black squares emphasizes the experimental results of (Cement + Pu) + ISA [94]. Black crosses illustrate the limit of detection at each ligand concentration. Green solid lines corresponding to the surface coverage in percentage (%) of the HCP by GTA, calculated according to one-site Langmuir-isotherm generated in this study.*

4. Summary and conclusions

The main objective of this PhD thesis was to determine the effect of small molecular weight organic molecules arising from the degradation of the UP2W ion exchange filter on the retention of Ni(II), Eu(III) and Pu(IV) by HCP under conditions relevant in the context of repositories for low- and intermediate level nuclear waste. Three organic ligands were defined as proxies for the degradation products of UP2W, *i.e.* glutaric acid (GTA), α-hydroxyisobutyric acid (HIBA) and 3-hydroxybutyric acid (HBA). These defined "proxy" ligands were applied in the subsequent experimental sections:

1. Characterization of $Ca(OH)_2$(cr), β-$Ni(OH)_2$(cr), $Nd(OH)_3$(s) and PuO_2(ncr,hyd) solubility in the presence of the proxy ligands
2. Determination of the proxy ligands sorption on cement phase
3. Examination of the uptake of RN (^{63}Ni, ^{152}Eu and ^{242}Pu) by HCP either in the absence or presence of proxy ligands

The final conclusions of each study are summarized in the following paragraphs:

1. Solubility of $Ca(OH)_2$(cr), β-$Ni(OH)_2$(cr), $Nd(OH)_3$(s) and PuO_2(ncr,hyd)

The solubility of M(II/III/IV) cations in the presence of proxy ligands (GTA, HIBA and HBA) derived from UP2W degradation solutions were measured and compared with the ligand-free systems as well as with previous solubility studies with ISA. From the experiments, it can be established that these proxy ligands have a minor effect on the solubility of Ca(II), Nd(III) and Pu(IV), while a slight increase in the solubility of Ni(II) was observed at $[Lig]_{tot} \geq 10^{-2}$ M. The latter observation suggests that Ni(II)-OH-Ligand ternary complexes might be formed in hyperalkaline conditions. The comparison of the formed M-Ligand (M = Ca(II), Ni(II), Nd(III) and Pu(IV), Ligand = GTA, HIBA, HBA) with previously reported Ca(II), Ni(II), Nd(III) and Pu(IV)-ISA under analogous boundary conditions unequivocally confirms that the latter organic molecule forms stronger complexes with the investigated radionuclides. Even though the HIBA (1 –COOH + 1 –C-OH in α-position) and HBA(1 –COOH + 1 –C-OH in β-position) contain the same functional groups like ISA (1 –COOH + 4 –C-OH), it is evident that more stable complexes are formed in the presence of ISA because of containing additional –OH functional groups or the different position/distance of –OH group to –COOH. This assumption was further validated by DFT + DFT/COSMO calculations implemented on

Pu(IV)-GTA/HIBA/HBA (performed by R. Polly of KIT-INE), which show that the alcoholic groups of HIBA and HBA do not participate in the complexation with Pu, neither protonated nor deprotonated form. This is clearly different for ISA, where it could be demonstrated, that alcoholic groups in α- and δ-position act as ligands under comparable conditions.

Solid phases of $Ca(OH)_2(cr)$, β-$Ni(OH)_2(cr)$, $Nd(OH)_3(s)$ and $PuO_2(ncr,hyd)$ were characterized by XRD from batch solutions comprising the highest ligand concentration of $[Lig]_{tot}$ = 0.1 M. The measurements confirmed the predominance of the original solid phases, although the formation of secondary solid phases possibly involving proxy ligands was hinted by the presence of new XRD patterns.

2. Sorption of proxy ligands on cement phase

The uptake of proxy ligands by Portland cement in hyperalkaline conditions was evaluated with a comprehensive series of sorption experiments with inactive and C-14 labelled ligands. The obtained results depicted that the uptake of HIBA and HBA occurs only at S:L = 50 $g \cdot dm^{-3}$, whereas a more pronounced uptake was observed for GTA. This observation can be attributed to the presence of two carboxylic functional groups in the molecule. This assumption was further supported by measurements of the zeta potential at S:L = 4 $g \cdot dm^{-3}$, which remains close the portlandite range in the presence of HIBA and HBA even at the highest ligand concentration ($[Lig]_{tot}$ = 0.1 M), whereas the GTA starts decreasing the surface potential from $[GTA]_{tot} \geq 10^{-3}$ M and reaches the isoelectric points (IEP) at $[GTA]_{tot} \geq 6 \cdot 10^{-2}$ M.

Considering the stronger uptake observed for GTA, additional batch measurements were implemented involving ^{14}C labelled GTA. Utilizing the obtained results from sorption experiments with labelled and non-labelled GTA, an one-site Langmuir isotherm was fitted to the experimental data, resulting in the adsorption affinity and capacity constants of K = (22.5 ± 6.1) $dm^3 \cdot mol^{-1}$ and q = (0.45 ± 0.12) $mol \cdot kg^{-1}$, respectively.

In order to gain additional insights into the retention process, the uptake of various organic compounds containing carboxylic and/or alcoholic groups were compared with the proxy ligands selected in this study. The main parameters affecting the strength of the uptake can be listed as follows: the number of functional groups, steric effects, pH of the system and the characteristics of HCP *i.e.* [Ca] and surface charge. Although the retention of the proxy ligands is much weaker than that of other ligands investigated in the literature, *e.g.* ISA or

GLU, the corresponding R_d values, characterized in this PhD thesis, allow a quantitative estimation of their retention properties in the context of cement-based repositories.

3. Uptake of RN (^{63}Ni, ^{152}Eu and ^{242}Pu) by HCP in the absence or presence of proxy ligands

Sorption behaviour of Ni(II), Eu(III) and Pu(III/IV) on Portland cement and the influence of the assigned proxy ligands on their uptake were investigated. For Pu experiments, redox conditions were additionally adjusted with hydroquinone and $SnCl_2$ in cementitious condition to Pu(IV) and Pu(IV/III), respectively. The retention of Pu(III/IV), Ni(II) and Eu(III) by HCP in ligand-free systems, assessed in the current work, is in good agreement with the results reported in previous experimental studies. Results obtained in this work for Ni(II) in combination with previous studies suggests that the uptake of ^{63}Ni might be driven by different processes, *i.e.* isotopic exchange with natural Ni present in pristine HCP and uptake by C-S-H phases. In the case of Eu(III), differences between experimental results using ultracentrifugation and centrifugation with standard lab centrifuge hints to the presence of colloidal Eu(III) fractions .

The proxy ligands in the order of addition of (Cement + RN) + Ligand affected the sorption process in different ways. Despite the fact the Pu(III/IV) retention was slightly reduced at high ligand concentration of $[Lig]_{tot} \geq 10^{-2}$ M, this decreasing trend can be considered to fall within the large uncertainty in the measurement of Pu at trace concentrations. Indeed, no clear effect of proxy ligands on the solubility was observed for Pu. In the case of Ni(II) ternary systems, the reduction of R_d values was ascribed to the formation of Ni(II)-OH-Ligand ternary complexes at high ligand concentrations, in line with observations made in the solubility experiments. Similarly in binary system, the datapoints gained from Eu(III) ternary systems were very close to detection limits in the presence of all 3 proxy ligands, suggesting that they have negligible low affinity to mobilize the Eu(III) from the HCP.

The inputs of all solubility and sorption experiments indicated that the proposed proxy ligands for the degradation of UP2W do not interact significantly with Ni(II), Eu(III) and Pu(III/IV). This proves that proxy ligands are not capable of mobilizing the radionuclides from cement phase. This study provides fundamental and thorough knowledge about the impact of these ligands on metal ions under hyperalkaline conditions representing cementitious environment at degradation stage II. In conclusion, the outcomes of the study contribute to the description

how the UP2W degradation products might interact both with cement paste and cationic radionuclides under cementitious condition. However, further experimental observations and measurements are required for constituting empirical basis over the influence of UP2W degradation products on the retention of radionuclides in repositories for L/ILW.

5. References

[1] Szabo, P., A. Tasi, X. Gaona, R. Polly, A. Maier, S. Hedström, M. Altmaier and H. Geckeis, *Solubility of Ca(II), Ni(II), Nd(III) and Pu(IV) in the presence of proxy ligands for the degradation of polyacrylonitrile in cementitious systems.* Dalton Transactions, 2022. **51**(24): p. 9432-9444.

[2] Szabo, P., A. Tasi, X. Gaona, A. Maier, S. Hedström, M. Altmaier and H. Geckeis, *Uptake of selected organic ligands by hardened cement paste: studies on proxy ligands for the degradation of polyacrylonitrile and general considerations on the role of different functionalities in the uptake process.* Frontiers in Nuclear Engineering: p. 8.

[3] Gaona, X., P. Szabo, A. Tasi, A.C. Maier, S. Hedström, M. Altmaier and H. Geckeis, *Uptake of Ni(II), Eu(III) and Pu(III/IV) by hardened cemenet paste in the presence of proxy ligands for the degradation of polyacrylonitrile.* Frontiers in Nuclear Engineering, 2023. **2**: p. 3.

[4] Karakosta, C., C. Pappas, V. Marinakis and J. Psarras, *Renewable energy and nuclear power towards sustainable development: Characteristics and prospects.* Renewable and Sustainable Energy Reviews, 2013. **22**: p. 187-197.

[5] Poinssot, C. and H. Geckeis, *Radionuclide behaviour in the natural environment: science, implications and lessons for the nuclear industry*, Elsevier (2012).

[6] Androniuk, I., *Effects of cement organic additives on the adsorption of uranyl ions on calcium silicate hydrate phases: experimental determination and computational molecular modelling*. 2017, Ecole nationale supérieure Mines-Télécom Atlantique Bretagne Pays de la Loire.

[7] Ouzounian, G., S. Voinis and F. Boissier, *Radioactive waste management in France: safety demonstration fundamentals.* Annals of the ICRP, 2012. **41**(3-4): p. 286-293.

[8] Darda, S.A., H.A. Gabbar, V. Damideh, M. Aboughaly and I. Hassen, *A comprehensive review on radioactive waste cycle from generation to disposal.* Journal of Radioanalytical and Nuclear Chemistry, 2021. **329**(1): p. 15-31.

[9] *Radioactivity.Eu.Com, Radioactivity: Intermediate-level waste (ILW-LL).* https://www.radioactivity.eu.com/site/pages/ML_LLW.htm.

[10] *Radioactivity.Eu.Com, Radioactivity:Low - and intermediate waste (LILW-SL).* https://www.radioactivity.eu.com/site/pages/LILW_SL_Waste.htm.

[11] Jungjohann, A., M. Besnard, M. Buser, I. Fairlie, G. MacKerron, A. Macfarlane, E. Matyas, Y. Marignac, E. Sequens and J. Swahn, *World nuclear waste report*. Focus Europe, 2019.

[12] *Design Principles and Approaches for Radioactive Waste Repositories, IAEA Nuclear Energy Series, No. NW-T-1.27.* 2020.

[13] Miller, W., R. Alexander, N. Chapman, J.C. McKinley and J. Smellie, *Geological disposal of radioactive wastes and natural analogues*, Vol. 2. Elsevier (2000).

[14] Tasi, A., *Solubility, redox and sorption behavior of plutonium in the presence of α-D-isosaccharinic acid and cement under reducing conditions.* 2018.

[15] Svensk Kärnbränslehantering, A., *Safety analysis SFR 1: Long-term safety*. 2008, SKB R-08-130, SKB.

[16] Tasdigh, H., *Assessment of the Impact of Fiber Mass UP2 Degradation Products on Ni(II) and Eu(III) Sorption*. 2015.

[17] Duro, L., M. Grivé, X. Gaona, J. Bruno, T. Andersson, H. Borén, M. Dario, B. Allard, J. Hagberg and K. Källström, *Study of the effect of the fibre mass UP2 degradation products on radionuclide mobilisation*. 2012, Swedish Nuclear Fuel and Waste Management Co.: Sweden.

[18] Tasi, A., X. Gaona, D. Fellhauer, M. Böttle, J. Rothe, K. Dardenne, R. Polly, M. Grivé, E. Colàs and J. Bruno, *Thermodynamic description of the plutonium–α-D-isosaccharinic acid system I: Solubility, complexation and redox behavior*. Applied Geochemistry, 2018. **98**: p. 247-264.

[19] Tasi, A., X. Gaona, D. Fellhauer, M. Böttle, J. Rothe, K. Dardenne, R. Polly, M. Grivé, E. Colàs and J. Bruno, *Thermodynamic description of the plutonium–α–d–isosaccharinic acid system ii: Formation of quaternary Ca(II)–Pu(IV)–OH–ISA complexes*. Applied Geochemistry, 2018. **98**: p. 351-366.

[20] Keith-Roach, M., M. Lindgren and K. Källström, *Assessment of complexing agent concentrations in SFR*. 2014, SKB R-14-03, Svensk Kärnbränslehantering AB.

[21] Breuer, H., *SH atlasz: Kémia*, Springer Verlag (1995).

[22] Ebong, F.S. and N. Evans, *Modelling the sorption of ^{63}Ni to granitic materials: application of the component additive model.* Journal of Environmental Science and Engineering. B, 2012. **1**(3B).

[23] González-Siso, M.R., X. Gaona, L. Duro, M. Altmaier and J. Bruno, *Thermodynamic model of Ni(II) solubility, hydrolysis and complex formation with ISA*. Radiochimica Acta, 2018. **106**(1): p. 31-45.

[24] Lindgren, M., M. Pettersson and M. Wiborgh, *Correlation factors for C-14, Cl-36, Ni-59, Ni-63, Mo-93, Tc-99, I-129 and Cs-135. In operational waste for SFR 1*. 2007, Swedish Nuclear Fuel and Waste Management Co.: Sweden.

[25] Gamsjäger, H., J. Bugajski and W. Preis, *Chemical thermodynamics of nickel*, Elsevier Amsterdam, Amsterdam (2005).

[26] Van Loon, L.R. and M.A. Glaus, *Experimental and theoretical studies on alkaline degradation of cellulose and its impact on the sorption of radionuclides*. 1998, Paul Scherrer Inst.: Switzerland.

[27] Felipe-Sotelo, M., J. Hinchliff, L. Field, A. Milodowski, J. Holt, S. Taylor and D. Read, *The solubility of nickel and its migration through the cementitious backfill of a geological disposal facility for nuclear waste.* Journal of hazardous materials, 2016. **314**: p. 211-219.

[28] Palmer, D.A. and H. Gamsjäger, *Solubility measurements of crystalline β-$Ni(OH)_2$ in aqueous solution as a function of temperature and pH.* Journal of coordination chemistry, 2010. **63**(14-16): p. 2888-2908.

[29] Gayer, K.H. and A. Garrett, *The equilibria of nickel hydroxide, $Ni(OH)_2$, in solutions of hydrochloric acid and sodium hydroxide at 25.* Journal of the American Chemical Society, 1949. **71**(9): p. 2973-2975.

[30] Plyasunova, N.V., Y. Zhang and M. Muhammed, *Critical evaluation of thermodynamics of complex formation of metal ions in aqueous solutions. IV. Hydrolysis and hydroxo-complexes of Ni^{2+} at 298.15 K*. Hydrometallurgy, 1998. **48**(1): p. 43-63.

[31] Ochs, M., D. Hager, S. Helfer and B. Lothenbach. *Solubility of Radionuclides in Fresh and Leached Cementitious Systems at 22 °C and 50 °C*. in *Materials Research Society Symposium Proceedings*. 1998. MATERIALS RESEARCH SOCIETY.

[32] Warwick, P., N. Evans, T. Hall and S. Vines, *Complexation of Ni(II) by α-isosaccharinic acid and gluconic acid from pH 7 to pH 13.* Radiochimica Acta, 2003. **91**(4): p. 233-240.

[33] Palmer, D.A., P. Bénézeth, C. Xiao, D.J. Wesolowski and L.M. Anovitz, *Solubility measurements of crystalline NiO in aqueous solution as a function of temperature and pH.* Journal of solution chemistry, 2011. **40**(4): p. 680-702.

[34] Ochs, M., D. Mallants and L. Wang, *Radionuclide and Metal Sorption on Cement and Concrete*, Vol. 29. Springer International Publishing Switzerland, Switzerland (2016).

[35] Cotton, S., *The Lanthanides-Principles and Energetics*. Lanthanide and Actinide Chemistry, 2006: p. 9-22.
[36] Cotton, S., *Lanthanide and actinide chemistry*, John Wiley & Sons (2013).
[37] Keller, R.N., *The lanthanide contraction as a teaching aid*. Journal of Chemical Education, 1951. **28**(6): p. 312.
[38] Cotton, S.A. and J.M. Harrowfield, *Lanthanides: Coordination Chemistry*. Encyclopedia of Inorganic and Bioinorganic Chemistry, 2011.
[39] Ganjali, M.R., V.K. Gupta, F. Faridbod, and P. Norouzi, *Lanthanides series determination by various analytical methods*, Elsevier (2016).
[40] Geoffrey, F. and N Cloke, *Zero oxidation state compounds of scandium, yttrium, and the lanthanides*. Chemical Society Reviews, 1993. **22**(1): p. 17-24.
[41] Newton, D.E., *Chemical Elements:from Carbon to Krypton*, (1999).
[42] Ugale, A., T.N. Kalyani and S.J. Dhoble, *Potential of europium and samarium β-diketonates as red light emitters in organic light-emitting diodes*, in *Lanthanide-Based Multifunctional Materials*. 2018, Elsevier. p. 59-97.
[43] Enders, K., E. Stachowska, G. Marx, C. Zölch, U. Georg, J. Dembczynski, G. Werth and I. Collaboration, *Ground-state hyperfine-structure measurements of unstable Eu^{+} isotopes in a Paul ion trap*. Physical Review A, 1997. **56**(1): p. 265.
[44] Dostal, J., *Rare earth element deposits of alkaline igneous rocks*. Resources, 2017. **6**(3): p. 34.
[45] Neck, V., M. Altmaier, T. Rabung, J. Lützenkirchen and T. Fanghänel, *Thermodynamics of trivalent actinides and neodymium in NaCl, $MgCl_2$, and $CaCl_2$ solutions: Solubility, hydrolysis, and ternary Ca-M(III)-OH complexes*. Pure and Applied Chemistry, 2009. **81**(9): p. 1555-1568.
[46] Tobias, R.S. and A. Garrett, *The thermodynamic properties of neodymium hydroxide $Nd(OH)_3$, in acid, neutral and alkaline solutions at 25°; the hydrolysis of the neodymium and praseodymium ions, Nd^{3+}, Pr^{3+}*. Journal of the American Chemical Society, 1958. **80**(14): p. 3532-3537.
[47] Icenhower, J., C. Sisk-Scott, L.D. Kirkes, J. Knox and C. Marrs, *Solubility of $Nd(OH)_3$ at high pH*. 2017, Sandia National Lab.(SNL-NM), Albuquerque, NM (United States).
[48] Giroux, S., S. Aury, B. Henry and P. Rubini, *Complexation of lanthanide(III) ions with polyhydroxy carboxylic acids in aqueous solutions*. European Journal of Inorganic Chemistry, 2002. **2002**(5): p. 1162-1168.
[49] Vercammen, K., *Complexation of calcium, thorium and europium by α-isosaccharinic acid under alkaline conditions*. 2000, ETH Zurich.
[50] Gugau, K., *Complexation of Nd(III) and Cm(III) with α-D-isosaccharinic acid under repository relevant conditions*. 2016: p. 99.
[51] Altmaier, M., X. Gaona and T. Fanghänel, *Recent advances in aqueous actinide chemistry and thermodynamics*. Chemical reviews, 2013. **113**(2): p. 901-943.
[52] Thyssen, P. and K. Binnemans, *Accommodation of the rare earths in the periodic table: A historical analysis*, in *Handbook on the Physics and Chemistry of Rare Earths*. 2011, Elsevier. p. 1-93.
[53] Tits, J.E. Wieland, *Actinide Sorption by Cementitious Materials*. 2018.
[54] Runde, W., *The chemical interactions of actinides in the environment*. Los Alamos Science, 2000. **26**: p. 392-411.
[55] Choppin, G., *Actinide speciation in the environment*. Journal of Radioanalytical and Nuclear Chemistry, 2007. **273**(3): p. 695-703.
[56] Choppin, G.R., *Actinide speciation in the environment*. Radiochimica Acta, 2003. **91**(11): p. 645-650.

[57] Knopp, R., V. Neck and J. Kim, *Solubility, hydrolysis and colloid formation of plutonium(IV).* Radiochimica Acta, 1999. **86**(3-4): p. 101-108.
[58] Neck, V. and J. Kim, *Solubility and hydrolysis of tetravalent actinides.* Radiochimica Acta, 2001. **89**(1): p. 1-16.
[59] Guillaumont, R.F.J. Mompean, *Update on the chemical thermodynamics of uranium, neptunium, plutonium, americium and technetium*, Vol. 5. Elsevier Amsterdam (2003).
[60] Seaborg, G., *The Transuranium Elements Present Status Nobel Lecture*. 1951, Radiation Lab., Univ. of Calif., Berkeley, CA.
[61] Kudo, A., *Plutonium in the Environment*, Elsevier (2001).
[62] Clark, D.L., *The chemical complexities of plutonium*. Los Alamos Science, 2000. **26**: p. 364-381.
[63] Neck, V., M. Altmaier and T. Fanghänel, *Solubility of plutonium hydroxides/hydrous oxides under reducing conditions and in the presence of oxygen.* Comptes Rendus Chimie, 2007. **10**(10-11): p. 959-977.
[64] Grenthe, I., X. Gaona, L. Rao, A. Plyasunov, W. Runde, B. Grambow, R. Konings, A. Smith, E. Moore and M.-E. Ragoussi, *Second update on the chemical thermodynamics of uranium, neptunium, plutonium, americium and technetium. Chemical thermodynamics volume 14*. 2020, Organisation for Economic Co-Operation and Development.
[65] Tasi, A., X. Gaona, D. Fellhauer, M. Böttle, J. Rothe, K. Dardenne, D. Schild, M. Grivé, E. Colàs and J. Bruno, *Redox behavior and solubility of plutonium under alkaline, reducing conditions.* Radiochimica Acta, 2018. **106**(4): p. 259-279.
[66] Altmaier, M., V. Neck, J. Lützenkirchen and T. Fanghänel, *Solubility of plutonium in $MgCl_2$ and $CaCl_2$ solutions in contact with metallic iron.* Radiochimica Acta, 2009. **97**(4-5): p. 187-192.
[67] Moreton, A.D., *Thermodynamic modelling of the effect of hydroxycarboxylic acids on the solubility of plutonium at high pH.* MRS Online Proceedings Library (OPL), 1992. **294**.
[68] Gaona, X., V. Montoya, E. Colàs, M. Grivé and L. Duro, *Review of the complexation of tetravalent actinides by ISA and gluconate under alkaline to hyperalkaline conditions.* Journal of Contaminant Hydrology, 2008. **102**(3-4): p. 217-227.
[69] Tits, J., K. Iijima, E. Wieland and G. Kamei, *The uptake of radium by calcium silicate hydrates and hardened cement paste.* Radiochimica Acta, 2006. **94**(9-11): p. 637-643.
[70] Glasser, F.M. Atkins, *Cements in radioactive waste disposal.* Mrs Bulletin, 1994. **19**(12): p. 33-38.
[71] Pointeau, I., P. Reiller, N. Macé, C. Landesman and N. Coreau, *Measurement and modeling of the surface potential evolution of hydrated cement pastes as a function of degradation.* Journal of colloid and interface science, 2006. **300**(1): p. 33-44.
[72] Wieland, E., B. Lothenbach, M. Glaus, T. Thoenen and B. Schwyn, *Influence of superplasticizers on the long-term properties of cement pastes and possible impact on radionuclide uptake in a cement-based repository for radioactive waste.* Applied geochemistry, 2014. **49**: p. 126-142.
[73] Gougar, M., B. Scheetz and D. Roy, *Ettringite and C-S-H Portland cement phases for waste ion immobilization: A review.* Waste management, 1996. **16**(4): p. 295-303.
[74] Tits, J., T. Fujita, M. Tsukamoto and E. Wieland, *Uranium(VI) uptake by synthetic calcium silicate hydrates.* MRS Online Proceedings Library (OPL), 2008. **1107**.
[75] Wang, L., E. Martens, D. Jacques, P. De Canniere, D. Mallants and J. Berry, *Review of sorption values for the cementitious near field of a near-surface radioactive waste disposal facility.* 2012.

[76] Lothenbach, B. and E. Wieland, *A thermodynamic approach to the hydration of sulphate-resisting Portland cement*. Waste Management, 2006. **26**(7): p. 706-719.
[77] Kamaruzaman, N.S., D.S. Kessel and C.-L. Kim, *Management of spent ion-exchange resins from nuclear power plant by blending method.* Journal of Nuclear Fuel Cycle and Waste Technology (JNFCWT), 2018. **16**(1): p. 65-82.
[78] Wang, Y.X., C.G. Wang, J.W. Wu and M. Jing, *High-temperature DSC study of polyacrylonitrile precursors during their conversion to carbon fibers.* Journal of applied polymer science, 2007. **106**(3): p. 1787-1792.
[79] Litmanovich, A.D. and N.A. Platé, *Alkaline hydrolysis of polyacrylonitrile. On the reaction mechanism*. Macromolecular Chemistry and Physics, 2000. **201**(16): p. 2176-2180.
[80] Glazkovskii, Y. and V.P. Mikhailov, *A spectroscopic study of the structure of products of chemical transformations of polyacrylonitrile.* Polymer Science USSR, 1966. **8**(10): p. 1844-1849.
[81] Bajaj, P., R. Chavan, and B. Manjeet, *Saponification kinetics of acrylonitrile terpolymer and polyacrylonitrile.* Journal of Macromolecular Science—Chemistry, 1985. **22**(9): p. 1219-1239.
[82] Bashir, Z., G. Manns, D. Service, D. Bott, I. Herbert, R. Ibbett, and S. Church, *Investigation of base induced cyclization and methine proton abstraction in polyacrylonitrile solutions.* Polymer, 1991. **32**(10): p. 1826-1833.
[83] Van Loon, L. and W. Hummel, *The degradation of strong basic anion exchange resins and mixed-bed ion-exchange resins: effect of degradation products on radionuclide speciation.* Nuclear Technology, 1999. **128**(3): p. 388-401.
[84] Tasi, A., P. Szabo, X. Gaona, M. Altmaier and H. Geckeis, *Contribution by KIT-INE to CORI Task 2*, in *Eurad European Joint Programme on Radiaoactive waste management, Milestone DMS97 – CORI Technical Report -Task 2 Hydrolytic/radiolytic degradation of organics: description of first results on hydrolytic and radiolytic organic degradation and identification of released species*, D. Ricard and J. Vandenborre, Editors. 2021.
[85] Gupta, A., D. Paliwal and P. Bajaj, *Melting behavior of acrylonitrile polymers.* Journal of applied polymer science, 1998. **70**(13): p. 2703-2709.
[86] Karacan, I. and G. Erdogan, *The influence of thermal stabilization stage on the molecular structure of polyacrylonitrile fibers prior to the carbonization stage.* Fibers and Polymers, 2012. **13**(3): p. 295-302.
[87] Wieland, E., A. Jakob, J. Tits, B. Lothenbach and D. Kunz, *Sorption and diffusion studies with low molecular weight organic compounds in cementitious systems.* Applied Geochemistry, 2016. **67**: p. 101-117.
[88] Miyashita, M., E. Yamada and M. Kawano, *Influence of low–molecular–weight dicarboxylic acids on the formation of calcium carbonate minerals in solutions with Mg^{2+} ions.* Journal of Mineralogical and Petrological Sciences, 2018. **113**(4): p. 207-217.
[89] Van Loon, L., M. Glaus, S. Stallone and A. Laube, *Sorption of isosaccharinic acid, a cellulose degradation product, on cement*. Environmental science & technology, 1997. **31**(4): p. 1243-1245.
[90] Plank, J. and C. Hirsch, *Impact of zeta potential of early cement hydration phases on superplasticizer adsorption.* Cement and concrete research, 2007. **37**(4): p. 537-542.
[91] Srinivasan, S., S. Barbhuiya, D. Charan, and S. Pandey, *Characterising cement–superplasticiser interaction using zeta potential measurements.* Construction and Building Materials, 2010. **24**(12): p. 2517-2521.

[92] Viallis-Terrisse, H., A. Nonat and J.-C. Petit, *Zeta-potential study of calcium silicate hydrates interacting with alkaline cations.* Journal of colloid and interface science, 2001. **244**(1): p. 58-65.
[93] Pointeau, I., N. Coreau and P.E. Reiller, *Uptake of anionic radionuclides onto degraded cement pastes and competing effect of organic ligands.* Radiochimica Acta, 2008. **96**(6): p. 367-374.
[94] Tasi, A., X. Gaona, T. Rabung, D. Fellhauer, J. Rothe, K. Dardenne, J. Lützenkirchen, M. Grivé, E. Colàs and J. Bruno, *Plutonium retention in the isosaccharinate–cement system*. Applied Geochemistry, 2021. **126**: p. 104862.
[95] Wieland, E., *Sorption data base for the cementitious near-field of L/ILW and ILW repositories for provisional safety analyses for SGT-E2*. 2014, Paul Scherrer Institute (PSI): Switzerland.
[96] Kulmala, S. and M. Hakanen, *The solubility of Zr, Nb and Ni in groundwater and concrete water, and sorption on crushed rock and cement*. 1993, Nuclear Waste Commission of Finnish Power Companies.
[97] Hietanen, R., E.-L. Kämäräinen and M. Alaluusua, *Sorption of strontium, cesium, nickel, iodine and carbon in concrete*. 1984, Voimayhtioeiden Ydinjaetetoimikunta.
[98] Wieland, E., J. Tits, P. Spieler and J.-P. Dobler, *Immobilisation of strontium, nickel and iodide by a sulphate-resisting Portland cement*. 1998.
[99] Noshita, K., T. Nishi, T. Yoshida, H. Fujihara, N. Saito and S. Tanaka, *Categorization of cement hydrates by radionuclide sorption mechanism*. MRS Online Proceedings Library (OPL), 2000. **663**.
[100] Scheidegger, A.M., E. Wieland, A.C. Scheinost, R. Dähn and P. Spieler, *Spectroscopic evidence for the formation of layered Ni−Al double hydroxides in cement*. Environmental science & technology, 2000. **34**(21): p. 4545-4548.
[101] Wieland, E. and L. Van Loon, *Cementitious near-field sorption data base for performance assessment of an ILW repository in Opalinus Clay*. 2003, Paul Scherrer Institut: Switzerland.
[102] Wieland, E., J. Tits, A. Ulrich and M.H. Bradbury, *Experimental evidence for solubility limitation of the aqueous Ni(II) concentration and isotopic exchange of ^{63}Ni in cementitious systems.* Radiochimica Acta, 2006. **94**(1): p. 29-36.
[103] Holgersson, S., Y. Albinsson, B. Allard, H. Borén, I. Pavasars and I. Engkvist, *Effects of gluco-isosaccharinate on Cs, Ni, Pm and Th sorption onto, and diffusion into cement*. Radiochimica Acta, 1998. **82**(s1): p. 393-398.
[104] Pilkington, N.N. Stone, *The solubility and sorption of nickel and niobium under high pH conditions*. 1990, United Kingdom Nirex.
[105] Missana, T., M. García-Gutiérrez, U. Alonso and O. Almendros-Ginestá, *Nickel retention by calcium silicate hydrate phases: Evaluation of the role of the Ca/Si ratio on adsorption and precipitation processes.* Applied Geochemistry, 2022: p. 105197.
[106] Dario, M., M. Molera and B. Allard, *Effect of organic ligands on the sorption of europium on TiO_2 and cement at high pH*. 2004, Swedish Nuclear Fuel and Waste Management Co.: Sweden.
[107] Randall, M., B. Rigby, O. Thomson and D. Trivedi, *Assessment of the effects of cellulose degradation products on the behaviour of europium and thorium*. Report prepared on behalf of NDA: National Nuclear Laboratory, 2012. **12239**.
[108] Wieland, E., J. Tits, P. Spieler and J. Dobler, *Interaction of Eu(III) and Th(IV) with sulfate-resisting Portland cement*. MRS Online Proceedings Library Archive, 1997. **506**.

[109] Pointeau, I., B. Piriou, M. Fedoroff, M.-G. Barthes, N. Marmier and F. Fromage, *Sorption mechanisms of Eu^{3+} on CSH phases of hydrated cements.* Journal of Colloid and Interface Science, 2001. **236**(2): p. 252-259.
[110] Schlegel, M.L., I. Pointeau, N. Coreau and P. Reiller, *Mechanism of europium retention by calcium silicate hydrates: an EXAFS study.* Environmental science & technology, 2004. **38**(16): p. 4423-4431.
[111] Mandaliev, P., T. Stumpf, J. Tits, R. Dähn, C. Walther and E. Wieland, *Uptake of Eu(III) by 11 Å tobermorite and xonotlite: a TRLFS and EXAFS study.* Geochimica et Cosmochimica Acta, 2011. **75**(8): p. 2017-2029.
[112] Tits, J., T. Stumpf, T. Rabung, E. Wieland and T. Fanghänel, *Uptake of Cm(III) and Eu(III) by calcium silicate hydrates: a solution chemistry and time-resolved laser fluorescence spectroscopy study.* Environmental science & technology, 2003. **37**(16): p. 3568-3573.
[113] Stumpf, T., J. Tits, C. Walther, E. Wieland and T. Fanghänel, *Uptake of trivalent actinides (curium(III)) by hardened cement paste: a time-resolved laser fluorescence spectroscopy study.* Journal of colloid and interface science, 2004. **276**(1): p. 118-124.
[114] Bradbury, M.H. and F.-A. Sarott, *Sorption databases for the cementitious near-field of a L/ILW repository for performance assessment*. 1995, Paul Scherrer Inst.(PSI).
[115] Rojo, H., M. García-Gutiérrez, T. Missana and H. Galán, *Sorption of Pu(IV) and Tc(IV) on concrete and mortar and effect of the complexation by isosaccharinic acid.* MRS Online Proceedings Library (OPL), 2012. **1475**.
[116] Häußler, V., S. Amayri, A. Beck, T. Platte, T.A. Stern, T. Vitova and T. Reich, *Uptake of actinides by calcium silicate hydrate (CSH) phases.* Applied Geochemistry, 2018. **98**: p. 426-434.
[117] Amayri, S., D.R. Fröhlich, U. Kaplan, N. Trautmann and T. Reich, *Distribution coefficients for the sorption of Th, U, Np, Pu, and Am on Opalinus Clay.* Radiochimica Acta, 2016. **104**(1): p. 33-40.
[118] Bayliss, S., R. McCrohon, P. Oliver, N. Pilkington and H. Thomason, *Near field sorption studies: January 1989 to June 1991, NSS/R227*. 1996, AEA-ESD-0353.
[119] Aggarwal, S., M. Angus and J. Ketchen, *Sorption of radionuclides onto specific mineral phases present in repository cements.* Report AEA Technology NSS, 2000. **312**(1).
[120] Pointeau, I., C. Landesman, E. Giffaut, P. Reiller, N. Coreau, C. Moisan and P. Reiller, *Etude de la rétention chimique des radionucléides Cs(I).* Am(III), Zr(IV), Pu(IV), Nb(V), U(VI) et Tc(IV) par es Matériaux Cimentaires Degradés: p. 03-037.
[121] Baston, G., J. Berry, M. Brownsword, T. Heath, C. Tweed and S. Williams, *Sorption of plutonium and americium on repository, backfill and geological materials relevant to the JNFL low-level radioactive waste repository at Rokkasho-Mura.* MRS Online Proceedings Library, 1994. **353**(1): p. 957-964.
[122] Van Loon, L.R., M.A. Glaus, A. Laube and S. Stallone, *Degradation of cellulosic materials under the alkaline conditions of a cementitious repository for low- and intermediate level radioactive waste. Part III: Effect of degradation products on the sorption of radionuclides on feldspar.* Radiochimica Acta, 1999. **86**(3-4): p. 183-189.
[123] Bruno, J., M.R. González-Siso, L. Duro, X. Gaona and M. Altmaier, *Key master variables affecting the mobility of Ni, Pu, Tc and U in the near field of the SFR repository*, in *Main Experimental Findings and PA Implications of the PhD Thesis, SKB Tehcnical Report, 18-01*. 2018, Svensk Kärnbränslehantering AB Solna, Sweden.
[124] Tits, J., E. Wieland and M. Bradbury, *The effect of isosaccharinic acid and gluconic acid on the retention of Eu(III), Am(III) and Th(IV) by calcite.* Applied Geochemistry, 2005. **20**(11): p. 2082-2096.

[125] Diesen, V., K. Forsberg and M. Jonsson, *Effects of cellulose degradation products on the mobility of Eu(III) in repositories for low and intermediate level radioactive waste.* Journal of hazardous materials, 2017. **340**: p. 384-389.
[126] Holgersson, S., I. Dubois and L. Börstell, *Batch experiments of Cs, Co and Eu sorption onto cement with dissolved fibre mass UP2 in the liquid phase.* 2011.
[127] Rojo, H., X. Gaona, T. Rabung, R. Polly, M. García-Gutiérrez, T. Missana and M. Altmaier, *Complexation of Nd(III)/Cm(III) with gluconate in alkaline NaCl and $CaCl_2$ solutions: Solubility, TRLFS and DFT studies.* Applied Geochemistry, 2021. **126**: p. 104864.
[128] Altmaier, M., V. Neck and T. Fanghänel, *Solubility of Zr(IV), Th(IV) and Pu(IV) hydrous oxides in $CaCl_2$ solutions and the formation of ternary Ca-M(IV)-OH complexes.* Radiochimica Acta, 2008. **96**(9-11): p. 541-550.
[129] Schepperle, J., *Untersuchungen zur Löslichkeit und Komplexierung von vierwertigem Plutonium und Neptunium in verdünnten und konzentrierten Salzlösungen (on-going), in Institute for Nuclear Waste Disposal (INE)*. 2017, Karlsruhe Institute of Technology: Karlsruhe, Germany.
[130] *Joint Committee on Powder Diffraction Standards, JCPDS-International center for diffraction data* (2000).
[131] Hohenberg, P. and W. Kohn, *Inhomogeneous electron gas.* Physical review, 1964. **136**(3B): p. B864.
[132] Kohn, W. and L.J. Sham, *Self-consistent equations including exchange and correlation effects.* Physical review, 1965. **140**(4A): p. A1133.
[133] Furche, F., R. Ahlrichs, C. Hättig, W. Klopper, M. Sierka and F. Weigend, *Turbomole.* Wiley Interdisciplinary Reviews: Computational Molecular Science, 2014. **4**(2): p. 91-100.
[134] Deglmann, P., K. May, F. Furche and R. Ahlrichs, *Nuclear second analytical derivative calculations using auxiliary basis set expansions.* Chemical physics letters, 2004. **384**(1-3): p. 103-107.
[135] Eichkorn, K., F. Weigend, O. Treutler and R. Ahlrichs, *Auxiliary basis sets for main row atoms and transition metals and their use to approximate Coulomb potentials.* Theoretical Chemistry Accounts, 1997. **97**(1): p. 119-124.
[136] Schäfer, A., H. Horn and R. Ahlrichs, *Fully optimized contracted Gaussian basis sets for atoms Li to Kr.* The Journal of Chemical Physics, 1992. **97**(4): p. 2571-2577.
[137] Treutler, O. and R. Ahlrichs, *Efficient molecular numerical integration schemes.* The Journal of Chemical Physics, 1995. **102**(1): p. 346-354.
[138] von Arnim, M. and R. Ahlrichs, *Geometry optimization in generalized natural internal coordinates.* The Journal of chemical physics, 1999. **111**(20): p. 9183-9190.
[139] Ahlrichs, R., F. Furche and S. Grimme, *Comment on "Assessment of exchange correlation functionals"[AJ Cohen, NC Handy, Chem. Phys. Lett. 316 (2000) 160–166]*. Chemical Physics Letters, 2000. **325**(1-3): p. 317-321.
[140] Klamt, A., *Conductor-like screening model for real solvents: a new approach to the quantitative calculation of solvation phenomena*. The Journal of Physical Chemistry, 1995. **99**(7): p. 2224-2235.
[141] Klamt, A. and G. Schüürmann, *COSMO: a new approach to dielectric screening in solvents with explicit expressions for the screening energy and its gradient*. Journal of the Chemical Society, Perkin Transactions 2, 1993(5): p. 799-805.
[142] Pointeau, I., C. Landesman, E. Giffaut and P. Reiller, *Reproducibility of the uptake of U(VI) onto degraded cement pastes and calcium silicate hydrate phases.* Radiochimica Acta, 2004. **92**(9-11): p. 645-650.

[143] Giffaut, E., M. Grivé, P. Blanc, P. Vieillard, E. Colàs, H. Gailhanou, S. Gaboreau, N. Marty, B. Made and L. Duro, *Andra thermodynamic database for performance assessment: ThermoChimie.* Applied Geochemistry, 2014. **49**: p. 225-236.
[144] Cannan, R.K. and A. Kibrick, *Complex formation between carboxylic acids and divalent metal cations.* Journal of the American Chemical Society, 1938. **60**(10): p. 2314-2320.
[145] Schubert, J. and A. Lindenbaum, *Stability of Alkaline Earth—Organic Acid Complexes Measured by Ion Exchange1.* Journal of the American Chemical Society, 1952. **74**(14): p. 3529-3532.
[146] Verbeek, F. and H. Thun, *The stability constants of the alkaline earth lactate and α-hydroxyisobutyrate complexes.* Analytica Chimica Acta, 1965. **33**: p. 378-383.
[147] Piispanen, J. and L. Lajunen, *Complex Formation Equilibria Of Some Aliphatic Alpha-Hydroxycarboxylic Acids. I: The Determination Of Protonation Constants And The Study Of Calcium(II) And Magnesium(II) Complexes.* Acta chemica scandinavica, 1995. **49**(4): p. 235-240.
[148] Dudás, C., B. Kutus, É. Böszörményi, G. Peintler, Z. Kele, I. Pálinkó and P. Sipos, *Comparison of the Ca^{2+} complexing properties of isosaccharinate and gluconate–is gluconate a reliable structural and functional model of isosaccharinate?* Dalton Transactions, 2017. **46**(40): p. 13888-13896.
[149] Prapaipong, P., E.L. Shock and C.M. Koretsky, *Metal-organic complexes in geochemical processes: Temperature dependence of the standard thermodynamic properties of aqueous complexes between metal cations and dicarboxylate ligands.* Geochimica et cosmochimica acta, 1999. **63**(17): p. 2547-2577.
[150] Grabarić, B., B. Mayer, I. Piljac and I. Filipović, *Spectrophotometric determination of stability constants of n-butyrate and 2-, 3-and 4-hydroxybutyrate of cobalt(II), nickel(II) and copper(II).* Journal of Inorganic and Nuclear Chemistry, 1974. **36**(12): p. 3809-3812.
[151] Inoue, T., K. Kojima and R. Shimozawa, *Kinetic and equilibrium studies of complex formation of nickel(II) with carboxylate ligands at high pressure. 1. Nickel(II) succinate and nickel(II) maleate.* Inorganic Chemistry, 1983. **22**(26): p. 3972-3977.
[152] Kojima, K., T. Inoue, M. Izaki and R. Shimozawa, *Kinetic and Equilibrium Studies of Complex Formation of Nickel(II) with Carboxylate Ligands at High Pressure. III. Nickel(II) Malonate and Nickel(II) Tartronate.* Bulletin of the Chemical Society of Japan, 1986. **59**(1): p. 139-144.
[153] Altmaier, M., V. Neck and T. Fanghänel, *Solubility and colloid formation of Th(IV) in concentrated NaCl and $MgCl_2$ solution.* Radiochimica Acta, 2004. **92**(9-11): p. 537-543.
[154] Choppin, G., A. Dadgar and E. Rizkalla, *Thermodynamics of complexation of lanthanides by dicarboxylate ligands.* Inorganic Chemistry, 1986. **25**(20): p. 3581-3584.
[155] Deelstra, H. and F. Verbeek, *The Ionization Constant of α-Hydroxy-Isobutyric Acid.* Bulletin des Sociétés Chimiques Belges, 1963. **72**(9-10): p. 612-618.
[156] Wang, Z.-M., L. Van de Burgt and G. Choppin, *Spectroscopic study of lanthanide(III) complexes with aliphatic dicarboxylic acids.* Inorganica Chimica Acta, 2000. **310**(2): p. 248-256.
[157] Thakur, P., P. Pathak, T. Gedris and G. Choppin, *Complexation of Eu(III), Am(III) and Cm(III) with dicarboxylates: thermodynamics and structural aspects of the binary and ternary complexes.* Journal of solution chemistry, 2009. **38**(3): p. 265.

[158] Kim, H.-K., K. Jeong, H.-R. Cho, K. Kwak, E.C. Jung and W. Cha, *Study of Aqueous Am(III)-Aliphatic Dicarboxylate Complexes: Coordination Mode-Dependent Optical Property and Stability Changes.* Inorganic Chemistry, 2020. **59**(19): p. 13912-13922.
[159] Tomat, G., L. Magon, R. Portanova and A. Cassol, *Complexes of thorium(IV) with dicarboxylate ligands in aqueous solution.* Zeitschrift für anorganische und allgemeine Chemie, 1972. **393**(2): p. 184-192.
[160] Magon, L., A. Bismondo, L. Maresca, G. Tomat and R. Portanova, *Stability-constants of Thorium(IV) complexes with alpha-hydroxymonoccarboxylate, beta-hydroxymonocarboxylate and gamma-hydroxymonocarboxylate ligands in aqueous-solution.* Journal Of Inorganic & Nuclear Chemistry, 1973. **35**(12): p. 4237-4243.
[161] Kobayashi, T., T. Sasaki, I. Takagi and H. Moriyama, *Solubility and solubility-limiting solid phase in M(IV)-OH-dicarboxylate ternary aqueous system*. Journal of nuclear science and technology, 2011. **48**(7): p. 993-1003.
[162] Jhung, S.H., J.H. Lee, P.M. Forster, G. Férey, A.K. Cheetham and J.S. Chang, *Microwave Synthesis of Hybrid Inorganic–Organic Porous Materials: Phase-Selective and Rapid Crystallization.* Chemistry–A European Journal, 2006. **12**(30): p. 7899-7905.
[163] Koleżyński, A., B. Handke and E. Drożdż-Cieśla, *Crystal structure, electronic structure, and bonding properties of anhydrous nickel oxalate.* Journal of thermal analysis and calorimetry, 2013. **113**(1): p. 319-328.
[164] Montney, M.R., R.M. Supkowski, R.J. Staples,and R.L. LaDuca, *Synthesis, crystal structure, and magnetic properties of two-dimensional divalent metal glutarate/dipyridylamine coordination polymers, with a single crystal-to-single crystal transformation in the copper derivative.* Journal of Solid State Chemistry, 2009. **182**(1): p. 8-17.
[165] Böszörményi, É., J. Lado, C. Dudás, B. Kutus, M. Szabados, G. Varga, I. Pálinkó and P. Sipos, *The structure and composition of solid complexes comprising of Nd(III), Ca(II) and D-gluconate isolated from solutions relevant to radioactive waste disposal.* Pure and Applied Chemistry, 2020. **92**(10): p. 1709-1715.
[166] García, D., P. Henocq, O. Riba, M. López-García, B. Madé and J.-C. Robinet, *Adsorption behaviour of isosaccharinic acid onto cementitious materials.* Applied Geochemistry, 2020. **118**: p. 104625.
[167] Glaus, M.A., A. Laube and L.R. Van Loon, *Solid–liquid distribution of selected concrete admixtures in hardened cement pastes.* Waste Management, 2006. **26**(7): p. 741-751.
[168] Kaneko, S., H. Tanabe, M. Sasoh, R. Takahashi, T. Shibano and S. Tateyama, *A study on the chemical forms and migration behavior of carbon-14 leached from the simulated hull waste in the underground condition.* MRS Online Proceedings Library (OPL), 2002. **757**.
[169] Matsumoto, J., T. Banba and S. Muraoka, *Adsorption of carbon-14 on mortar.* MRS Online Proceedings Library Archive, 1994. **353**.
[170] Androniuk, I. and A.G. Kalinichev, *Molecular dynamics simulation of the interaction of uranium(VI) with the C–S–H phase of cement in the presence of gluconate.* Applied Geochemistry, 2020. **113**: p. 104496.
[171] Smith, R., A. Martell and R. Motekaitis, *NIST standard reference database 46.* NIST Critically Selected Stability Constants of Metal Complexes Database Ver, 2004. **2**.
[172] Hummel, W., F.J. Mompean, M. Illemassène and J. Perrone, *Chemical thermodynamics of compounds and complexes of U, Np, Pu, Am, Tc, Se, Ni and Zr with selected organic ligands*, Vol. 9. Elsevier Amsterdam (2005).

[173] Kutus, B., X. Gaona, A. Pallagi, I. Pálinkó, M. Altmaier and P. Sipos, *Recent advances in the aqueous chemistry of the calcium(II)-gluconate system–Equilibria, structure and composition of the complexes forming in neutral and in alkaline solutions*. Coordination Chemistry Reviews, 2020. **417**: p. 213337.
[174] Ballinger, P. and F. Long, *Acid Ionization Constants of Alcohols. II. Acidities of Some Substituted Methanols and Related Compounds1, 2*. Journal of the American Chemical Society, 1960. **82**(4): p. 795-798.
[175] Pallagi, A., É.G. Bajnóczi, S.E. Canton, T. Bolin, G. Peintler, B. Kutus, Z. Kele, I. Pálinkó and P. Sipos, *Multinuclear complex formation between Ca(II) and gluconate ions in hyperalkaline solutions*. Environmental science & technology, 2014. **48**(12): p. 6604-6611.
[176] Pointeau, I., D. Hainos, N. Coreau and P. Reiller, *Effect of organics on selenite uptake by cementitious materials*. Waste Management, 2006. **26**(7): p. 733-740.
[177] Svensk Kärnbränslehantering, A., *Data report for the safety assessment SR-PSU*. 2014, SKB TR-14-10, SKB.
[178] Wieland, E., J. Tits, P. Spieler, J. Dobler and A. Scheidegger, *Uptake of nickel and strontium by a sulphate-resisting Portland cement*. Applied mineralogy, 2000. **2**: p. 705.

6. Appendix

6.1 Auxiliary thermodynamic data on nuclide aqueous species and solid compounds

Table A-1 *Solubility and hydrolysis constants of Ni(II) used in this work (I = 0, T = 25 °C) [23, 25].*

Hydrolysis equilibria	log $\beta°$ / log $K°_{s,0}$
$Ni^{2+}+H_2O(l) \rightleftarrows NiOH^+ + H^+$	–(9.54 ± 0.14)
$Ni^{2+}+2\ H_2O(l) \rightleftarrows Ni(OH)_2(aq) + 2\ H^+$	–(19.7 ± 0.4)
$Ni^{2+}+3\ H_2O(l) \rightleftarrows Ni(OH)_3^- + 3\ H^+$	–(29.2 ± 1.7)
$2\ Ni^{2+}+H_2O(l) \rightleftarrows Ni_2OH^{3+} + H^+$	–(10.6 ± 1.0)
$4\ Ni^{2+}+4\ H_2O(l) \rightleftarrows Ni_4(OH)_4^{2-} + 4\ H^+$	–(27.52 ± 0.15)
β–$Ni(OH)_2(cr) + 2\ H^+ \rightleftarrows Ni^{2+} + 2\ H_2O(l)$	(11.03 ± 0.28)
β–$Ni(OH)_2(cr) \rightleftarrows Ni(OH)_2(aq)$	–(7.6 ± 0.4)

Table A-2*. Solubility and hydrolysis constants of Nd(III) used in this work (I = 0, T = 25 °C) [45].*

Hydrolysis equilibria	log $\beta°$ / log $K°_{s,0}$
$Nd^{3+} + H_2O(l) \rightleftarrows NdOH^{2+} + H^+$	–(7.4 ± 0.4)
$Nd^{3+} + 2\ H_2O(l) \rightleftarrows Nd(OH)_2^+ + 2H^+$	–(15.7 ± 0.7)
$Nd^{3+} + 3\ H_2O(l) \rightleftarrows Nd(OH)_3(aq) + 3\ H^+$	–(26.2 ± 0.5)
$Nd^{3+} + 4\ H_2O(l) \rightleftarrows Nd(OH)_4^- + 4\ H^+$	–(40.7 ± 0.7)
$Nd(OH)_3(s) + 3\ H^+ \rightleftarrows Nd^{3+} + 3\ H_2O(l)$	(17.2 ± 0.4)[a]

a*: represented in* log $K°_{s,0}$

Table A-3*. Solubility and hydrolysis constants of Pu(IV) used in this work (I = 0, T = 25 °C) [14, 63-65].*

Hydrolysis equilibria	log $\beta°$ / log $K°_{s,0}$
$PuO_2(am, hyd) \rightleftarrows Pu^{4+} + 4\ OH^-$	−(58.3 ± 0.5)
$PuO_2(am) + 2\ H_2O(l) + e^- \rightleftarrows Pu^{3+} + 4\ OH^-$	−(58.1 ± 0.4)
$PuO_2(am, hyd) + 2\ H_2O(l) + e^- \rightleftarrows Pu^{4+} + 4\ OH^-$	−(58.1 ± 0.4)
$PuO_2\ (am, hyd)\ + 2\ H_2O(l) \rightleftarrows Pu(OH)_4(aq)$	−(10.4 ± 0.5)
$Pu^{4+} + OH^- \rightleftarrows Pu(OH)^{3+}$	(14.6 ± 0.2)
$Pu^{4+} + 2\ OH^- \rightleftarrows Pu(OH)_2^{2+}$	(28.6 ± 0.3)
$Pu^{4+} + 3\ OH^- \rightleftarrows Pu(OH)_3^+$	(39.7 ± 0.4)
$Pu^{4+} + 4\ OH^- \rightleftarrows Pu(OH)_4(aq)$	(47.5 ± 0.5)

Table A-4. *Solubility and hydrolysis constants of Pu(III) used in this work (I = 0, T = 25 °C) [14, 63-65].*

Hydrolysis equilibria	**log $\beta°$ / log $K°_{s,0}$**
$Pu(OH)_3(am) \rightleftarrows Pu^{3+} + 3\ OH^-$	–(26.2 ± 1.5)
$Pu^{3+} + OH^- \rightleftarrows Pu(OH)^{2+}$	(7.1 ± 0.3)
$Pu^{3+} + 2\ OH^- \rightleftarrows Pu(OH)_2^+$	(12.9 ± 0.7)
$Pu^{3+} + 3\ OH^- \rightleftarrows Pu(OH)_3^0(aq)$	(15.8 ± 0.5)

6.2 Supplementary PuO_2(ncr,hyd) solid phase analyze in XRD plot

The extended XRD pattern of PuO_2(ncr,hyd) from the solubility experiments after the equilibration with $[Lig]_{in}$ = 0.1 M (where the Lig = GTA, HIBA and HBA) in stage II cement porewater is represented in the Figure A-1 – A-3. Blue, red and green solid lines illustrate the XRD pattern of PuO_2 in GTA, HIBA and HBA, whilst black lines correspond to the XRD diffractogram of the dried supernatant. Inverted blue and black triangles represent reference patterns of PuO_2(cr) (PDF 75-2011) and portlandite (PDF 44-1481).

Besides the peaks of the reference materials, additional reflection signals emerged in all 3 proxy ligands systems (see blue, red, green and black arrow in Figure A-1 – A-3), which could not be assigned neither to PuO_2(ncr,hyd) nor to portlandite. As discussed in the main text, this could imply the formation of a secondary phase.

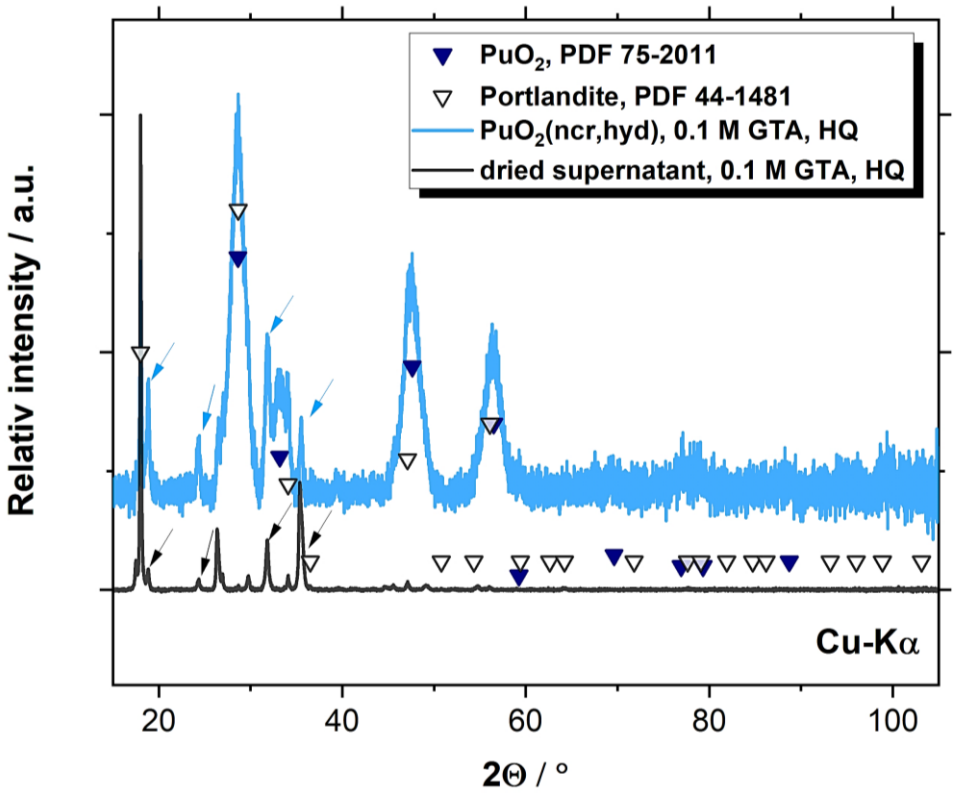

Figure A-1. *Blue line corresponding to the XRD diffractogram of PuO_2(ncr,hyd) after equilibration in solubility experiments with GTA at $[Lig]_{tot}$ = 0.1 M, buffered by HQ. Black line presents XRD pattern of the batch solution supernatant containing [Ca] ≈ 0.02 M and [Pu] ≈ 10^{-11} M, which was dried under Ar atmosphere and room temperature. Purple and unfilled up-side down triangles reflect the pattern of PuO_2(cr) (PDF 75-2011) and portlandite ($Ca(OH)_2$(cr), PDF 44-1481) reference materials, respectively. Blue and black arrows emphasize the additional signals which appear only in the solid phase and dried supernatant, but not in PuO_2(cr) nor $Ca(OH)_2$(cr).*

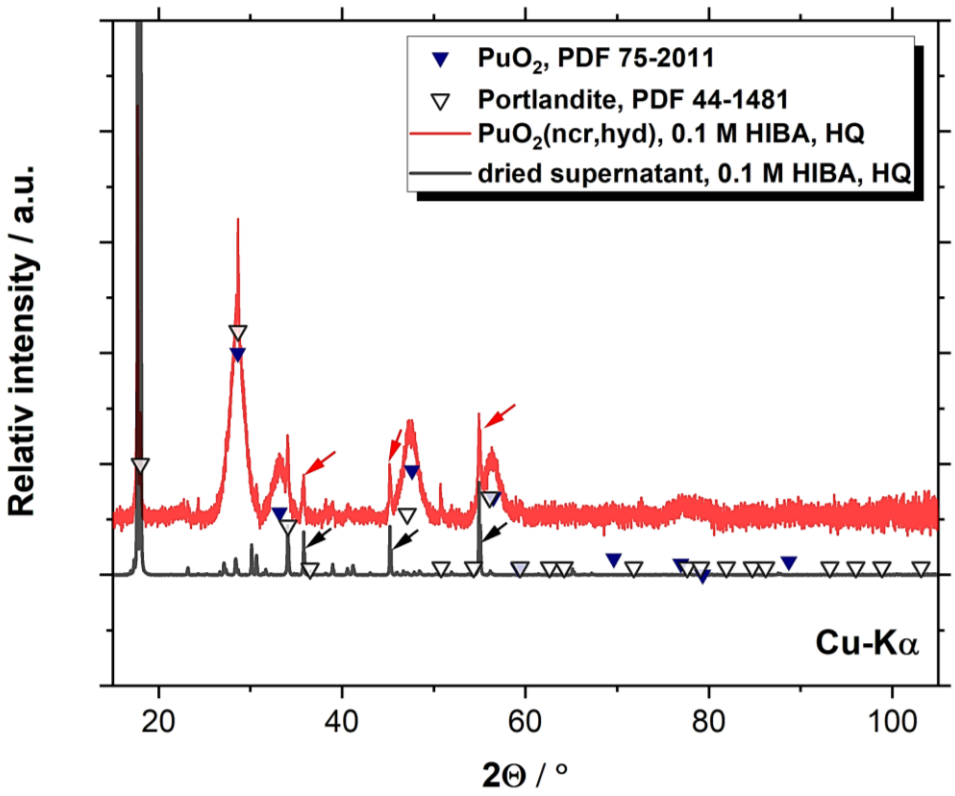

Figure A-2. *Red line corresponding to the XRD diffractogram of PuO_2(ncr,hyd) after equilibration in solubility experiments with HIBA at $[Lig]_{tot}$ = 0.1 M, buffered by HQ. Black line presents XRD pattern of the batch solution supernatant containing [Ca] ≈ 0.02 M and [Pu] ≈ 10^{-11} M, which was dried under Ar atmosphere and room temperature. Purple and unfilled up-side down triangles reflect the pattern of PuO_2(cr) (PDF 75-2011) and portlandite ($Ca(OH)_2$(cr), PDF 44-1481) reference materials, respectively. Red and black arrows emphasize the additional signals which appear only in the solid phase and dried supernatant, but not in PuO_2(cr) nor $Ca(OH)_2$(cr).*

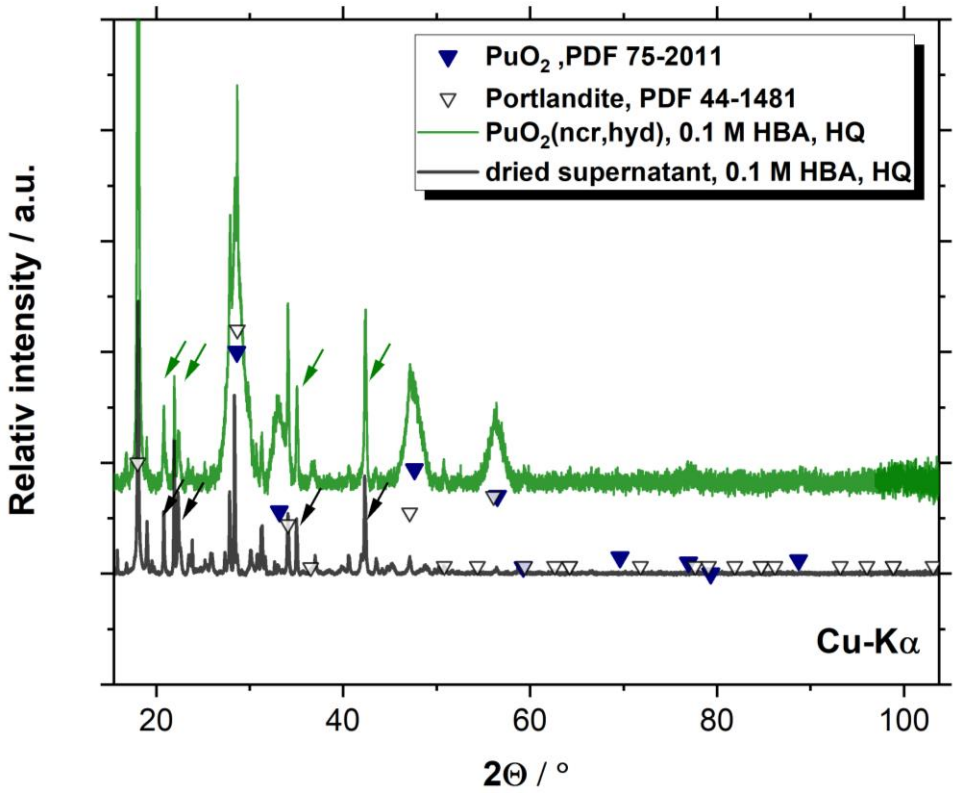

Figure A-3. *Green line corresponding to the XRD diffractogram of PuO_2(ncr,hyd) after equilibration in solubility experiments with HBA at $[Lig]_{tot}$ = 0.1 M, buffered by HQ. Black line presents XRD pattern of the batch solution supernatant containing [Ca] ≈ 0.02 M and [Pu] ≈ 10^{-11} M, which was dried under Ar atmosphere and room temperature. Purple and unfilled up-side down triangles reflect the pattern of PuO_2(cr) (PDF 75-2011) and portlandite ($Ca(OH)_2$(cr), PDF 44-1481) reference materials, respectively. Green and black arrows emphasize the additional signals which appear only in the solid phase and dried supernatant, but not in PuO_2(cr) nor $Ca(OH)_2$(cr).*

6.3 Effect of NaCl and $NaClO_4$ on the uptake of Pu by HCP

Continuing the same sorption experimental thread as it was interpreted in the previous Section 3.3.4.2, the retention of Pu(IV) on Portland cement was complemented with additional experimental results applying of NaCl and $NaClO_4$ as it is showed in the Figure A-4. The batch solutions were prepared in order of addition of the components (Cement + Pu) + NaCl/$NaClO_4$ and according the Na^+ concentration within the proxy ligands. Moreover, two $NaClO_4$ series were created, which reflect the Na^+ content in GTA (yellow symbol) and HIBA/HBA (purple symbol) systems.

At given initial concentration of plutonium of log $([Pu]_{in}$ /M) = –8 and S:L = 1 $g \cdot dm^{-3}$, the detected log R_d values were noticed to display scattering in each batch solution after 49 and 83 days in the batch solutions, equilibrated with $NaClO_4$ (yellow and purple symbols) and NaCl (blue symbols).

In the frame of solubility approaches, the effect of NaCl and $NaClO_4$ on PuO_2(ncr,hyd) under alkaline conditions is considerably low or none, thus solubility increase in high ionic strength can be disregarded [58]. Other aspect within the sorption experiment was observed that proxy ligands decrease the uptake of Pu at log $([Lig]_{in}$ /M) $\geq$ –2 (Figure 31), however this statement basically was formed due to the higher dilution used at high ligand concentration, which eventuates the decrease of the detection limit and discrepancy (see Section 3.3.4.2). Meanwhile, the Figure A-4 signifies only large dispersion occurred in every solution containing NaCl and $NaClO_4$. This overrules the theory that the Na^+ contributes to the release of Pu to the aqueous phase.

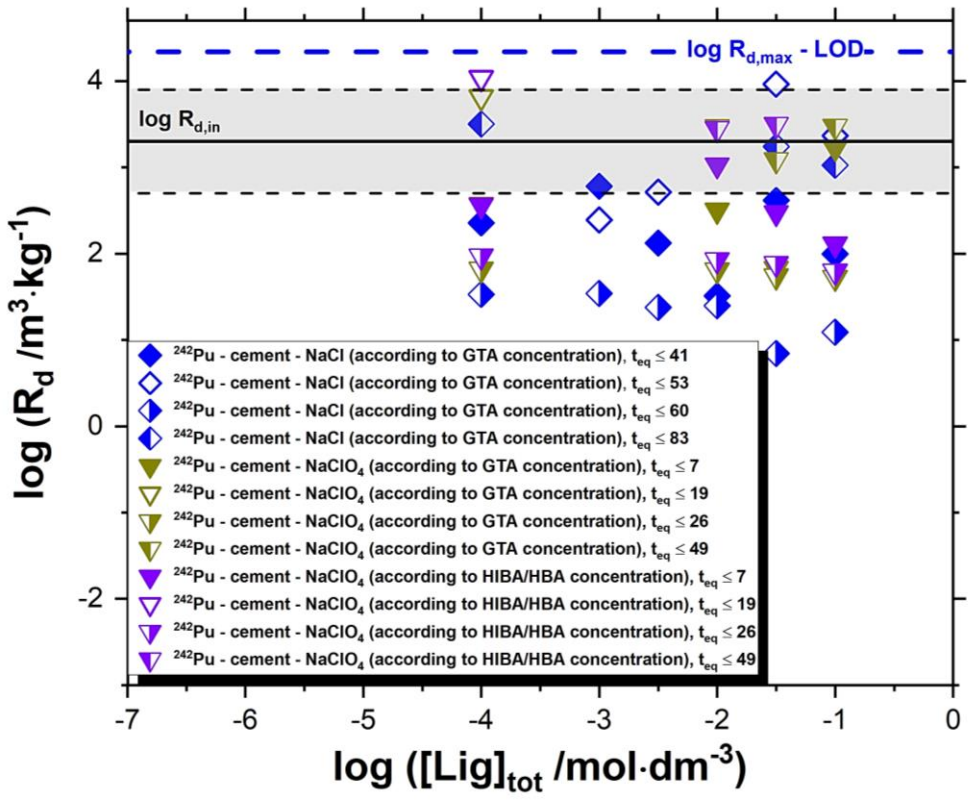

Figure A-4. *Effect of NaCl and $NaClO_4$ on the uptake of Pu by HCP in HQ buffered media and order of addition of individual components of (Cement + Pu) + NaCl/$NaClO_4$. The batch samples were generated according to the Na^+ concentration in GTA, HIBA and HBA batch solutions. Blue symbols correspond to the NaCl sorption datapoints, while the yellow and purple present the $NaClO_4$ experimental results at $t_{eq} \leq 83$ and 49 d, respectively. The blue dash line illustrates the highest log R_d that can be quantified, based on the detection limit of SF-ICP-MS for [Pu]. Solid black lines and grey shades are the distribution ratio of Pu and its uncertainty in organic ligand-free system (log ($R_{d,in}$/m^3·kg^{-1}) = (3.3 ± 0.6) [94].*